NUREG/CR-3736

Field and Theoretical Investigations of Fractured Crystalline Rock Near Oracle, Arizona

Prepared by J. W. Jones, E. S. Simpson, S. P. Neuman, W. S. Keys

Department of Hydrology and Water Resources
University of Arizona

Prepared for
U.S. Nuclear Regulatory
Commission

NUREG/CR-3736
RW

Field and Theoretical Investigations of Fractured Crystalline Rock Near Oracle, Arizona

Manuscript Completed: May 1985
Date Published: August 1985

Prepared by
J. W. Jones, E. S. Simpson, S. P. Neuman, W. S. Keys*

Department of Hydrology and Water Resources
University of Arizona
Tucson, AZ 85721

*U. S. Geological Survey, Denver Federal Center, Denver CO 80225

Prepared for
Division of Radiation Programs and Earth Sciences
Office of Nuclear Regulatory Research
U.S. Nuclear Regulatory Commission
Washington, D.C. 20555
NRC FIN B5753

ABSTRACT

A combination of geophysical and hydraulic testing has been conducted in granite near Oracle, Arizona. The purpose of the work is to determine relationships, if any, among (1) fracture distribution, (2) geophysical properties, and (3) hydraulic properties of fractured rock of low hydraulic conductivity. To date, eight vertical borings spaced 20 to 50 feet apart, ranging from 250 to 300 feet in depth, have been drilled. The data obtained from neutron, gamma, acoustic-velocity, electrical-resistivity, and acoustic-televiewer logs, with the results of over 100 single-hole, straddle-packer injection tests make possible a detailed description of the fracture system. Geophysical logs readily detect fractures and are sensitive to subtle lithologic variations of the granite. Orientation and distribution of individual fractures were determined from interpretation of the acoustic-televiewer data, and from the analysis of core obtained from one borehole. Fracture densities over the 13-foot long straddle-packer test intervals did not correlate with measured hydraulic conductivity for each interval. A strong correlation between the neutron-log response and measured hydraulic conductivity does exist; it was used to supplant conductivity measurements. The geostatistical technique of kriging provided a three-dimensional map of hydraulic conductivity that can be compared with subsurface interpretations of the geophysical logs.

This method can be applied in a general sense to any naturally fractured rock system. Reconstruction of the geologic history provides a framework for the interpretation of geophysical and hydraulic testing. A continuum approach to the analysis of the volume-averaged measurements is then applied and the techniques of geostatistics give estimates of the uncertainties inherent to the data.

TABLE OF CONTENTS

TABLE OF CONTENTS (CONT'D)

LIST OF ILLUSTRATIONS

LIST OF ILLUSTRATIONS (CONT'D)

LIST OF ILLUSTRATIONS (CONT'D)

LIST OF TABLES

INTRODUCTION

1.1 Site Location

This report summarizes field investigations to establish the relationship among geophysical and hydraulic characteristics and fracture distribution of granitic rocks, informally called Oracle granite in this report, about five miles southeast of the town of Oracle, Arizona (Figure 1.1). The report is part of a larger investigation concerned with fluid flow and solute transport through fractured rocks of low hydraulic conductivity. The study site is on a pediment surface, flanking the northwest end of the Santa Catalina Mountains. Surface elevation of the granite ranges from about 5,000 feet above sea level near the mountains, to about 4,000 feet at its contact with a basin-fill sedimentary sequence, 15 miles to the east. At the study site, surface elevation is about 4,250 feet above mean sea level. A contour map of the regional water table is shown in Figure 1.2, based on data from 30 wells. In most of the area, the water table is less than 100 feet below land surface; at the study site, it is about 40 feet below land surface. Average annual precipitation ranges from 19 inches at Oracle, to a maximum of 25 inches at highest elevations (approximately 9,000 feet) of the Santa Catalina Mountains. About half the precipitation occurs during a summer wet season, from July through September; most of the remainder occurs in a winter wet season from December through February.

1.2 Boreholes

Eight boreholes were drilled at the site (Figure 1.3 and Table 1.1). During initial exploration, borehole H1 was drilled about 1,500 feet north of the site; however, the granite was too fractured, and the site was abandoned. Nevertheless, this borehole provides useful geological and water-level data. Drilling of the eight boreholes at the study site was accomplished in two phases. During phase 1, boreholes M1, H1, H2, H3, and H4 were drilled; completion was in February 1981. During phase 2, boreholes H5, H6, H7, and H8 were drilled; completion was in December 1982. Weathered granite was cased off in all holes. Depth of weathering ranged from about 40 to about 65 feet. (It should be mentioned that the core taken from boring M1 was used for experiments in borehole sealing as part of project NRC-04-78-271, Dr. Jack Daemen, Principal Investigator).

1.3 Purpose and Scope

These investigations were generic; the purpose was the study of flow and transport through fractured rocks in general, and the evaluation of techniques for determining hydrologic properties of such rock. The Oracle site served as a convenient field laboratory. Neither the study site nor its vicinity was intended for nuclear-waste disposal. However, to properly design and interpret hydrological tests at the site, its geology must be characterized in the context of the regional setting. One purpose of this report is to provide such a site characterization, and to interpret the nature and distribution of

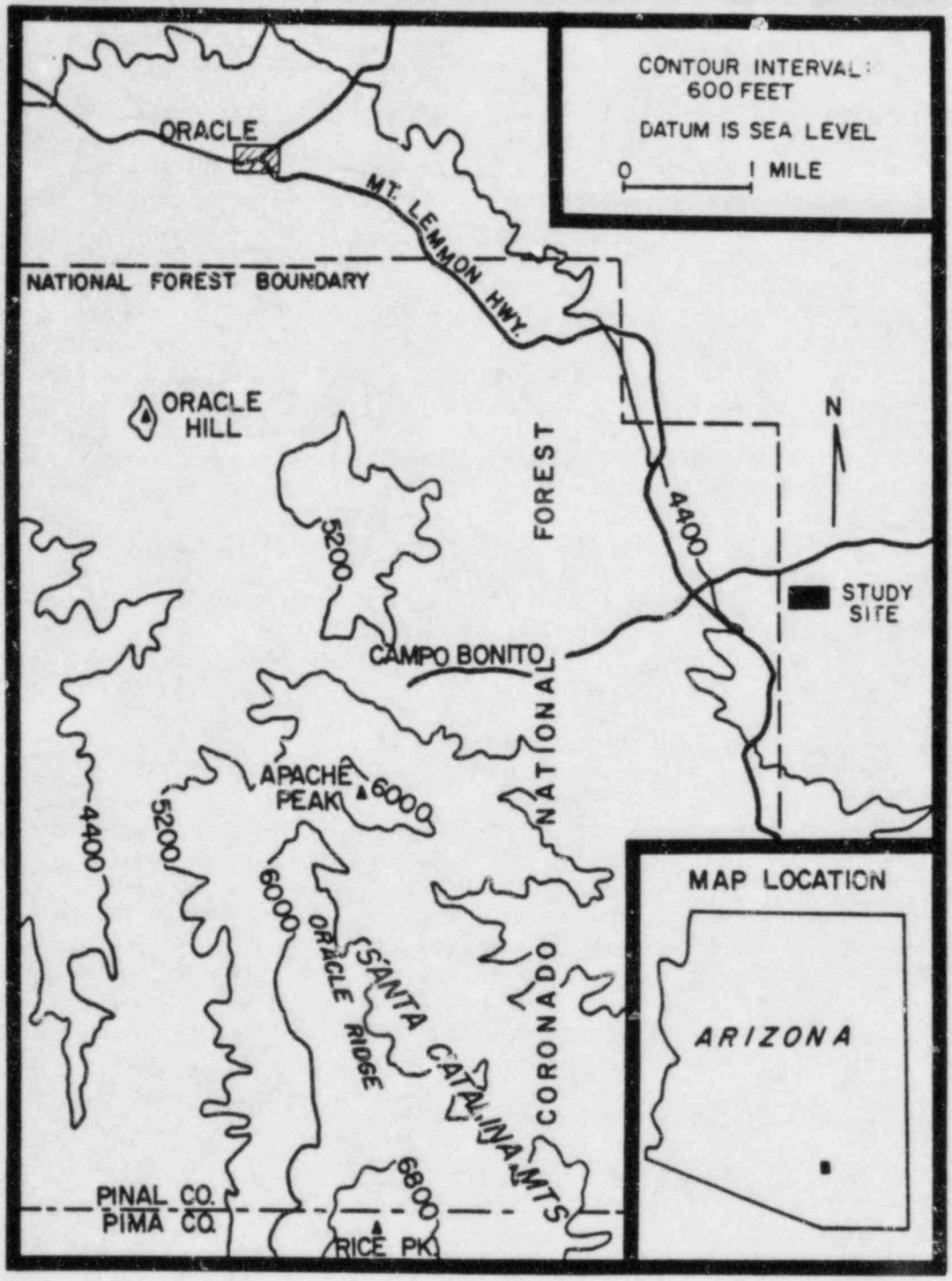

Figure 1.1. Topographic map of northern Santa Catalina Mountains.

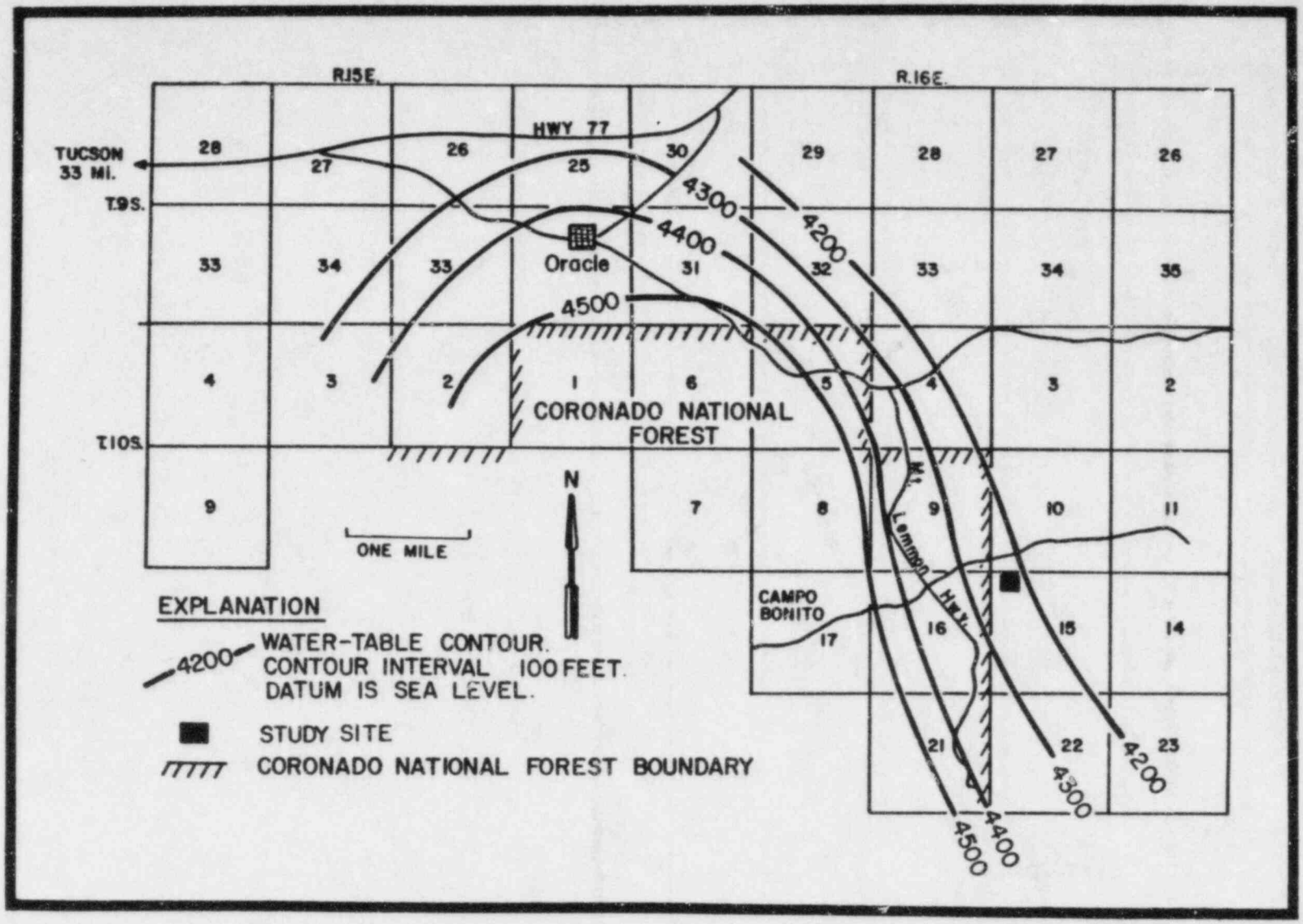

Figure 1.2. Regional water table.

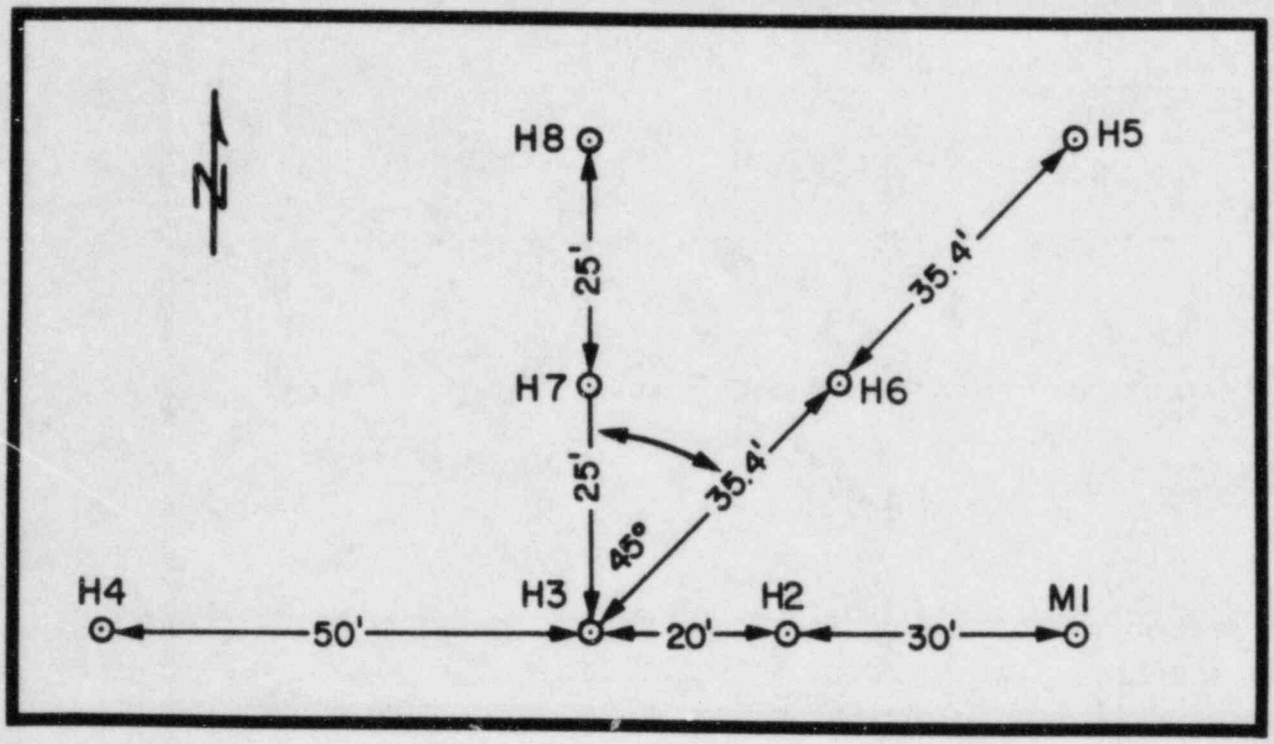

Figure 1.3. Location of boreholes.

Table 1.1 Boreholes at the Study Site

BOREHOLE NO.	TOTAL DEPTH (FEET)	CASING DEPTH (FEET)	CASING DIAMETER (INCHES)	NOMINAL HOLE DIAMETER (INCHES)	DRILLING METHOD AND DEPTH INTERVAL (FEET)
M1	300	58	8	6 3/4	0-58, mud rotary; 59-106, cored; 106-300, air hammer
H2	300	59	5	4 1/2	0-59, mud rotary; 59-300, air hammer
H3	300	58	7	6 3/4	0-58, mud rotary; 58-300, air hammer
H4	288	43	5	4 1/4	0-43, mud rotary; 43-288, cored
H5	250	61	5	4 1/2	0-250, air hammer/ foam
H6	250	63	5	4 1/2	0-250, air hammer/ foam
H7	250	66	5	4	0-66, air hammer/ foam; 66-250, cored
H8	250	59	5	4	0-59, air hammer/ foam; 59-250, cored

the fractures in light of their genesis and hydraulic properties. Other aims of the report are: (1) To describe investigations of the potential use of selected borehole-geophysical techniques as aids in the determination of hydraulic parameters; and (2) to show how geostatistical methods can be used to interpolate the spatial variability of such parameters. The distribution of hydraulic conductivity is given as an example.

Some researchers believe that fractured rocks exhibit a larger degree of hydraulic anisotropy and spatial variability than porous sedimentary formations do. This leads them to insist that field tests in fractured rock be designed on a grand scale (megascale) to measure the average (effective) properties of large rock volumes. Other researchers prefer the microscale; they examine the properties of individual fractures, with the expectation that these can be integrated into a large-scale picture. Examples of the latter approach include the works of Snow (1965), Schwartz (1983), and Long et al. (1982). Megascale hydrologic tests are outside the present scope of this project; most of our work is somewhere between megascale and microscale. Our measurements were conducted over distances of a few feet to a few tens of feet; however, we collected sufficient data on individual fractures to determine whether or not microscale theoretical analyses would be feasible and applicable to the Oracle granite. We found that these data are useful in reaching qualitative conclusions of the effect of fracture geometry on fluid flow and solute transport; however, we were skeptical that such data (with the exception of major fractures) could be used to obtain quantitative estimates of hydraulic parameters, such as hydraulic conductivity and kinematic (also called effective) porosity. Our analysis suggested that such parameters must be measured directly by appropriate hydraulic, geophysical, and tracer tests on a scale not smaller than a few feet or a few tens of feet. The choice of an optimum test scale is open for debate.

Our approach to the study of fracture patterns was to relate them to geological and tectonic events. Chapter 2 considers those aspects of the local and regional geology that are relevant to fracture formation. This chapter indicates that certain fracture sets can be related to definable events that occurred during the emplacement and cooling of the granite. Later tectonic events were, in part, controlled by planes of weakness in the rock. Thus, an understanding of geological and tectonic history is needed to genetically and conceptually classify the mapped fractures. The division of fractures into sets is further facilitated by stereographic projections that indicate central tendencies and the degree of scatter of the orientations of fractures.

A statistical analysis of fracture spacings and an attempt to correlate fractures between and among boreholes are described in Chapter 3. We found that the degree of interconnectivity among fractures in different boreholes was generally difficult to determine on the basis of location and orientation data alone (with the exception of major features such as faults). Reliable information concerning fracture continuity was obtainable by cross-hole packer tests of the kind described by Hsieh et al. (1983), and also by tracer tests.

Chapter 4 describes attempts to use the responses of selected borehole geophysical instruments to improve our understanding of fracture patterns and our knowledge of hydraulic parameters. A major difficulty in the interpretation of geophysical logs in crystalline rock is that many of the probes have not

been calibrated for response in igneous and metamorphic rocks as they have been for sedimentary rock. Nevertheless, we were able to show discernable correlations between neutron logs and in situ hydraulic conductivity. However, we were unable to correlate neutron- and acoustic-velocity responses with rock porosity as determined by laboratory analysis of core samples. In this case, we used empirical equations relating instrument response to porosity, which has been standard practice in petroleum exploration for a long time. Another negative result is the apparent lack of correlation between fracture density and hydraulic conductivity. This raises doubts about the applicability of fluid-flow and solute-transport models that are based on the distribution of discrete fractures, at least insofar as rock formations similar to the Oracle granite are concerned. Acoustic-televiewer logs were particularly useful for providing data on fracture location, orientation, and character, and providing data in major fracture zones, where core recovery was not possible.

The report closes (Chapter 5) with an analysis of the spatial variability of hydraulic conductivities (as obtained by single-hole packer tests) using geostatistical methods. This analysis shows that the logarithm of hydraulic conductivity can be fitted to a spherical-semivariogram function, representing a so-called intrinsic stochastic process. The parameters of this function have been used (Winter et al., 1984a,b) to predict the far-field dispersivity tensor of the Oracle granite. In this report, the same function is used to estimate hydraulic conductivity of the rock between boreholes in three dimensions by means of a stochastic interpolation method called kriging. The "kriged" estimate then is used as the basis for generating equally likely log-hydraulic-conductivity distributions by conditional Monte Carlo simulations. These estimates and simulations have considerable potential for the investigation of three-dimensional fluid flow and solute transport through the Oracle rock mass, as well as through other fractured rocks.

1.4 U.S. Geological Survey Cooperation

The U.S. Geological Survey has a research project on borehole geophysics as applied to groundwater hydrology. For the past five years, Geological Survey personnel have been working at several research sites in crystalline rocks in Canada in cooperation with Atomic Energy of Canada Limited (Davison, et al., 1982; Keys, 1984). The work at the Oracle study site was a logical extension of that experience, in an area where core and hydraulic-test data were available for comparison with geophysical logs.

2. GEOLOGY AND FRACTURE CLASSIFICATION

The following description of the granite near Oracle provides a framework for the analysis of fluid flow and contaminant transport in the rock; it is not meant to be a comprehensive geological treatise. We start with a description of the texture and composition of the rock fabric in relation to the evolution of the granite. Next we discuss regional features such as dikes and faults. Finally, we provide an overview of the geological history to show the interrelationship between local and regional features. Additional discussion and interpretation of features observed during testing at the site are given in subsequent chapters. A glossary of geologic terms is given in Appendix B.

2.1 Petrology

Oracle granite is a coarse-grained porphyritic biotite quartz monzonite of light-gray to light-pink color. (The term granite, though technically inaccurate, will be retained). Potassium feldspar (K-spar) occurs as large (2 to 6 cm) subhedral to euhedral phenocrysts. Biotite schlieren, quartz-schist inclusions, and mafic (diabase) inclusions are common in the exposures of the Oracle granite. These inclusions, when tabular, consistently strike NE within the area of the study, as do the K-spar phenocrysts.

Biotite is often replaced by chlorite, especially near zones of movement and hydrothermal action. Examination of cores showed that recrystallization of the coarse-grained rock to a fine-grained, nearly mylonitically textured rock took place over short (3 to 100 cm) intervals around some fractures. In zones of brecciation, the rock is often highly weathered. Common weathering products are kaolinite and various iron and magnesium oxides, that impart reddish brown to purple stains to many fracture surfaces.

A significant feature of the Oracle granite is the abundance of dikes. A wide range of dike compositions exists, including coarse- and fine-grained diabase and pegmatite, aplite, quartz veins, latite, trachyte, andesite, and rhyolite, all of which have been identified in the vicinity of the study site (Figure 2.1). Most of the dikes have preferred orientations and can be detected on aerial photographs and by surface mapping. The exact temporal relationship among the intrusives is not clear. Pegmatite and aplite dikes usually form during the last stages of the cooling of a granitic pluton, and tend to fill preexisting fractures that formed during the emplacement and cooling of the magma.

2.2 Regional Structural Setting

Approximately 40 mi^2 of the Oracle granite is exposed at the north end of the Santa Catalina-Rincon-Tortolita crystalline complex (Figures 2.2 and 2.3). The Oracle granite was dated to be approximately 1,400 million years (MY) old by Rb-Sr, K-Ar, and other radioisotope dating techniques (Keith et al., 1980). Equivalent units of similar age throughout the region include the Ruin granite, the Rincon Valley granodiorite, the Continental granodiorite, and many of the dark augen gneisses of the Catalina forerange (Keith et al.,

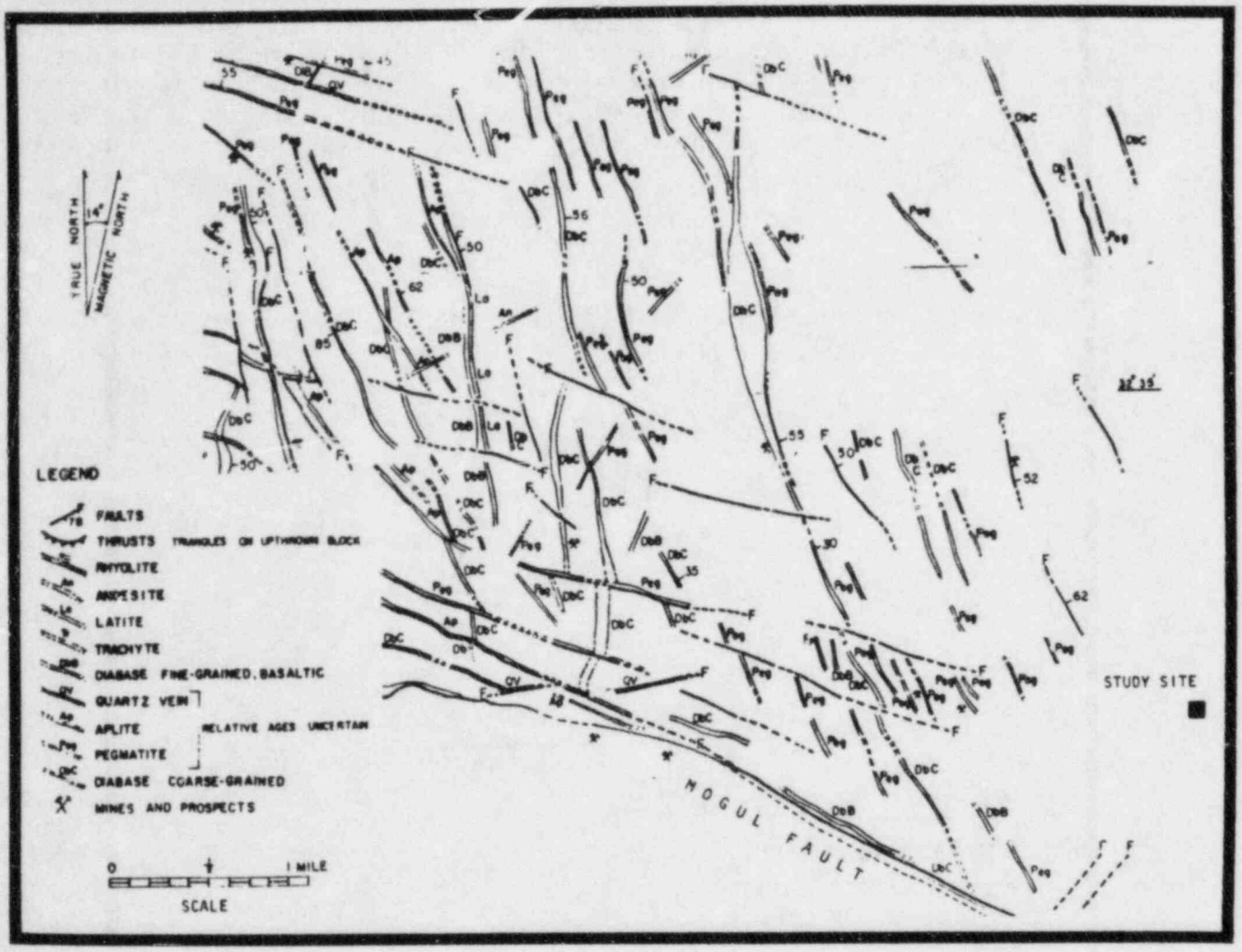

Figure 2.1. Faults and dikes in the granite near Oracle (modified after Banerjee, 1957).

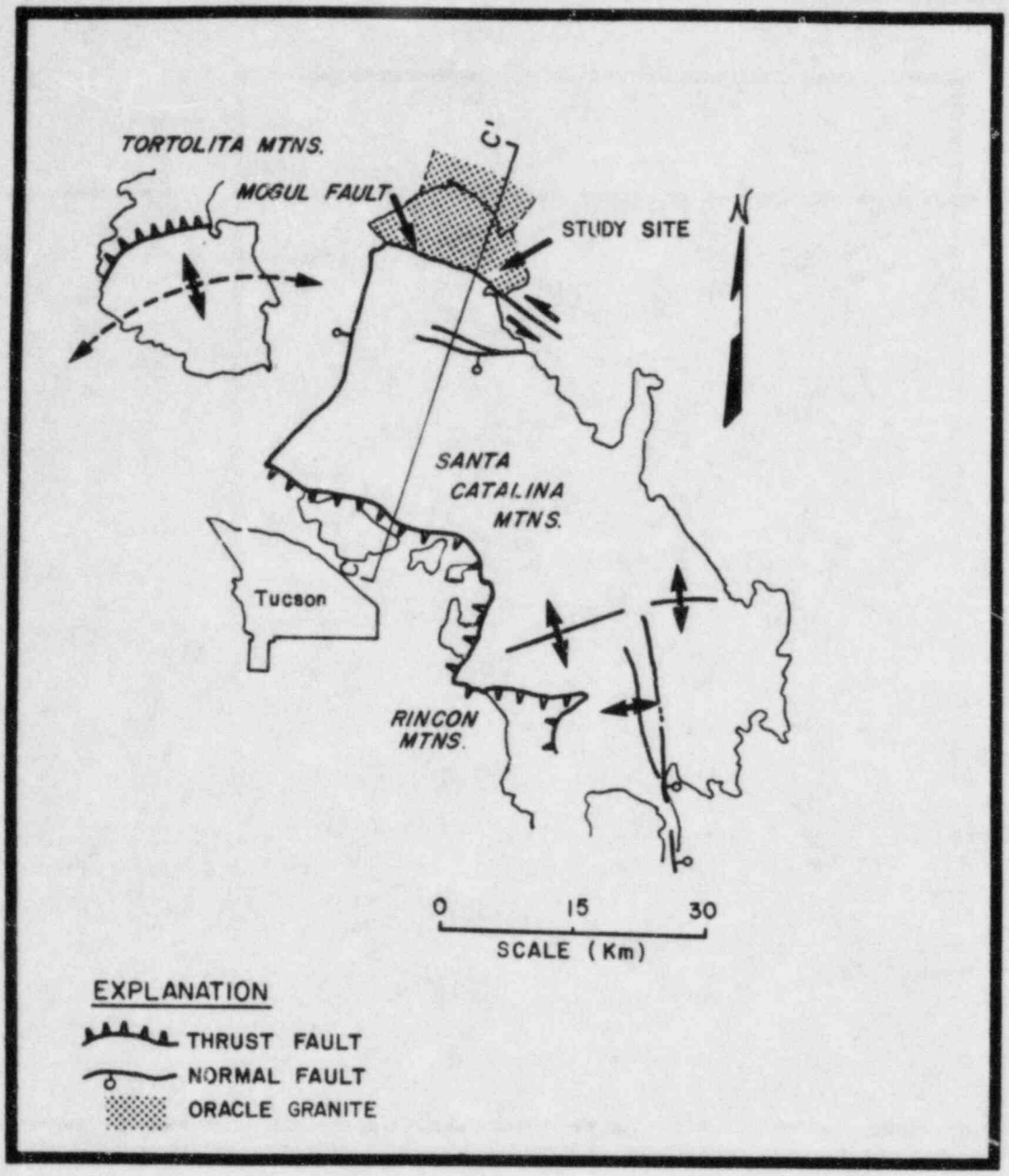

Figure 2.2. Generalized geological map of the Santa Catalina-Rincon-Tortolita Mountain crystalline complex (after Crittenden et al., 1980).

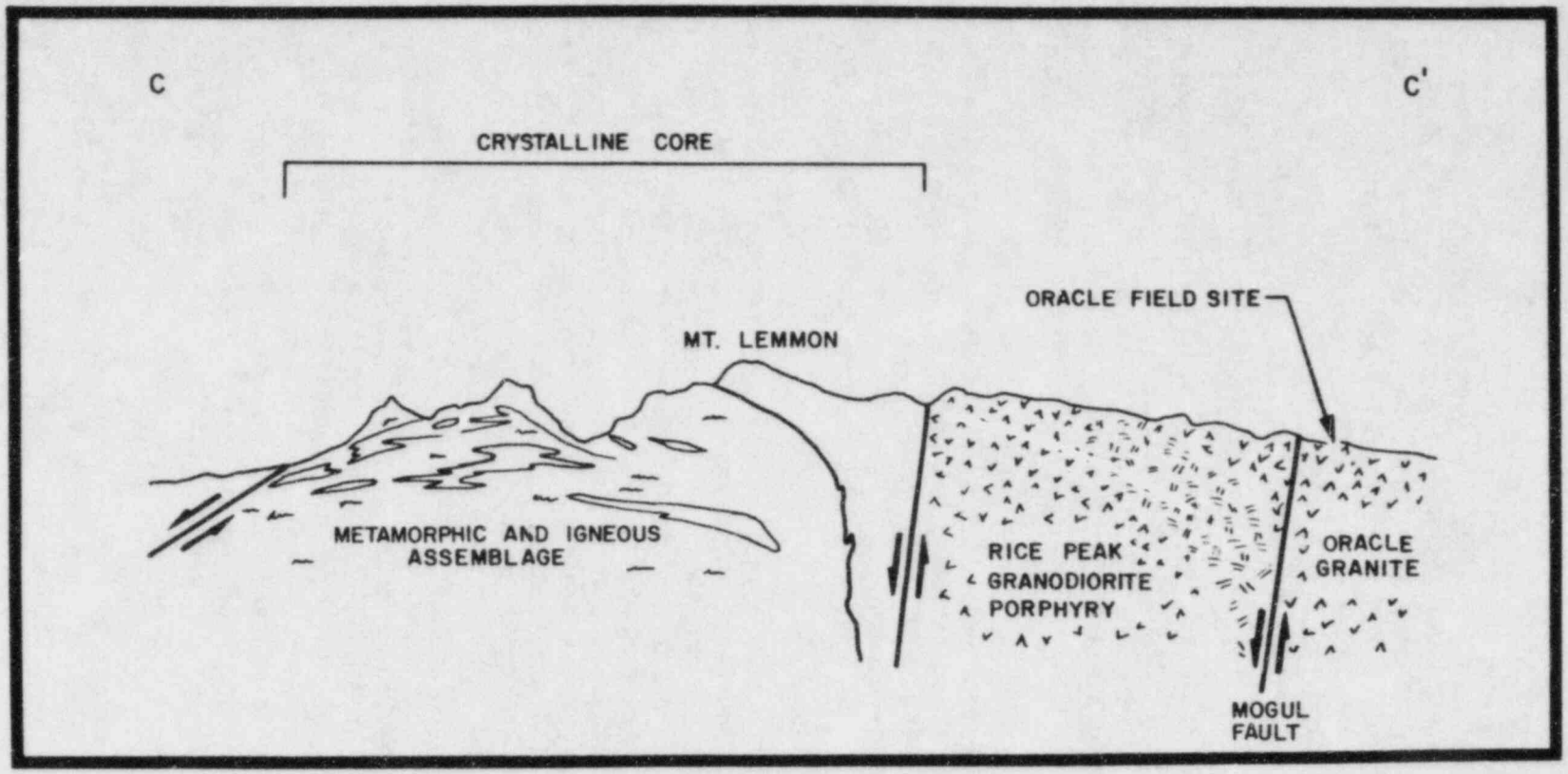

Figure 2.3. Cross section through central Santa Catalinas and the Oracle site (after Crittenden et al., 1980).

1980). The Oracle granite appears to be part of a structurally complex, major Precambrian granitic system.

The Oracle granite is separated from the Santa Catalina complex by the west-northwest trending Mogul fault (Figures 2.2 and 2.3). This fault is believed to be part of a zone of faults that has been active since Precambrian time, and may be part of a major continental-scale tectonic feature (Drewes, 1981). Both uplift and left lateral movements of the Oracle granite have been recorded along the fault zone (Banerjee, 1957). The post-Paleozoic intrusive units of the Santa Catalina complex have been divided into three suites of Late Cretaceous (75-65 MY), Eocene (50-44 MY), and middle Tertiary (28-25 MY) age and represent periods of major tectonic activity in southeastern Arizona (Keith et al., 1980). Some of the dikes in the study area may be representative of these intrusion pulses. Dikes in the immediate vicinity of the study area have been little studied to date, primarily because of a lack of economic mineralization. The only available isotopic age date is for the north-northwest trending diabase system, a regional intrusive event dated at 1100 MY (Drewes, 1981).

Intrusive events represent only part of the regional geologic history. Davis (1981) recognized at least seven superimposed deformational episodes since emplacement of the granite. Two local fault systems affecting the Oracle region are comparatively well-documented; the Mogul and the San Manuel faults. Motion from this faulting was, in part, accommodated by preexisting fractures in the granitic rock.

The Mogul fault is part of a series of anastomosing faults that trend west-northwest throughout southeastern Arizona. In this study, the fault is important because of its close proximity (1 mile) to the Oracle study site (Figure 2.1). Two modes of movement have been recorded along this fault: (1) Left lateral strike slip that dragged foliae of the granite into parallelism with the fault, and (2) uplift of the Oracle granite. Strike-slip movement may have been taking place throughout geologic time. The uplift was part of the Basin and Range movements (14 MY), and motion was not restricted to the Mogul fault. Subsequent erosion lowered the present exposure of the Oracle granite below the Santa Catalina Mountains (with a relief of approximately 5,000 feet).

The San Manuel fault (not shown on Figure 2.1) is five miles northeast of the study site, within the Oracle granite, where it bisects the San Manuel-Kalamazoo porphyry system. Ten to fifteen thousand feet of southwest displacement (toward the Oracle site) is documented along this lystric normal fault, that is oriented approximately N45W/30SW (Lowell, 1968). This fault has been dated as middle Miocene by the depositional relationship of the Gila Conglomerate. The motion, fault morphology, and timing are consistent with middle Miocene (25 MY) lystric normal faulting seen throughout the region (Davis, 1981).

The major structural events that have influenced the Oracle granite follow:

1. 1400 MY — Emplacement of granitic batholiths, including the Oracle granite.

2.	1100 MY	Emplacement of coarse-grained diabase dikes, typically trending NNW. Hydrothermal alteration of granite close to these dikes.
3.	Precambrian to (?)	Left-lateral, strike-slip movement of the Mogul fault.
4.	75-65 MY	
	44-50 MY	Emplacement of Santa Catalina-Rincon-Tortolita plutonic suites.
	28-25 MY	
5.	25 (?) MY	Middle Miocene low-angle lystric normal faulting and widespread hydrothermal alteration of granite due to thermo-tectonic activity.
6.	14 MY	Basin and Range block faulting.
7.	14 MY (?) to present	Erosion of Oracle granite below level of Santa Catalina Mountains.

2.3 Primary Magmatic Features

During the formation of a plutonic mass, a definable system of internal petrological structures, dikes, and fractures develops. The so-called primary magmatic features occur in all granitic plutons. Subsequent tectonic events later may cause the superposition of additional features on the primary system, the properties of which often are influenced by the preexisting primary features. Two important elements in the Oracle granite in the environs of the site are: (1) The northeast-trending mafic inclusions and elongate K-spar phenocrysts of the rock fabric; and (2) the northwest-trending aplite and pegmatite dikes. The dikes are the most prominent mappable feature (Figure 2.4).

Foliation and lineation (the planar and linear orientation of the internal petrological structures) provide a record of the style and history of magma emplacement. Elongate inclusions and phenocrysts align themselves with the direction in which the magma flows within the Earth's crust. Granite at Oracle contains mafic and silicic inclusions, such as pieces of older Pinal Schist (1,700 MY), that were incorporated into the magma as it penetrated the country rock. These inclusions, as well as K-spar phenocrysts that have formed in the magma, are both aligned in a NE direction, which was the last flow direction of the local magma as it cooled.

The fracture patterns that develop subsequent to foliation and lineation, and the orientation of magma differentiates, such as pegmatite and aplite that later fill some of these fractures, depend on the stress evolution and late emplacement history of the rock mass (Knapp and Norton, 1981). A generic classification of these patterns has been suggested by Balk (1937) and is illustrated in Figure 2.5. According to this classification, the primary fractures often form three mutually orthogonal sets: (1) Cross joints oriented perpendicular to the flow line; (2) steeply dipping longitudinal joints

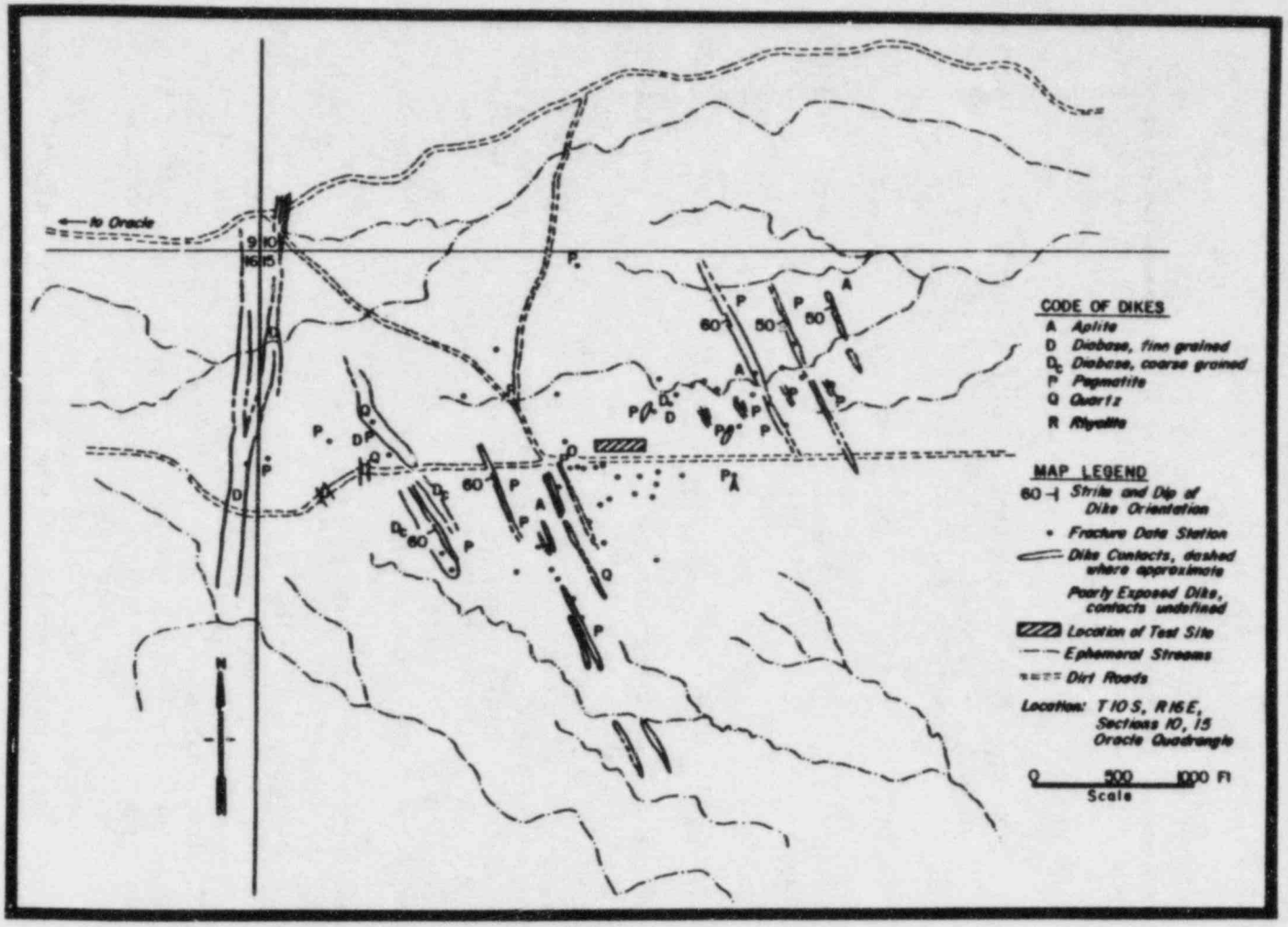

Figure 2.4. Local geologic map of the Oracle site.

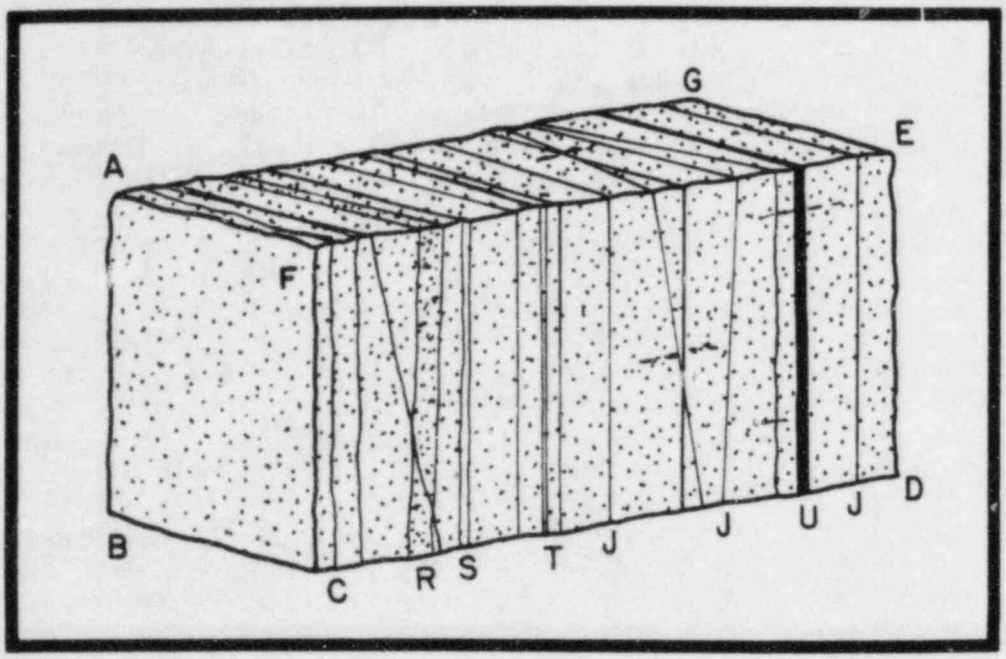

EXPLANATION

J	-	CROSS JOINT
CFED	-	LONGITUDINAL JOINT, ALONG FLOW TREND DIRECTION.
AFEG	-	FLAT-LYING JOINT, FOLLOWING GENERAL DIRECTION OF FLOW PLANES.
RSTU	-	DIKE EMPLACED PREDOMINANTLY IN CROSS JOINTS -- FLOW LINES ARE HORIZONTAL.

Figure 2.5. Schematic relationship between flow lines in magma and directions of parting (from Balk, 1937).

running parallel to the flow lines; and (3) primary flat-lying joints, which are subparallel to the exterior boundary of the magma chamber. Pegmatite and aplite dikes often are observed to form in the cross joints of many granitic systems. Further details about the nature of these three sets of primary fractures are listed in Table 2.1 (after Balk, 1937; and McEwen, 1980).

Information about fractures at the Oracle test site is derived from three major sources: (1) Surface mapping; (2) cores and thin sections obtained from boreholes M1 and H4; and (3) acoustic-televiewer logs from boreholes M1, H2, H3, and H4. The acoustic-televiewer logs were used to orient the cores from M1 and H4. While cores also are available from boreholes H7 and H8, these cannot be oriented at the present time as acoustic-televiewer logs are not yet available. In general, surface mapping is biased toward steeply dipping fractures, and data from vertical boreholes is biased toward low angle fractures.

While surface mapping at the site is difficult because of deep weathering, it nevertheless reveals a regular fracture pattern, when cracks within dikes are disregarded. A lower-hemisphere stereographic projection of fractures found in surface exposures is shown in Figure 2.6. A stereographic projection, or stereonet, is a technique for plotting planar, three-dimensional data on a two-dimensional projection of the lower half of a sphere. The position in space of each plane is represented by the intersection of its normal line (pole) with the surface of the hemisphere. For example, the pole of a horizontal plane will project to the center of the stereonet; near-vertical planes will be represented by points along the periphery of the stereonet. For the sake of clarity, the lines of latitude and longitude that ordinarily appear on a stereonet are omitted. The areal density of points are then contoured as the percent of total points per one percent area of the hemisphere. In this way, the groupings of planes of similar orientation can be identified.

The stereonet of Figure 2.6 shows three distinct clusters or groups of fractures that are nearly orthogonal to each other. One of these clusters represents a set of fractures striking approximately NW and dipping 50° to 60° to the SW. Since these fractures are perpendicular to the NE direction of magma flow, as evidenced by the orientation of inclusions and phenocrysts, they may be classified as cross joints. We saw earlier that most pegmatite and aplite dikes have a similar orientation, which is further evidence that we are dealing with cross joints as defined by Balk (1937). The NW trending dikes are resistant to weathering and form low ridges. Within the dikes, fractures are densely spaced and seem to be randomly oriented.

Another group on the stereonet in Figure 2.6 represents a near-vertical set of fractures striking ENE, roughly parallel to the magma flow lines. As such, these fractures can be classified as longitudinal according to Balk (1937). Where exposed in ENE trending stream channels (Figure 2.4), the spacing of these fractures varies between 2 inches and 2 feet; in the few outcrops found outside of stream channels, their spacing ranges from 1 to 4 feet. Denser spacing of longitudinal fractures in stream channels may reflect the tendency of local streams to occupy zones of relative weakness in the rock. Stream channels in the area tend to follow the longitudinal and cross-joint features, resulting in channels that take right-angle turns.

Table 2.1. Primary Joints of Granitic Systems

CROSS JOINTS (Synonyms: Principal joints, "Q", or Querklufte - German after Cloos, 1922). These develop as a tensional feature due to differential expansion and contraction of the magma and the walls of the chamber. Observed to be:

- long and straight, regularly spaced.
- coated with hydrothermal minerals; chlorite, muscovite, quartz, and pyrite.
- the preferred host for magma differentiates such as aplite and pegmatite.
- exhibiting slickensides.
- orthogonal to flow patterns of magma.

LONGITUDINAL JOINTS (Synonym: "S", or Spaltseite - German) these strike approximately parallel with the flow lines, again appear to be a tensional feature observed to be:

- steeply dipping.
- best developed where flow lines lie flat in the magma chamber.
- typically rougher than cross joints and show little relative movement suggesting a conchoidally fractured surface and possible feather fractures (Hodgson, 1961).
- weathered more readily, therefore include kaolinite, iron oxides tend to be locally closely spaced.
- containing much less dike material than cross joints, often at an observed ratio of 1:5 to 1:10.
- following bubble trains, microcracks.

PRIMARY FLAT JOINTS (Synonym: "L", or Lager - German) represent a subhorizontal magma border and are evidenced by subhorizontal masses of intrusives. Observed to:

- appear along flat surfaces of plutonic masses.
- contain chlorite, muscovite, and pyrite.
- be not the same as sheeting or exfoliation.

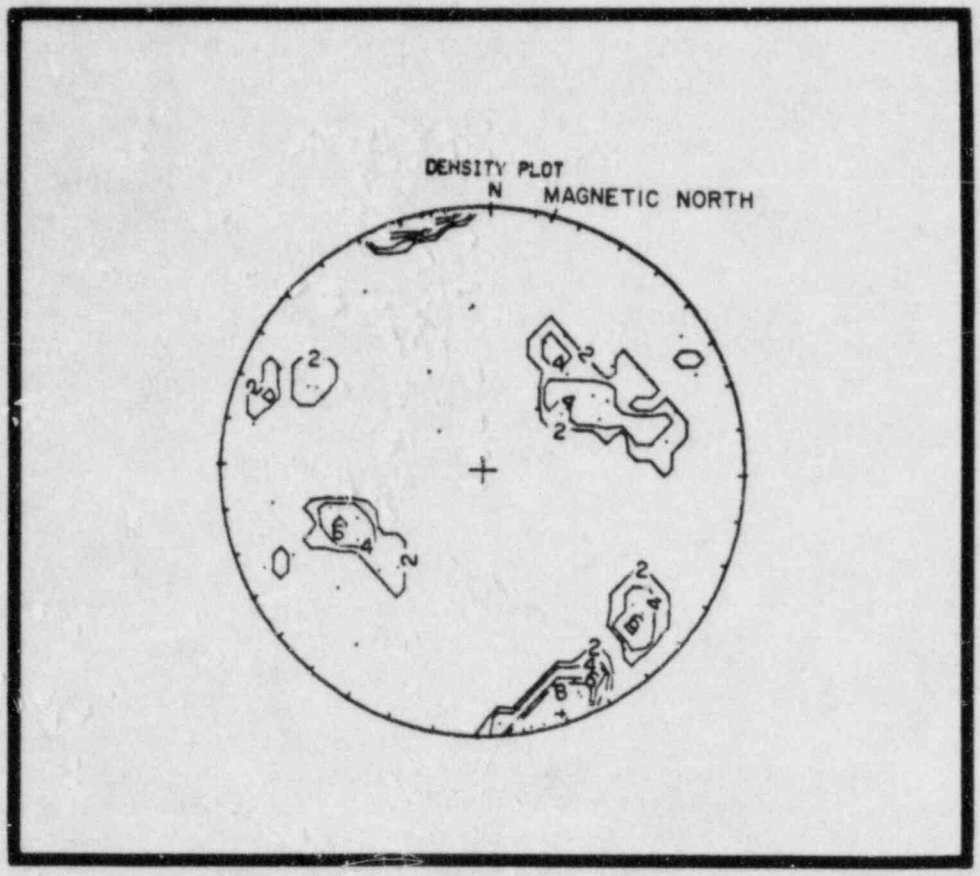

Figure 2.6. Stereonet of fractures mapped on the surface.

The third group in Figure 2.6 represents fractures striking parallel to the dikes, but dipping to the NE, orthogonally to the dikes. Even though they are not flat lying with respect to the surface, these fractures appear to form the third primary set, in accord with Balk's (1937) classification. The relationship among all three sets of primary fractures is illustrated schematically in Figure 2.7. In this figure, the NE-dipping fractures (the cross-joint set) are designated as primary set 1; whereas, the longitudinal fractures are referred to as primary set 2.

Lower-hemisphere stereographic projections of fractures detected below the surface in boreholes M1, H2, H3, and H4 are shown in Figures 2.8 and 2.9. Only fractures in Oracle granite are represented; fractures within dikes are not included, as surface mapping showed that they have random orientations. The cross joints and fractures of primary set 1 can be recognized in all four stereonets. However, since all four boreholes are nearly vertical, fractures of the longitudinal set (primary set 2) are undersampled; thus, they are underrepresented in Figures 2.8 and 2.9. Some of the longitudinal fractures that are represented have been intersected vertically by the boreholes along depth intervals of up to 40 feet. Cores obtained from these intervals show that the fractures are highly weathered and have irregular surfaces, which could suggest formation under tension (Hodgson, 1961). Some cores, including fractures of primary set 1, show a minor degree of chloritization, possibly due to shear or translation along their surfaces, or as a product of hydrothermal activity.

Balk's (1937) classification of primary magmatic features extends beyond the previously discussed three orthogonal sets to include diagonal conjugate shear fractures at roughly 45° from the direction of the magma flow lines. Such fractures tend to cut through the cross joints at a similar angle and to exhibit a minor displacement. Two additional primary sets, marginal joints and flat-lying faults, have also been included in Balk's classification. Marginal joints form along the boundaries of intrusive masses and are related to the updoming of a pluton. Flat-lying faults are low-angle reverse faults caused by dilation in the upper part of a cooling pluton. None of these three features has been conclusively identified at Oracle since large-scale geometry of the pluton is not known. A conjugate-joint set exists that may be of primary origin; however, this interpretation is tentative until further data are obtained.

2.4 Secondary Features

Primary features described in the preceding section date back to the time of the formation of the Oracle granite (more than 1,400 MY). Since that time, the area has experienced a series of major tectonic episodes that caused the superposition of younger features, such as fractures, dikes, and faults, on the old ones. The orientation and nature of the younger features were influenced by preexisting primary discontinuities in the rock mass. A combined analysis of all the surface and subsurface fracture-orientation data in Figures 2.6, 2.8, and 2.9 suggest that there are six identifiable fracture sets at the study site. Tentative outlines of these sets and their central tendencies (average orientations) are shown in Figure 2.10. These outlines are based on a somewhat subjective interpretation of the data in Figures 2.6,

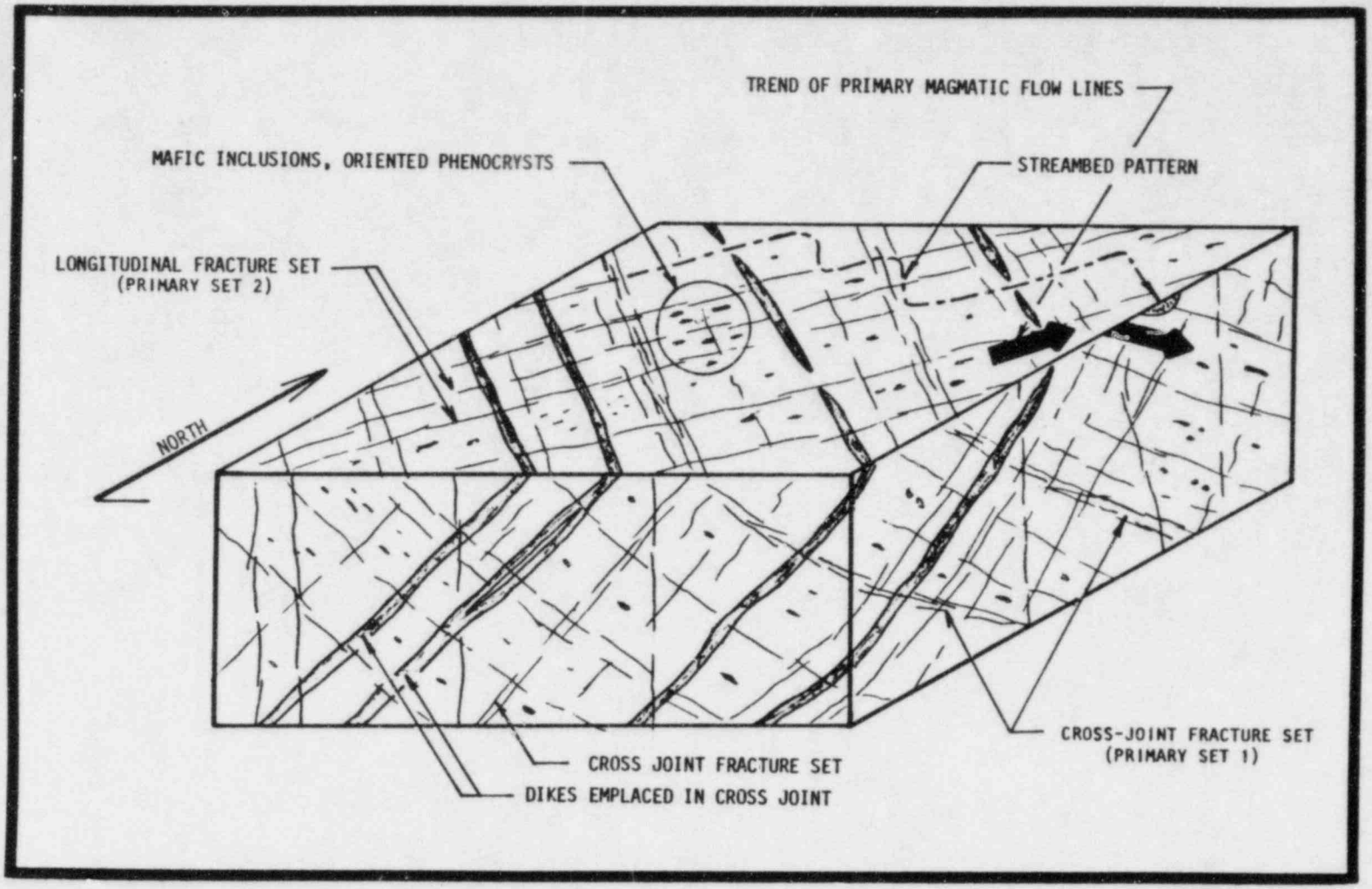

Figure 2.7. Schematic diagram of primary features.

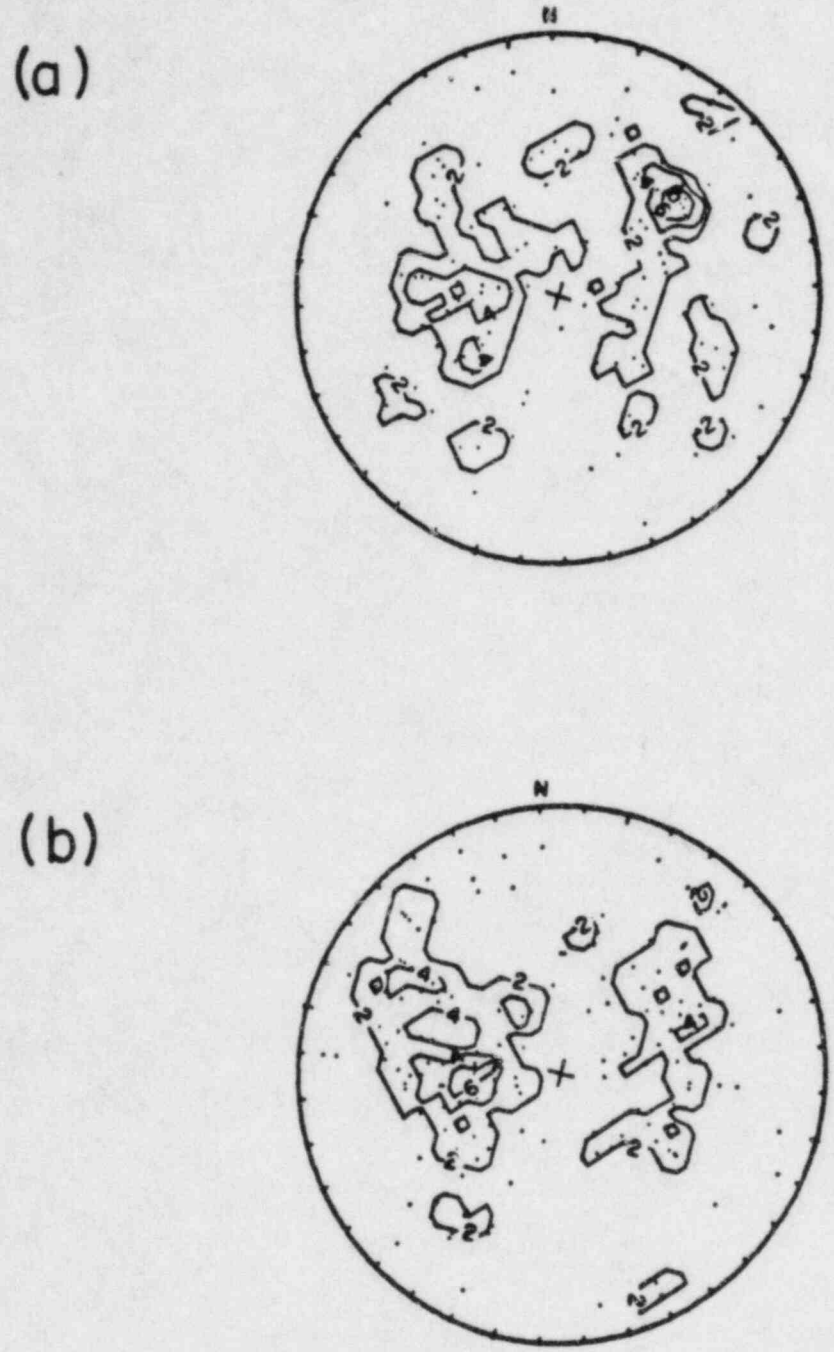

Figure 2.8. Stereonets showing fracture-plane normals in (a) borehole M1, and (b) borehole H2.

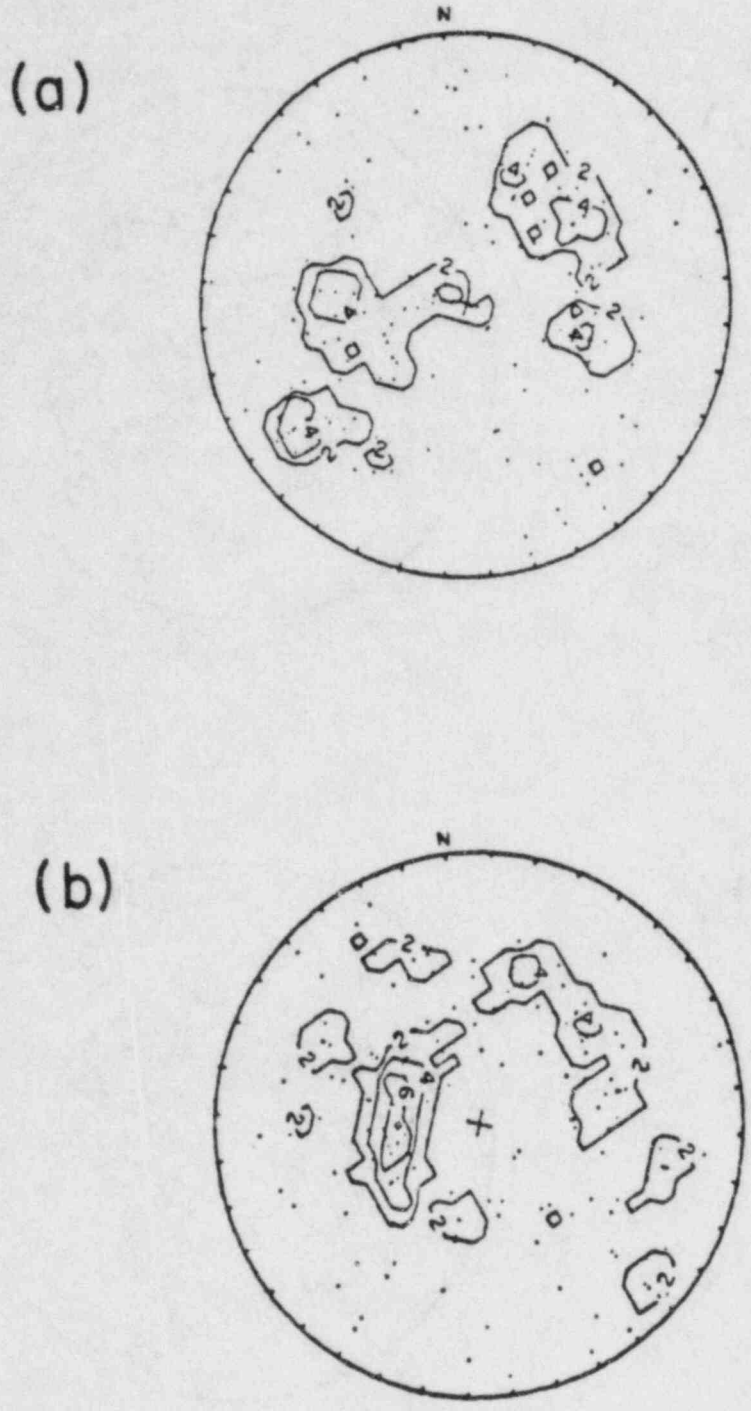

Figure 2.9. Stereonets showing fracture-plane normals in (a) borehole H3, and (b) borehole H4.

2.8, and 2.9, and, in part, on the spacing characteristics discussed in a following section. In addition to the cross joints and the two additional primary sets, Figure 2.10 depicts two sets that are conjugate (mutually orthogonal) labeled A and B, and another near-horizontal set between them. Sets A and B strike NNE. However, their orientation is not consistent with the conjugate fractures of Balk's (1937) classification, so we consider them to be of secondary origin.

The large scatter of orientations about the central tendency of each fracture set in Figure 2.10 could be due, in part, to the curved or irregular nature of many fracture surfaces, as well as to sampling errors. The absolute and relative sizes of the samples used to define each set, with the central tendencies determined for each set from surface and subsurface data, are listed in Table 2.2. Note that the definition of the three primary-fracture sets is more reliable than that of the three secondary sets, because the former definition is based on the majority of both surface and subsurface orientation data.

While most pegmatite and aplite dikes in Figure 2.4 are primary features associated with cross joints, some other dikes in the area may be of secondary origin. In particular, the large north-trending dike of fine-grained diabase on the west side of the figure appears to be part of a regional diabase system (see Figure 2.1) formed about 1,100 MY ago, after the emplacement of the Oracle granite. Another westerly-dipping dike of similar composition, which may belong to the same system, was identified in boreholes H3, H4, H7, and H8. The orientation of that dike most probably was controlled by the primary cross-joint set. A few exposures of rhyolite and quartz dikes also exist at the site, which may be secondary in origin. In a few instances, these dikes follow the trend of the primary longitudinal fracture set.

The orientation of slickensides observed in some of the core obtained from borehole H4 is shown in Figure 2.11. These marks have been preserved only in tight fractures that have not been exposed to weathering and alteration. They indicate the most recent direction of motion that has taken place in these fractures. As seen in Figure 2.11, most striations on the slickensides are oriented in a broad northwesterly direction. Some are parallel to the cross joints and associated dikes, (which is consistent with findings of others; e.g., Balk, 1937). Striations on slickensides point to the southwest and may be related to motion similar to that along the San Manuel fault.

Another indication of movement along fracture planes is the presence of chlorite, a mineral that can form as a result of localized forces involved in faulting. Fractures containing more than 25% chlorite by volume (as determined in the core from borehole H4) are plotted on the stereonet of Figure 2.12. A cluster of poles occurring in the SW quadrant of the stereonet sheet represent low-angle NE-dipping fractures. These fractures are subparallel to the major fracture (fault) zone of unusually high hydraulic conductivity found in the boreholes at depths exceeding 200 feet. Perpendicular to this set of fractures are other chlorite-filled fractures, whose normals roughly define a great circle on the stereonet. If the major fracture zone is indeed a fault, then the fractures represented by the points along the great circle are likely related to it, being antithetic faults with minor displacements. The set of fractures in Figure 2.12 are believed related to regional Miocene normal faulting.

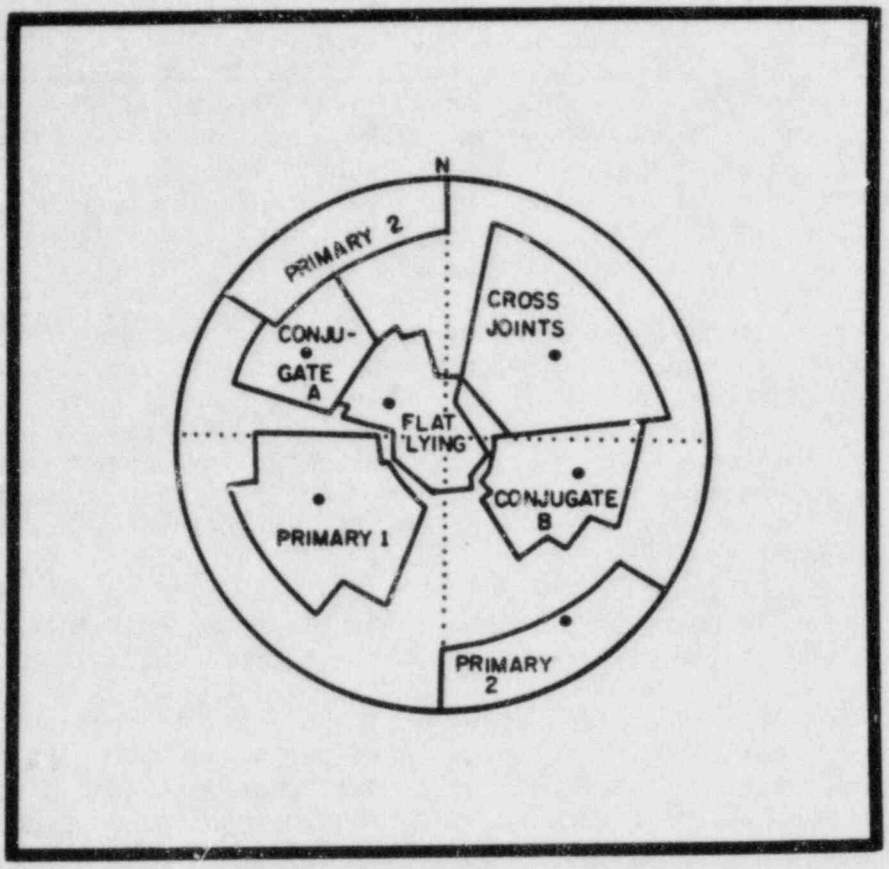

Figure 2.10. Stereonet showing areal distribution of fracture sets.

Table 2.2 Fracture Set Sample Sizes and Central Tendencies

FRACTURE SET	SUBSURFACE CENTRAL TENDENCY (STRIKE/DIP)	MAJOR FRACTURES (PERCENT)	SURFACE CENTRAL TENDENCY (STRIKE/DIP)	PERCENT OF TOTAL FRACTURES
Cross Joints	320/45W	19.5	327/41W	25
Primary 1	338/44E	29.4	338.48E	15
Primary 2	057/80NWW	4.5	070/88NW	38
Flat lying	040/21E	8.9	*	
Conjugate A	035/54E	7.0	020/70E	8
Conjugate B	018/41W	10.9	*	
TOTAL PERCENT		80.2		76
TOTAL FRACTURES		678		134

*Insufficient Data

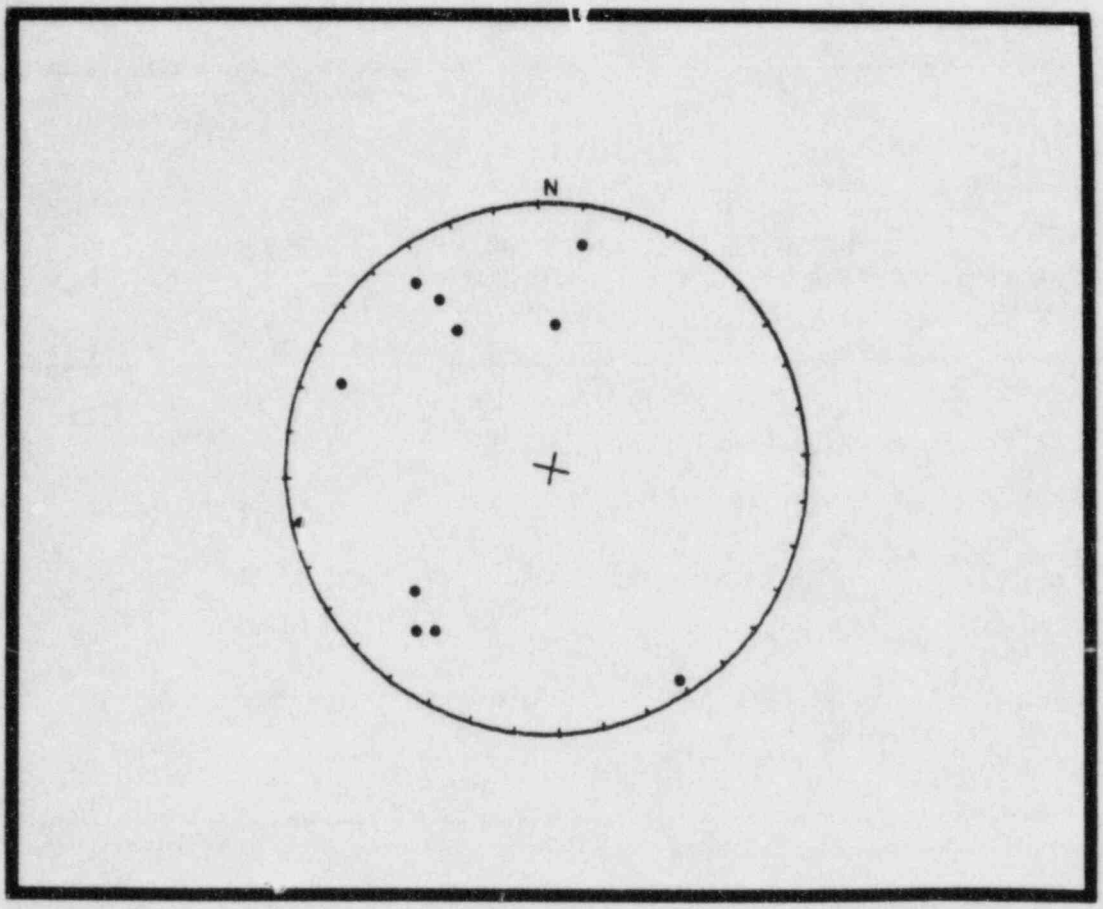

Figure 2.11. Stereonet showing linear directions of movement along fracture surfaces.

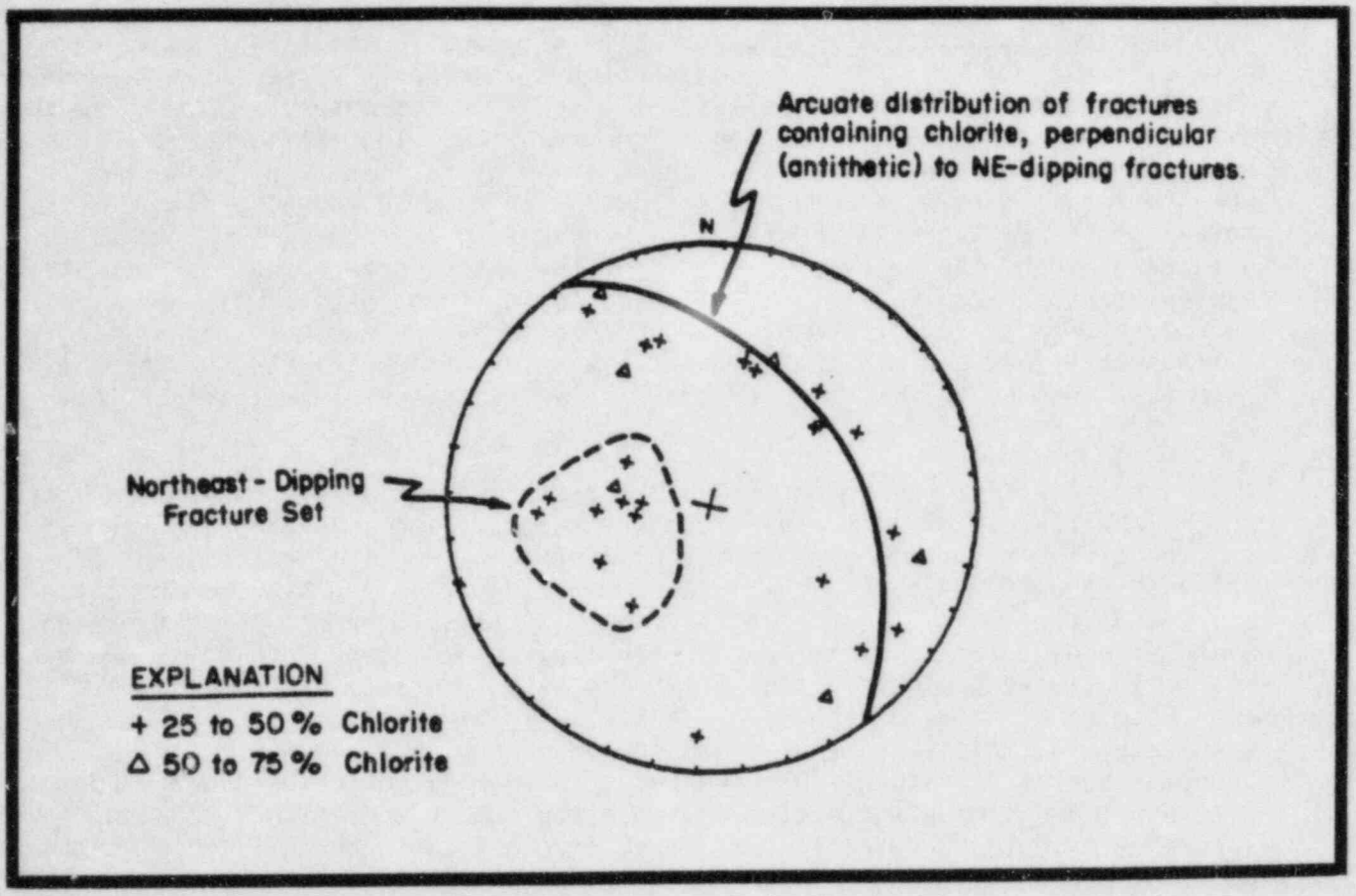

Figure 2.12. Stereonet showing fractures that contain chlorite.

3. SPATIAL-FRACTURE DISTRIBUTION

Having classified the fractures at the Oracle study site into distinguishable sets, we are now ready to investigate the frequency and pattern of their distribution in space. Since surface exposures are poor because of deep weathering, this analysis is based exclusively on subsurface data obtained from boreholes M1, H2, H3, and H4. As mentioned earlier, fracture geometry data were obtained from the interpretation of acoustic-televiewer logs for boreholes M1, H2, H3, and H4 in conjunction with cores obtained from M1 and H4. The total length of the televiewer logs is approximately 910 feet. Some difficulties in the interpretation of the televiewer logs stem from the fact that, in zones of high fracture frequency such as faults, some resolution has been lost due to reduced acoustic reflection in altered rocks, and to hole-diameter variations. Furthermore, cores show fractures which had not been recorded by the televiewer. Most of these fractures appear to have very narrow apertures and fresh surfaces which could indicate that they were induced by stress relief and agitation during drilling and core recovery. The televiewer has been demonstrated to have sufficient sensitivity to detect all permeable or open fractures in crystalline rocks down to 1 mm (Davison, et al., 1982).

According to Priest and Hudson (1976), the spacing between fractures tends to follow one of the following four modes of spatial distribution: (1) Even spacing giving rise to a peaked histogram of the kind illustrated schematically in Figure 3.1 (part 3); (2) random spacing, with a histogram showing a sharp peak near zero (Figure 3.1, part 5); (3) clustering occurring near contacts with dikes or in fault zones, resulting in a histogram to which one can fit a negative-exponential, probability-density function (Figure 3.1, part 4); and (4) a combination of these, as indicated in Figure 3.1 (part 6). In the last case, (4), clustered and random spacings combine to form a relatively steep histogram near the origin, whereas the combination of even and random spacings may cause an inflection in the histogram at some higher spacing value. When data representing different fracture sets are analyzed simultaneously, the result tends to be a negative-exponential histogram typical of a random distribution. For a random distribution, the mean and standard deviation of the values of the distances between fractures should equal the inverse of the number of fractures per unit length.

When all televiewer data from boreholes M1, H2, H3, and H4 are treated as belonging to one population, the resulting histogram of fracture spacings resembles a negative exponential (Figure 3.2). If we fit the probability density function

$$f(x) = \lambda e^{-\lambda x}, \quad x > 0 \qquad (3\text{-}1)$$
$$= 0, \quad x \leq 0$$

to this histogram, where x is spacing; f(x) is fracture frequency in the interval (x, x+dx); and λ is mean number of fractures per unit length of sample line, we find that the inverse of the density, $1/\lambda$, equals 1.34 feet. The mean spacing equals 1.38 feet, with a standard deviation of 1.63 feet. Equation (3-1) can also be tested by examining the variance of the density of the fractures; in this case fracture is defined as the number of observed fractures per 10-foot interval along the borehole. If the fractures are statistically

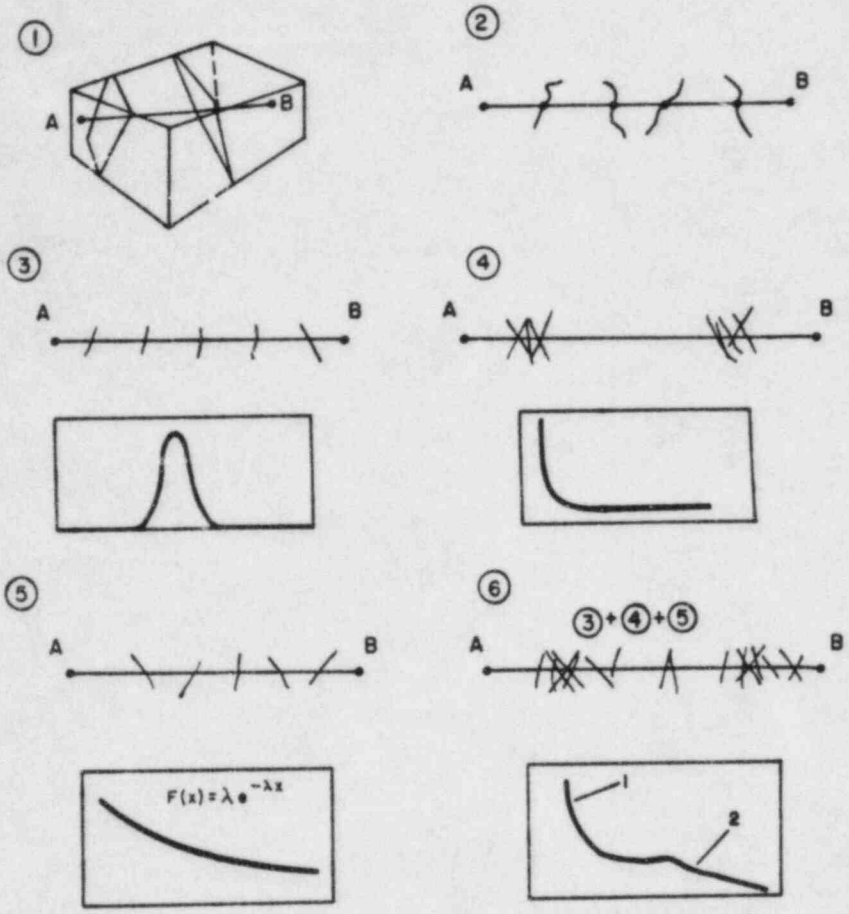

(1) Discontinuity intersection points along a straight line (AB) through the rock mass.

(2) Scanline along exposed surface or borehole. Spacing values are given as the distance between the scanline and its intersection with a fracture.

(3) Fairly evenly spaced distribution.

(4) Clustered distribution.

(5) Random distribution.
NOTE:
$F(x) = \lambda e^{-\lambda x}$ negative exponential

(6) Combination of distributions.
NOTE: [1]Clustered and random distributions mutually reinforce at narrow spacings.

[2]Evenly spaced and random distributions mutually interfere at wide spacings.

Figure 3.1. Examples of fracture spacing histograms (modified from Priest and Hudson, 1976).

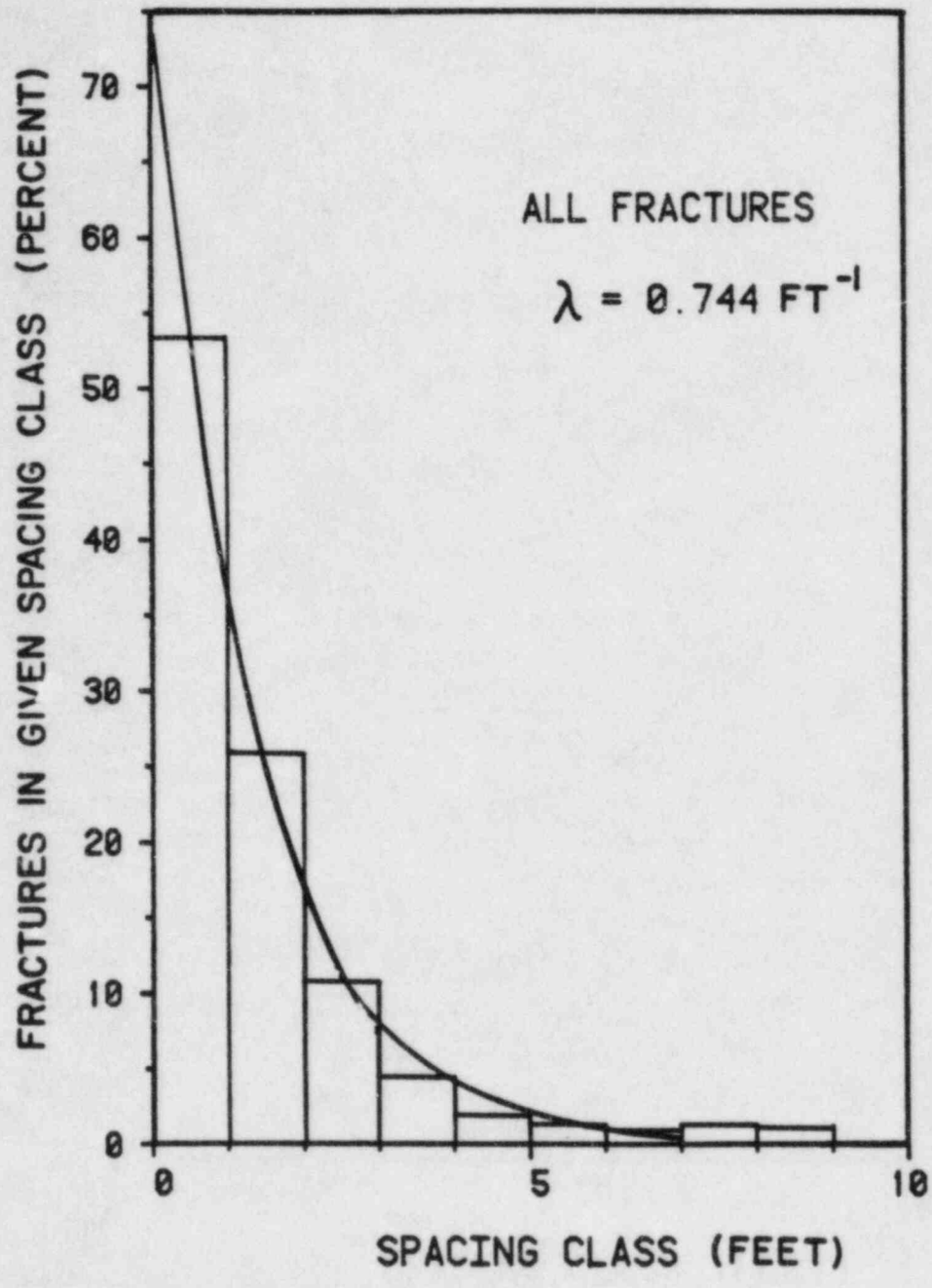

Figure 3.2. Histogram of fracture spacings for all data.

random, fracture densities can be described by a Poisson distribution, where the mean will equal the variance. The mean number of fractures per 10-foot interval is 6.7, with a variance of 12.0. This test indicates that the Poisson distribution of fracture density (and, hence the negative-exponential distribution of fracture spacing) may not be an adequate description of fracturing at the site.

A better approach to the analysis of fracture-spacing distribution is to sample separately each individual fracture set along a line parallel to its central tendency (Figure 2.10). Results of such sampling for the cross joints and primary set 1 are shown in Figure 3.3; results for the flat-lying set and conjugate sets A and B are shown in Figure 3.4. The length of each scanline, number of samples, and λ value fitted to each histogram are listed in Table 3.1. The cross joints and primary set 1 fit negative-exponential distributions with $\lambda = 0.209$ ft^{-1} and $\lambda = 0.304$ ft^{-1}, respectively (Figure 3.3). Other researchers (e.g., Snow, 1970; Hudson and Priest, 1979) also found that fracture spacings tend to follow a negative-exponential distribution. Primary set 1 shows a strong clustering effect (Figure 3.3); many of these fractures are concentrated near a fault. Primary set 2 consists of steeply dipping fractures that are undersampled in the near-vertical boreholes; therefore, its spacing cannot be analyzed statistically. The flat-lying set is relatively sparse and clustered; its histogram is poorly fitted with a negative exponential, having a λ value of 0.070 ft^{-1} (Figure 3.4). Histograms of conjugate sets A and B are similar; they show inflections typical of evenly spaced fractures superimposed on fractures with a random spacing (Figure 3.4). Both of these functions are characterized by $\lambda \simeq 0.1$ ft^{-1}; $1/\lambda \simeq 10$ ft; and by some degree of clustering. Although the spacing of fractures involves a strong random element, many fracture sets are also characterized by systematic tendencies either to be evenly spaced or to cluster in narrow zones. Where clustering occurs, the properties of the rock often change sufficiently to appear as strong anomalies on certain geophysical logs and usually to produce high permeabilities. This tendency, with core and acoustic-televiewer data, makes it possible to correlate such zones between boreholes. Our attempts to correlate individual fractures between boreholes have been much less successful because of possible curvature of fracture surfaces, spatial variations in the aperture of a given fracture, nonuniform mineralogy, lack of fracture continuity between boreholes, and sampling errors.

Our attempts at cross-hole correlation of fractures are summarized in Figures 3.5 and 3.6. Figure 3.5 shows the angles (apparent dips) at which mappable fractures intersect the vertical plane formed by boreholes M1 and H2-H4. While the apparent dips appear to be quite chaotic, nevertheless they can be used in conjunction with other data (such as selected geophysical logs or hydraulic conductivities measured by Hsieh et al., 1983) to delineate the trace produced on this plane by some key features. The usefulness of geophysical logs for fracture correlation is evident from the example in Figure 3.6, representing a part of borehole H4 below the diabase dike. Besides the acoustic televiewer that provides a visual record of fractures intersecting the borehole, fracture identification also can be performed by other logs including single-point resistance, acoustic velocity, neutron, and natural gamma. The single-point resistance tool is similar in response to the 16-inch normal resistivity probe (not available for boreholes M1 and H2-H4) and provides a fairly detailed record of fracture zones. The acoustic-velocity probe is

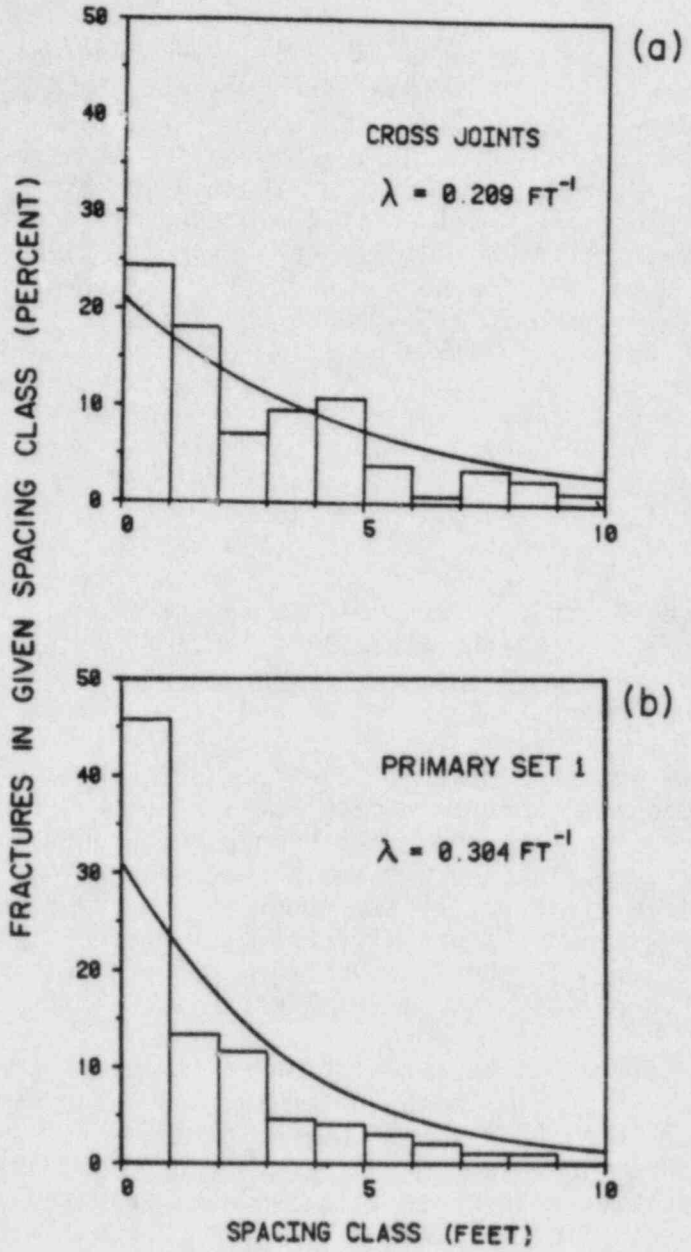

Figure 3.3. Histogram of fracture spacings for (a) cross joints, and (b) primary set 1.

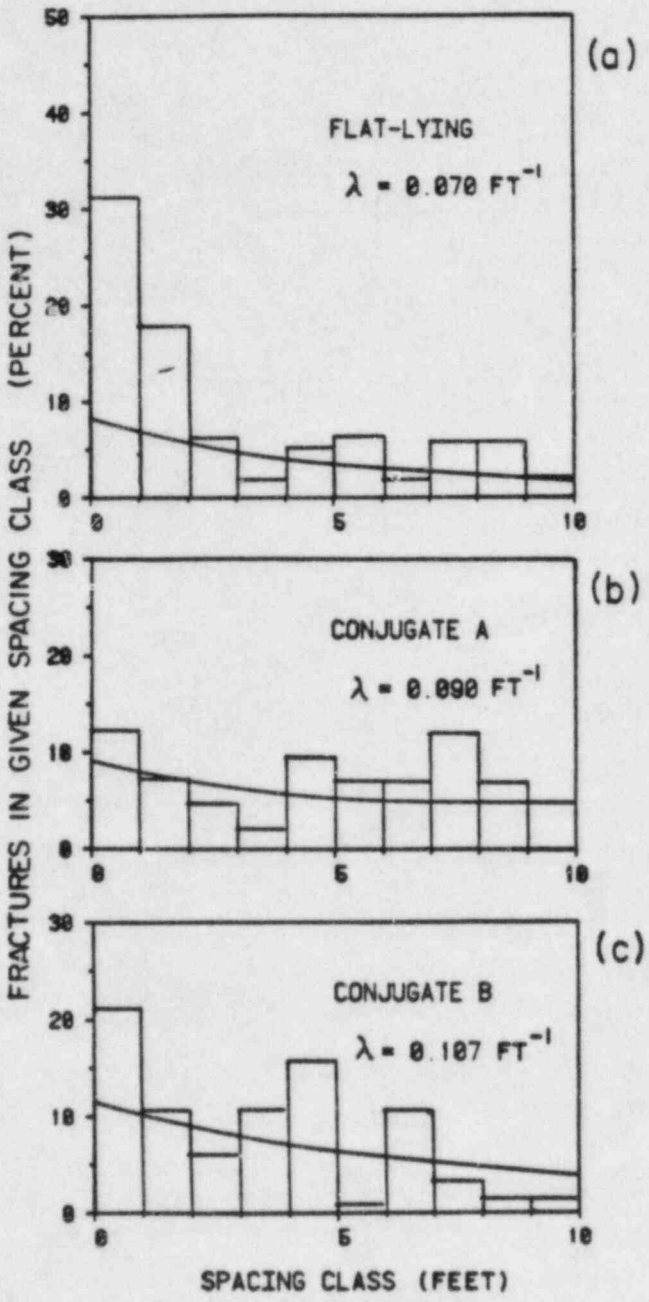

Figure 3.4. Histogram of fracture spacings for (a) flat-lying set; (b) conjugate set A; and (c) conjugate set B.

Table 3.1 Spatial Frequency Analysis

FRACTURE SET	LENGTH OF SCANLINE[a] (FEET)	NUMBER OF SAMPLES	λ (FEET^{-1})
All data	911	678	.744
Cross joints	632	132	.209
Primary set 1	655	199	.304
Primary set 2	158	31	.196
Low dip	850	60	.071
Conjugate set A	535	48	.090
Conjugate set B	687	74	.108

a. Scanline for fracture sets is the length along the central tendency of a fracture set sampled sampled by the borings.

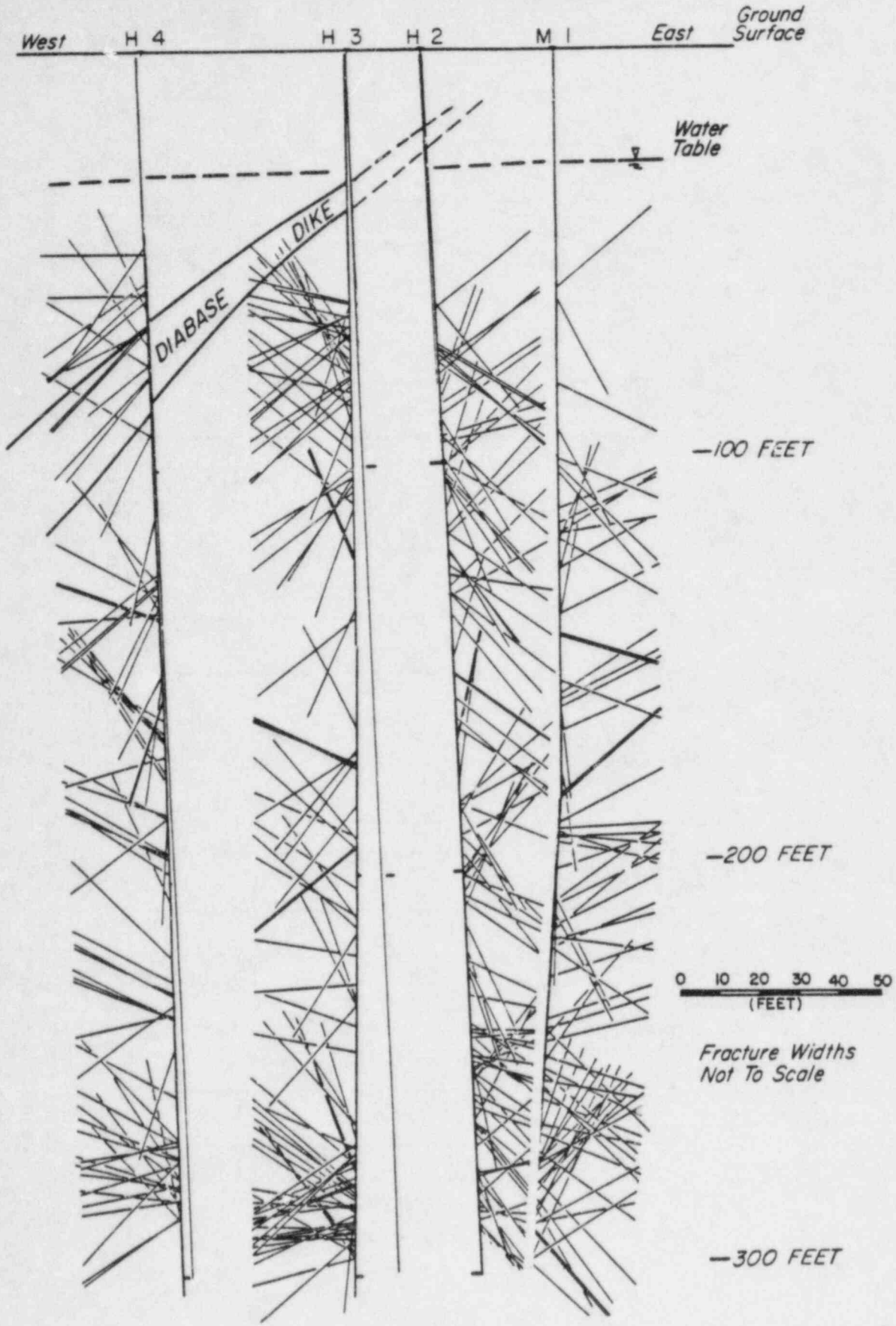

Figure 3.5. Cross section of apparent dips of fractures identified by acoustic televiewer, boreholes H4, H3, H2, and M1.

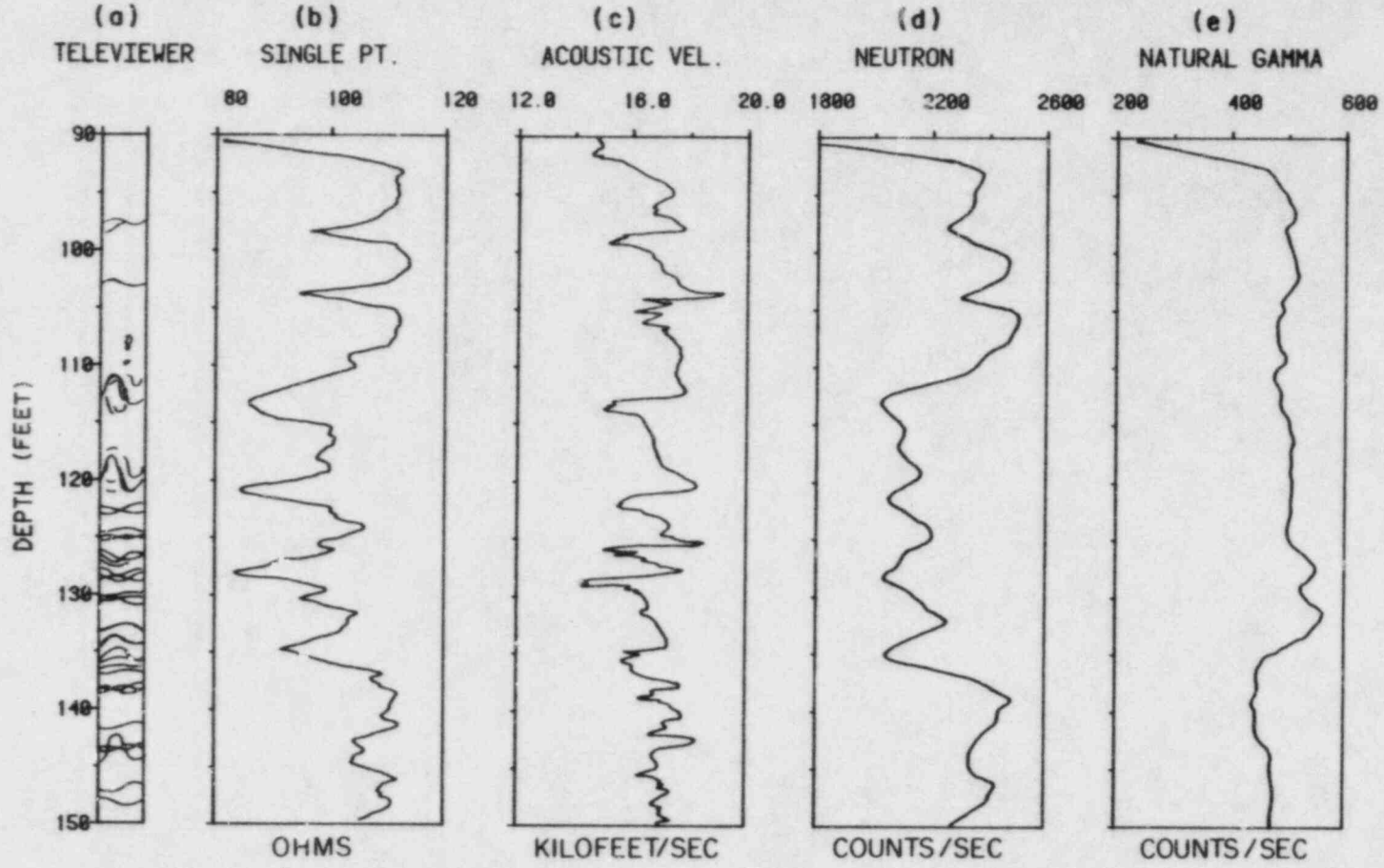

Figure 3.6. Relationship between fractures appearing on (a) acoustic televiewer; (b) single-point resistance; (c) acoustic velocity; (d) neutron-; and (e) gamma-geophysical records, in portion of borehole H4.

sensitive to irregularities in the borehole wall caused by fractures. Its response usually is distinct in densely fractured intervals; otherwise, it is somewhat erratic. Cycle skipping is a typical response of the acoustic-velocity log to discontinuities in the borehole wall, but it cannot be related quantitatively to fracture aperture. Neutron and gamma tools have relatively minimal resolution, because they represent rock properties integrated over a radius of 10 to 30 inches around the probe. Many other geophysical instruments and techniques are available that have not been utilized in this study. The interested reader may wish to consult Keys and MacCary (1971), Nelson and Glenn (1975), Nelson et al. (1979), and Davison et al. (1982).

Results of our correlation effort are depicted in Figure 3.7, which is a tentative, "eye-ball" analysis. Its construction is based upon interpretation of geophysical logs, acoustic-televiewer records, and core and chip samples. Uncorrected neutron logs are included because of their coordination with permeable zones. Indicated also are zones of measurable permeability, as well as the diabase dike mentioned earlier, which is easily traced between holes H3 and H4 (note the strong neutron signal in H4). Whereas most diabase-dike exposures appear to be densely fractured, diabase cores from borehole H4 show a lesser degree of fracturing. Many preexisting fractures in the dike appear to have been "healed" by calcite deposition. Calcite also has been deposited in fractures immediately below the dike, which causes the permeability of this zone to be relatively low. Clustering of subparallel fractures about the diabase dike is clearly discernible in Figure 3.7.

The correlations shown in Figure 3.7 are incomplete; yet, they proved valuable in designing cross-hole hydraulic tests (Hsieh et al., 1983) and tracer tests at the study site. In the future, we expect to compare these correlations with results obtained from such tests. For the present, the cross section suggests that the rock at the site is intersected by fractures in many different directions; these fractures should impart a considerable degree of nonuniformity and anisotropy to local hydraulic properties.

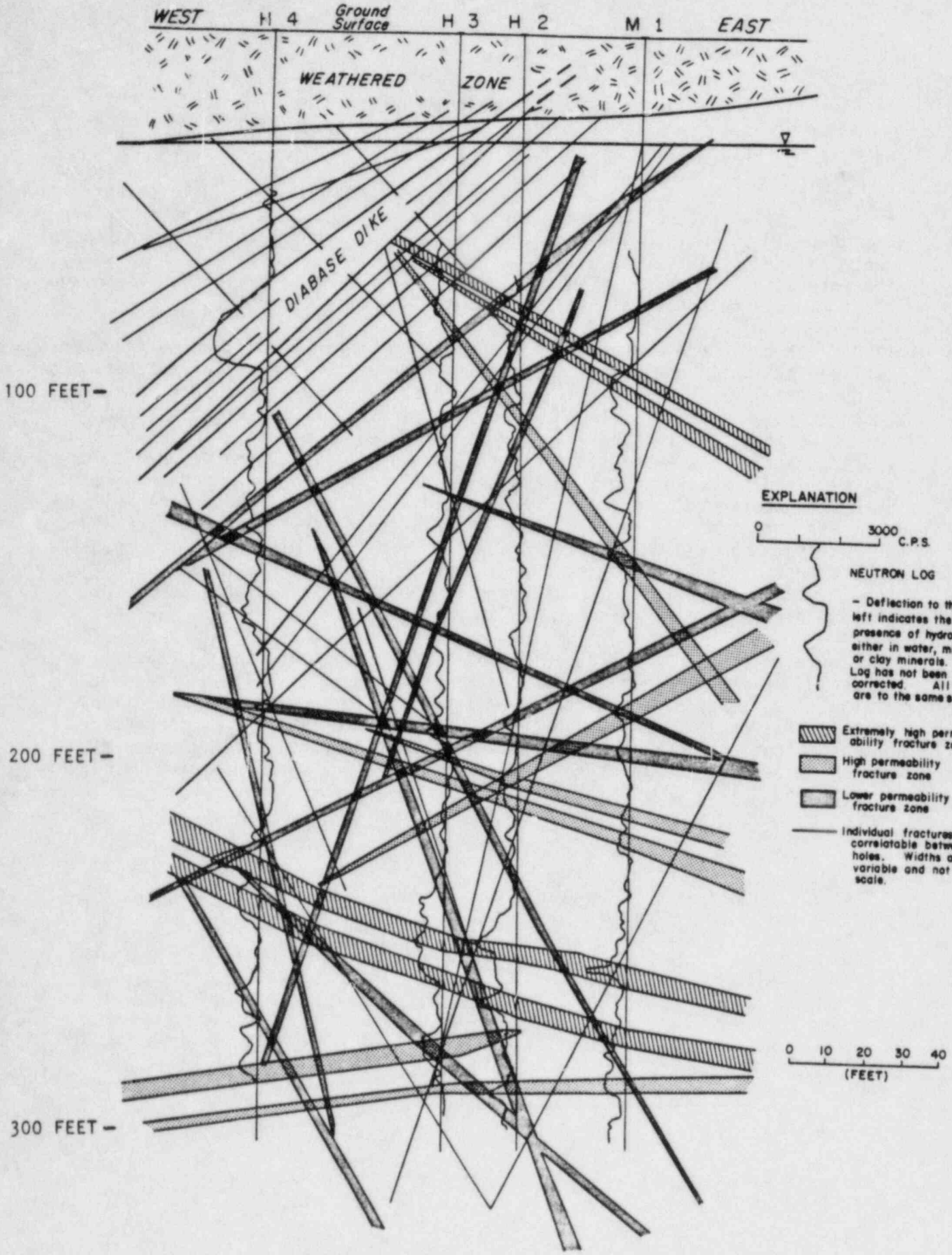

Figure 3.7. West-east cross section showing inferred interconnections of fracture zones in boreholes H4, H3, H2, and M1.

4. RELATIONSHIPS OF FRACTURE GEOMETRY AND GEOPHYSICAL LOGS TO HYDRAULIC PROPERTIES

In this chapter, we investigate the extent to which fracture geometry and the response of selected geophysical logs can be used to estimate hydraulic properties of the rock such as conductivity and porosity. The information available about fracture geometry has been discussed in the preceding chapter. Geophysical data to be considered include data from gamma, neutron, and acoustic-velocity logs. Electrical-resistivity logs are not available for boreholes M1 and H4 and are not evaluated in this report.

4.1 Effects of Fracture Density on Hydraulic Conductivity

In the past, several theoretical models have been postulated that relate the hydraulic conductivity and porosity of a fractured rock mass to various geometric parameters of the fractures, such as orientation, spacing or density, aperture, roughness, and size (Romm and Pozinenko, 1963; Snow, 1965; Wilson and Witherspoon, 1970; Long et al., 1982). Data from the study site are not sufficient to test any of these theories because of the lack of reliable, independent information about fracture apertures and roughness, and the availability of only limited information about fracture size. These fractures may have variable apertures, curved surfaces, and irregularly shaped boundaries, factors that are disregarded in most existing theoretical models. Despite shortcomings of the data base and the available models, we can test one particular hypothesis that is common to all discrete fracture models--that hydraulic conductivity increases with fracture density (i.e., decreases as fracture spacing increases).

To test this hypothesis, we used information of the kind shown in Figure 4.1. On the right side of this figure, we plotted the variation of hydraulic conductivity with depth as reported for borehole H2 by Hsieh et al. (1983), based on pressure-injection tests between two packers spaced 13 feet apart. On the left side, the figure displays the number of fractures identified within each interval between the packers. These fractures have varying orientations, as shown in the middle diagram of Figure 4.1. The bottom scale indicates apparent dip in the vertical plane of boreholes M1, H2, H3, and H4; the contours mark the percent of fractures plotting within 1% of the rectangular display area (i.e., percent per 1-percent area). Thus, horizontal fractures having zero apparent dip plot along the center of the diagram, whereas easterly-dipping fractures plot to the right of the center and westerly dipping fractures plot to the left. For example, point A represents a cluster of fractures at a depth of 170 feet, having an apparent dip of 15° due east and a density of more than 3 percent per 1-percent area. The extent to which a set of (apparently) parallel fractures persists with depth can be established by noting the rate at which the densities of fractures with a given apparent dip vary along the borehole.

Based on core and acoustic-televiewer data, it is possible to divide the fractures into rough classes such as open (X), partly open (A), possibly open (B), and closed (C), as explained in Appendix A. By plotting the number of fractures per packed-off interval versus the logarithm of hydraulic conductivity for boreholes M1, H2, H3, and H4, we obtain the scatter diagram in Figure 4.2.

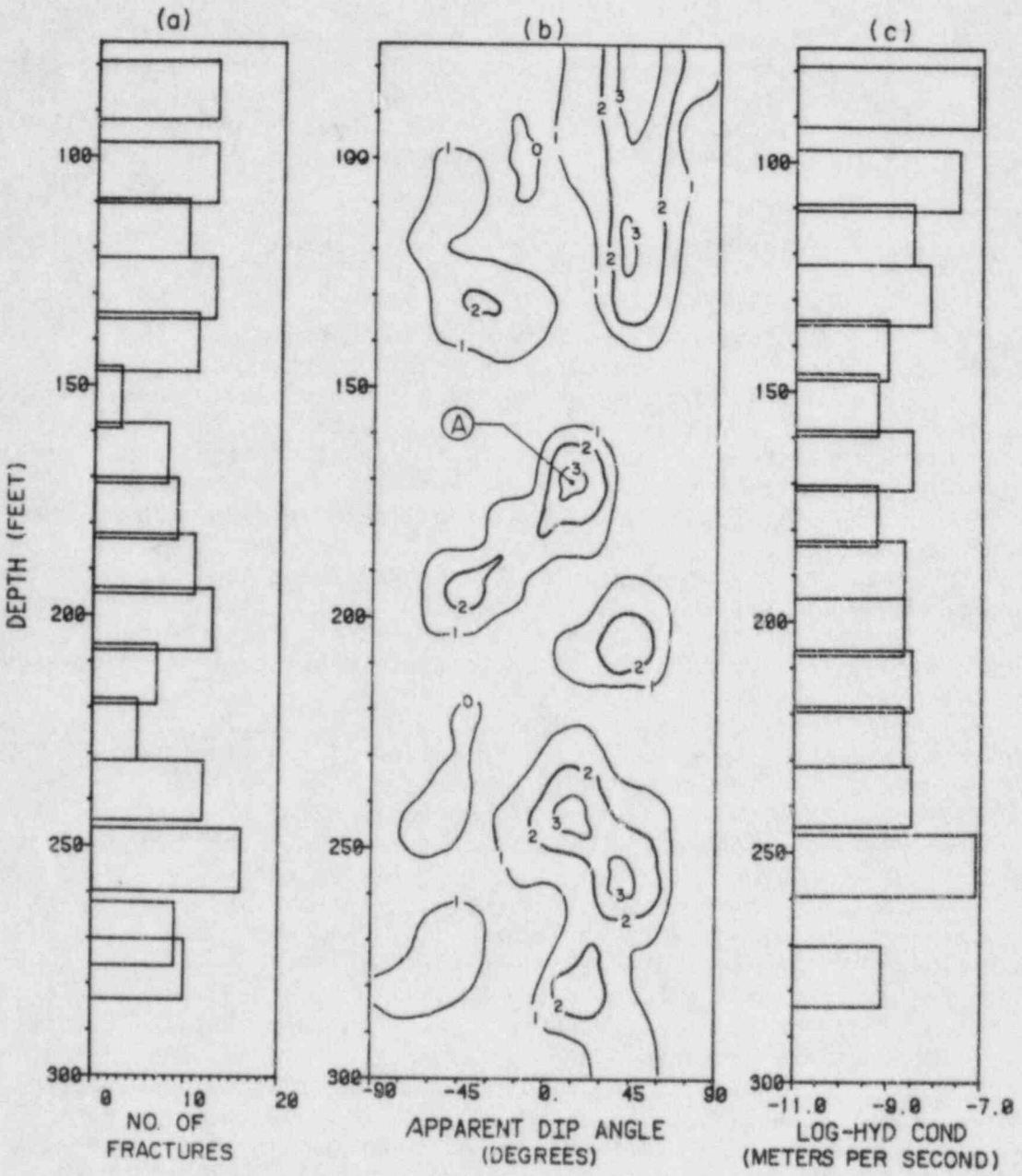

Figure 4.1. Comparison of (a) fracture density; (b) fracture orientation; and (c) measured hydraulic conductivity as a function of depth in borehole H2. Contours indicate percent of fractures plotting in 1% of rectangular display area. See text for explanation of point A.

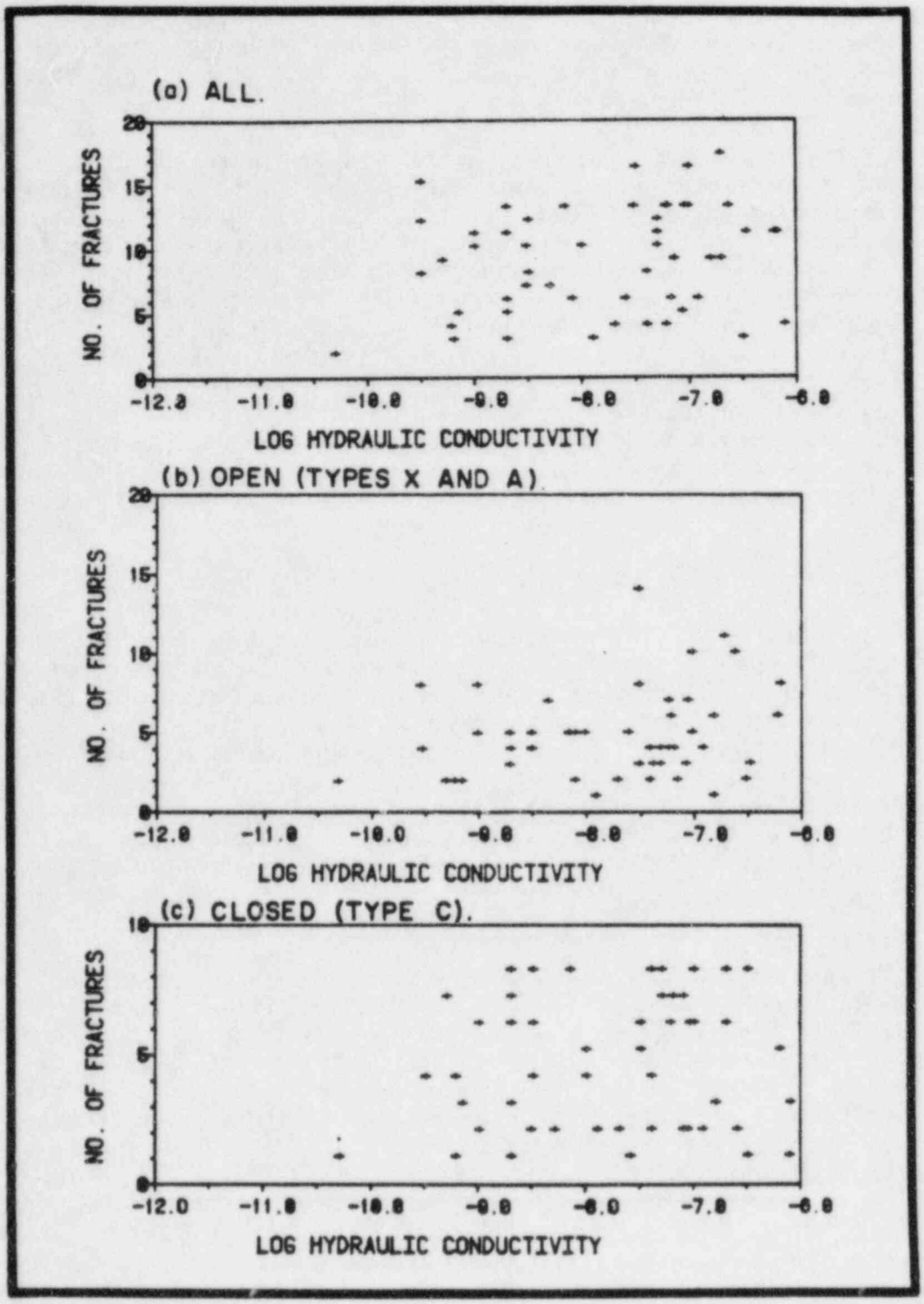

Figure 4.2. Fracture density versus measured log-hydraulic conductivity for (a) all; (b) open (types X and A); and (c) closed (type C) fractures, in boreholes M1, H2, H3, and H4.

(Some of the log-hydraulic conductivity data are over-estimated because of problems of leakage past the packers; however, we believe these errors are not large enough to invalidate our method of analysis or our conclusions. See Appendix C for a listing of such errors).

It is clear from Figure 4.2 that, no matter what class of fractures is considered, the correlation between fracture density and log-hydraulic conductivity is surprisingly weak. Our analysis further suggests that fracture orientation has little apparent influence on this relationship (or lack of it). This raises a serious question about the validity of existing conceptual models of fluid flow and contaminant transport through networks of discrete fractures when these models are applied to rocks, such as the Oracle granite. An alternative model based on a continuum concept, coupled with the geostatistical analysis of hydrologic test data, will be proposed in Chapter 5. Similar investigations carried out in Canadian Shield crystalline rock also showed little relationship between fracture density and hydraulic conductivity due to the fact that discrete fractures provided most of the fluid flow (Davison, et al., 1982; Keys, 1984).

4.2 Interpretation of Geophysical Logs

Our objectives in the interpretation of geophysical logs at the Oracle site are: (1) To evaluate geophysical responses to lithologic variations as determined from core samples, and (2) to determine the relationship between these responses and hydraulic parameters, such as porosity measured in the laboratory and hydraulic parameters from packer tests. Geophysical logs long have been used in oil-field exploration to identify lithologic and hydraulic properties of sedimentary rocks, but their application to fractured crystalline rocks has been relatively limited. Recent applications of borehole geophysics to crystalline rocks have been reported by Keys (1979), Keys and Sullivan (1979), Davison et al. (1982), and Nelson et al. (1979).

It will be recalled from Chapter 2 that the geological history of the Oracle granite was dominated by three major events: (1) Emplacement and cooling of the plutonic mass, resulting in the formation of primary magmatic flow structures, fractures, and dikes; (2) intrusion of diabase dikes, accompanied by hydrothermal alteration of granite close to the intrusions; and (3) thermotectonic middle-Miocene activity producing low-angle lystric normal faulting, and another phase of widespread hydrothermal alteration. Hydrothermal alteration of granite typically is accompanied by the redistribution of elements such as potassium; by the alteration of feldspars to sericite, kaolinite, or zeolites; and by the alteration of muscovite and biotite to chlorite. Further alterations may later take place along fracture planes due to weathering processes or further tectonic activity. Many of the resulting chemical and physical changes have an effect on the response of borehole-geophysical logs. Four such geophysical logs are briefly discussed below.

4.2.1 Gamma Log

The gamma log used in this study measures the total gamma radiation produced by naturally occurring radioactive isotopes. Among the principal sources of

such radiation in granite are potassium-40 and the daughter products of uranium and thorium.

As of April 1983, gamma logs were available at the study site for boreholes M1, H2, H3, H4, and H7. The gamma logs for M1, H1, H2, and H3 were corrected for borehole-diameter effects (to a nominal 8-inch diameter, according to chart Por-7 in Schlumberger, 1979); they are reproduced in Figure 4.3. Superimposed on this figure are the diabase dike and fault zone as established by a combination of data. One of the most striking features is the large decrease in gamma activity in the diabase dike in borehole H4, which is typical of basic rocks. A gamma peak occurs at the top of the fault zones in borehole H2 at a depth of approximately 245 feet; this might be the result of enrichment in uranium as noted for shallow fracture zones in other granitic environments by Keys and Sullivan (1979), Nelson et al. (1979), and Davison et al. (1982).

Redistribution of uranium daughter products is controlled by oxidation potential of groundwater, since the radioactive elements normally are soluble under oxidizing conditions. Substantial enrichment or depletion of uranium may indicate groundwater flow in the zone of oxidation. Another source of increased gamma intensity in such zones may be due to potassium-40 in clay minerals. Hydrothermal alteration, commonly indicated by potassium redistribution, is marked in the zone beneath the diabase dike in borehole H4 by an increase in the gamma-log response between the depths of 90 and 130 ft. (Keys, 1979).

Interestingly, the fault zone in Figure 4.3 is characterized by a decreased gamma intensity, and may in fact be correlated between the boreholes on this basis. Little low radioactivity along large segments of this highly permeable fault zone (see Hsieh et al., 1983, as well as Chapter 5) may result from the solution and migration of radioisotopes in circulating meteoric groundwater. Gamma logs are useful for the delineation of lithologic variations (as diabase versus granite) and major fracture zones that affect site hydrology. However, no known method exists to obtain quantitative hydrologic information from these logs in crystalline rock.

4.2.2 Neutron Log

The neutron probe consists of an isotopic source of fast neutrons and an epithermal-neutron detector separated by a distance of about 15 inches or more. High-energy rapidly moving neutrons are emitted from the source, and are slowed and ultimately captured when they encounter hydrogen, chlorine, or other elements that have a large effective-neutron cross section. Because the detector is relatively far from the source, the neutron flux decreases as the quantity of hydrogen near the probe increases. In sections of a borehole with little porosity, neutron density typically is high, because neutrons can travel further toward the detector before they are captured. The log responds inversely to the concentration of hydrogen; changes in this response can be attributed to spatial variations in porosity if most of the hydrogen is present in free water.

In Oracle granite, chlorine does not appear to be important in neutron-log response. On the other hand, hydrogen is present not only in the water that

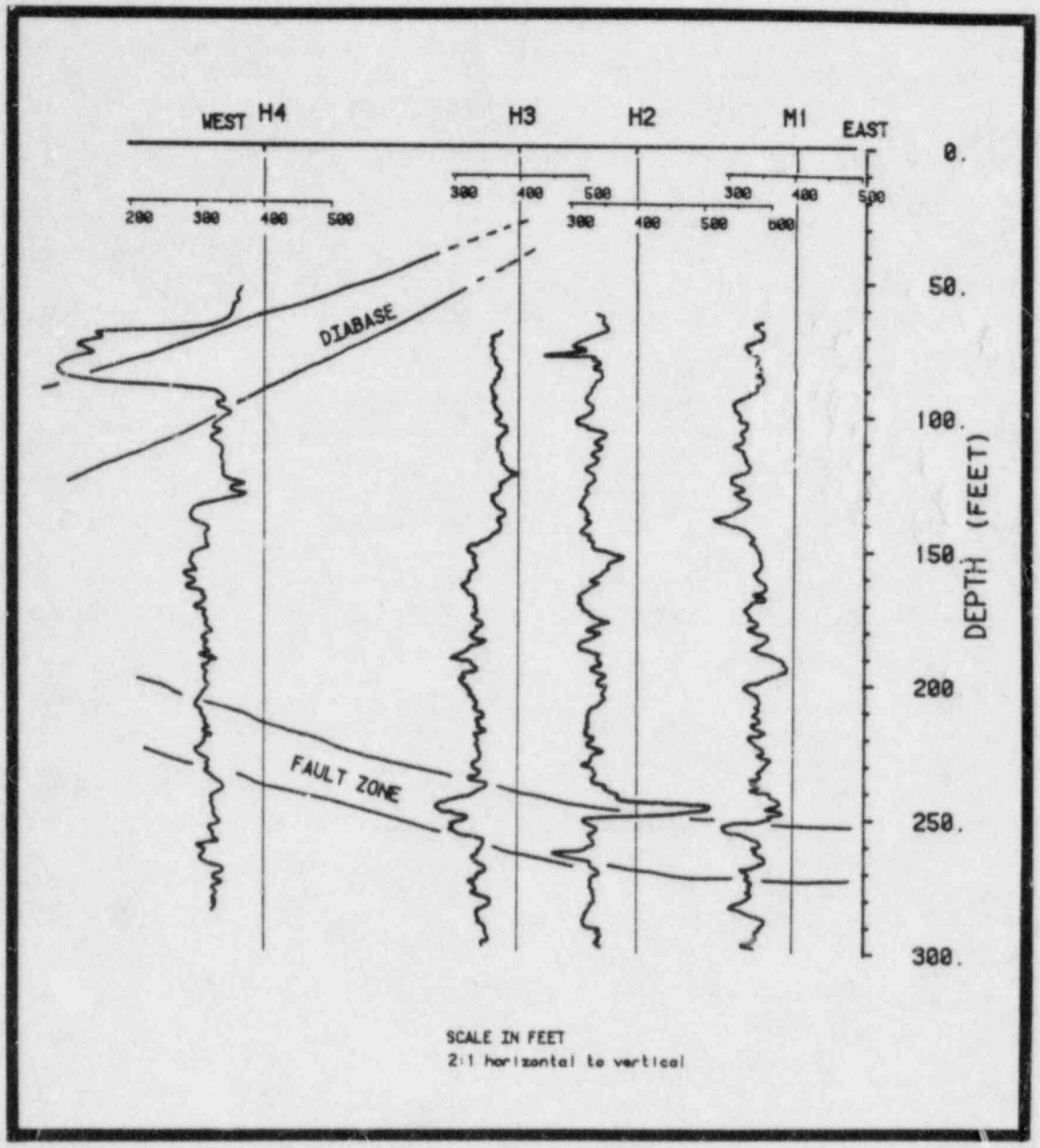

Figure 4.3. Gamma logs in boreholes H4, H3, H2 and M1.

occupies pores and fractures, but also in micas, clays, and other minerals. Hydrothermal alteration and weathering produces minerals with increased amounts of hydrogen. Thus, the neutron-log response reflects the combined effects of primary porosity from pores and microcracks, secondary porosity from fractures, and the presence of hydrous minerals.

In a study of andesite and latite rock by Nelson and Glenn (1975), the amount of bound water in the rock was measured and compared with the neutron-log response. They found that bound water ranged from one to four percent by weight. A similar study by Alexander et al. (1981) also indicated that bound water in other granitic rock can be a few percent, and that total porosity of the rock generally is of the same order of magnitude as bound water. In both cases, when the contribution of bound water was determined, the neutron log appeared to be capable of resolving porosity changes of one percent at low porosity.

To assess the effect of hydrous minerals on neutron-log response at the study site, and to determine primary porosity of the granite, the porosity of 18 core samples from borehole H4 was measured in the laboratory. These samples were taken from depth zones below the alteration halo of the diabase dike where there were no visible fractures. After measuring bulk density of each sample, the rock was crushed, and the density of its grains was determined on the basis of pycnometer measurements, using kerosene.

Each sample (approximately 10 inches of the core) was considered representative of the unfractured interval. The neutron-log response over unfractured zones generally was smooth, so that a single value of the log response could be found for each interval and, thus, each sample. All neutron-log values were corrected for the lag or difference between the position of the neutron probe and the reading indicated on the log (i.e., lag = time constant of the logging device multiplied by the rate of logging). After this correction was applied, a value of the neutron-log response for each interval could be compared to measured core porosity. The relationship between resulting porosities and the corresponding log responses are shown in Figure 4.4. One reason for the apparent lack of correlation between the neutron-log response and core porosities may stem from differences in measurement scale: Rock volume sampled by the log is much larger than laboratory samples. Another reason may be the effect of hydrous minerals illustrated in the experiments of Nelson and Glenn (1975). In any event, the large scatter of points in Figure 4.4 casts doubt about the direct applicability of core data to the calibration of in situ, neutron-log measurements in the altered rock at the study site.

Large volumes of rock with known porosity are required to calibrate neutron logging equipment. This is the standard approach used in oil-field applications; igneous rock pits have recently become available at the Denver Federal Center, Colorado.

Neutron logs for boreholes M1 and H2-H4 are shown in Figure 3.6. We mentioned earlier in Chapter 3 that these logs were the most helpful geophysical tools to correlate fractures between the four boreholes. Since porosity variations are much smaller than spatial variations in hydraulic conductivity, and since the neutron-log provides a fairly large volume of investigation in low-porosity rock, we suspected the possibility that small-scale variations in

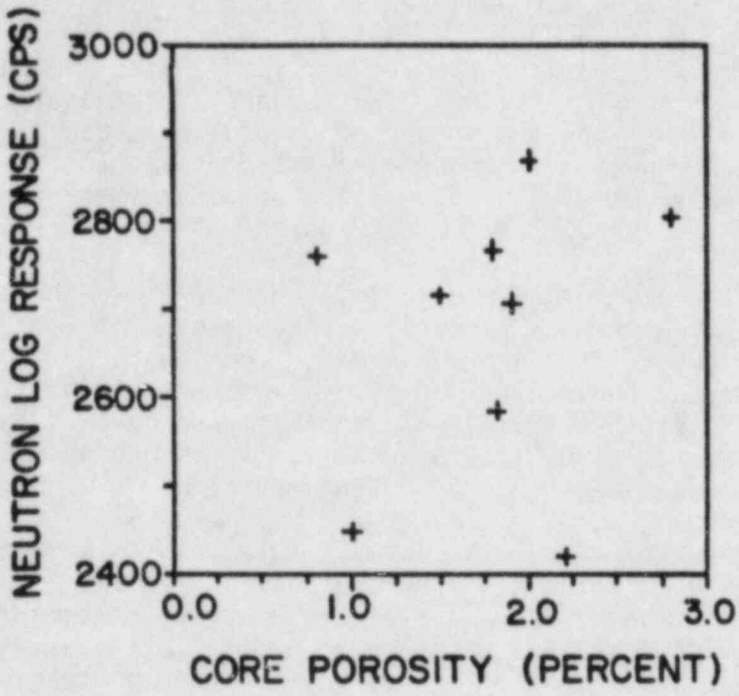

Figure 4.4. Measured core porosity versus neutron-log response in unfractured sections of borehole H4.

porosity might average out, so that the neutron-log data could be compared to measured hydraulic conductivity. In Figure 4.5, inverted neutron-log response in each borehole (actual response subtracted from an arbitrary reference value to facilitate numerical integration) is plotted, versus the logarithm of the hydraulic conductivity, as obtained from packer tests. (As mentioned previously, page 42, some of the hydraulic-conductivity data are overestimated because of leakage past the packers.) To achieve consistency in scale, the neutron records were integrated over 13-foot intervals, coinciding with intervals packed-off during the hydraulic tests. Because neutron-log response varies with hole diameter and porosity in a highly nonlinear fashion (e.g., chart Por-9a, Schlumberger, 1978), the data were separated into three groups according to the nominal diameter of each hole. To further avoid anomalies resulting from the presence of hydrous minerals in the large-scale zones of strong hydrothermal alteration and weathering, data from such zones were excluded from Figure 4.5.

Data in Figure 4.5 point to the existence of a linear relationship between inverted-integral, neutron-log response and log-hydraulic conductivity, over at least two orders of magnitude of hydraulic-conductivity variation. A similar relationship was noted by Schimschal (1981) in carbonate rocks. Interestingly, all three straight lines fitted to the data by least squares in Figure 4.5 have similar slopes. This similarity suggests that there may be an advantage in using one standard nominal borehole diameter in all crystalline rock investigations, to achieve a better definition of the relationship between neutron logs and hydraulic conductivity at a given site, and to enable transferring experimental results from one site to another. (Field standards in logging trucks may be used to standardize the response of various neutron probes.) This similarity also suggests that a correlation between total porosity of the rock and measured hydraulic conductivity exists, because the neutron log responds to total porosity (a large part of which is fracture porosity) and to hydrous minerals, because of alteration along fractures. However, the relation between neutron-log response and hydraulic conductivity may be only a local phenomenon, and is not appropriate for use in a predictive sense.

4.2.3 Acoustic-Velocity Log

The acoustic-velocity log provides a continuous record of compressional-wave velocity measured parallel to the borehole. The receiver spacing and thus the sample interval is typically one foot in length. The acoustic velocity can be expressed as a function of elastic properties and bulk density according to Dobrin, 1976:

$$V_p = \frac{[\ K + 4\mu/3\ ]^{1/2}}{\rho} \quad , \qquad (4\text{-}1)$$

where V_p = acoustic velocity $[LT^{-1}]$;

K = bulk modulus of elasticity $[FL^{-2}]$;

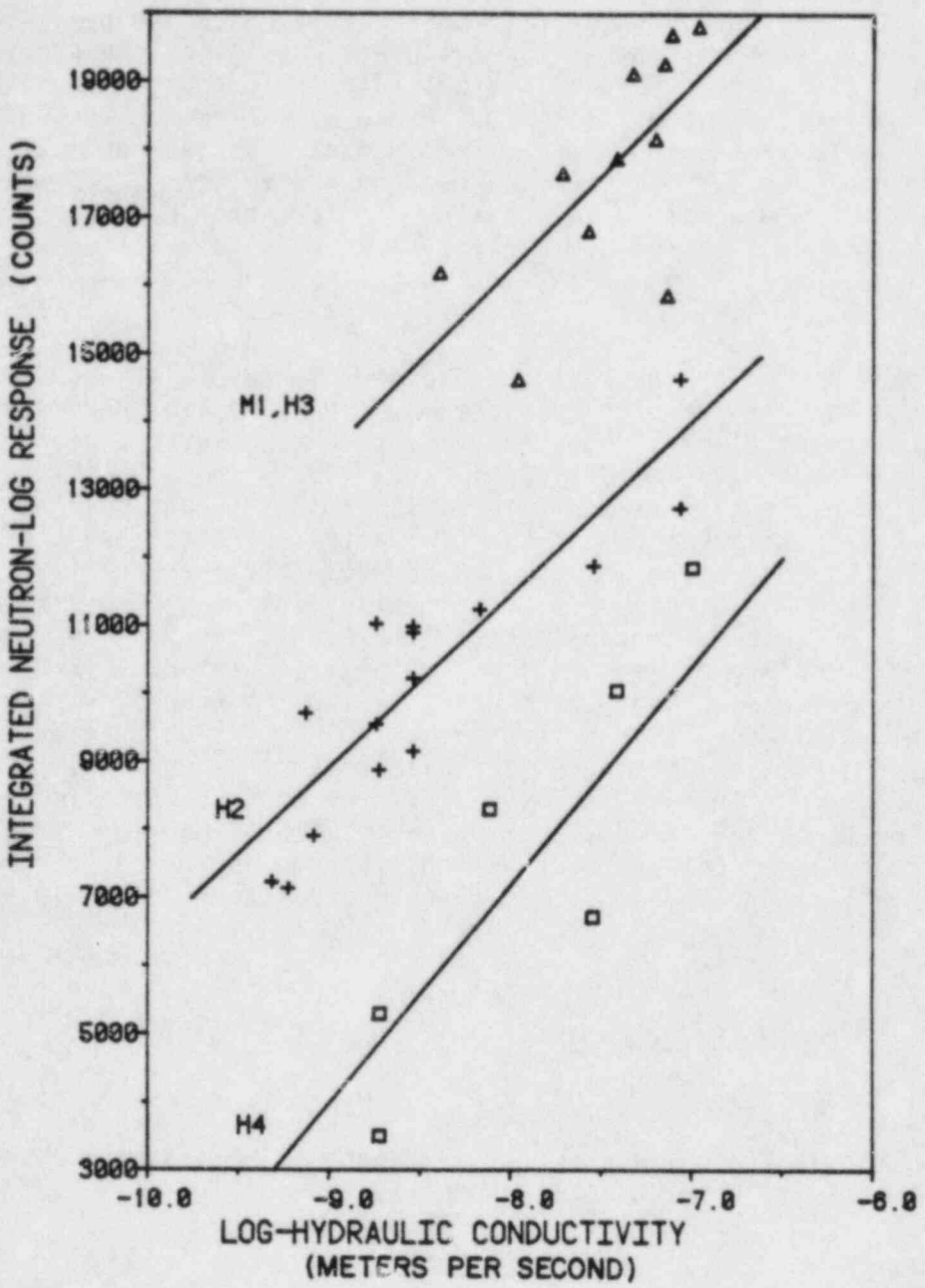

Figure 4.5. Neutron-log response versus log-hydraulic conductivity for straddle-packer intervals of boreholes M1, H2, H3, and H4.

μ = shear modulus of elasticity [FL^{-2}]; and

ρ = bulk density [ML^{-3}].

In oil-field technology, the acoustic log is used to obtain estimates of formation porosity by the following formula (Wyllie et al., 1952; Schlumberger, 1978):

$$\phi_a = \frac{t_{log} - t_{ma}}{t_{fl} - t_{ma}} \times 100, \qquad (4\text{-}2)$$

where ϕ_a = porosity in percent;

t_{log} = measured interval-transit time [TL^{-1}];

t_{ma} = interval-transit time in rock matrix [TL^{-1}]; and

t_{fl} = interval-transit time in fluid, equal to 189 s/ft.

In sedimentary-rock applications, compressional-wave velocity of the rock matrix generally is known, and calculation of porosity is straightforward. Fracture porosity usually is not considered included in the porosity inferred from the acoustic-velocity log. However, much less is known about the effects of fracture aperture, density, and orientation upon compressional-wave velocities in crystalline rock (Paillet, 1980). Generally, as observed at the study site, velocity increases with depth due to the effect of increasing lithostatic pressure. This pressure closes or decreases the width of many fractures and elastic moduli increase (Simmons, et al., 1975). Weathering of the rock also decreases with depth. Variations from this general trend with depth indicate changes in lithology and porosity. A cross section through the plane of boreholes M1 and H2-H4 that shows the velocity logs of these holes is shown in Figure 4.6. Lines of equal compressional-wave velocity are superimposed on the plot in zones of competent rock, where no macrofracturing is evident. The rock is hydrothermally altered and the velocity is slower around the diabase dike. The velocity log appears to be useful in the qualitative interpretation of rock characteristics. Major fracture and fault zones also can be discerned on the acoustic logs.

To test the applicability of Equation (4-2) to the Oracle granite, we plotted (Figure 4.7) the porosity from this equation against porosity determined from core samples in the laboratory (refer to Section 4.2.2). At contact with the diabase (depth of 91 feet) porosity is maximum; bulk density is decreased; and grain density increases by 0.1 g/cm^3 in the altered zone. Porosity value calculated from the acoustic log can be compared to measured core porosity. Under the assumption that acoustic velocity in water is constant, a value for matrix velocity is determined by a linear approximation to the trend of measured velocity with depth, as indicated in Figure 4.8. The line was determined under the assumption that Equation (4.2) is valid for core porosity values obtained from depths greater than 200 feet. Figure 4.7 shows that

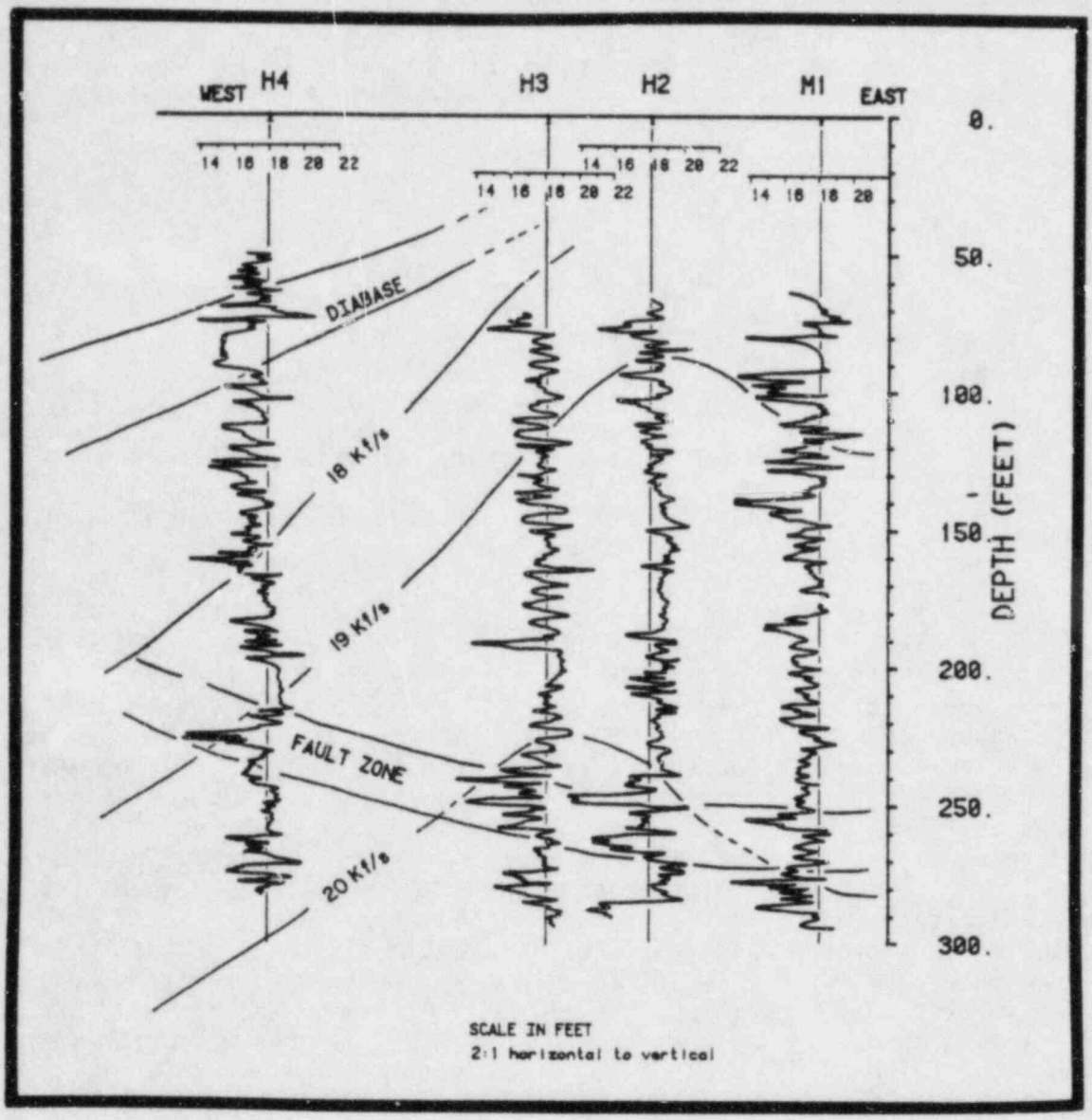

Figure 4.6. Interval acoustic-velocity data for a cross section defined by boreholes H4, H3, H2, and M1. Log scales are in kilofeet per second. Contours relate to acoustic velocity of unfractured rock only. Cycle skips are not shown.

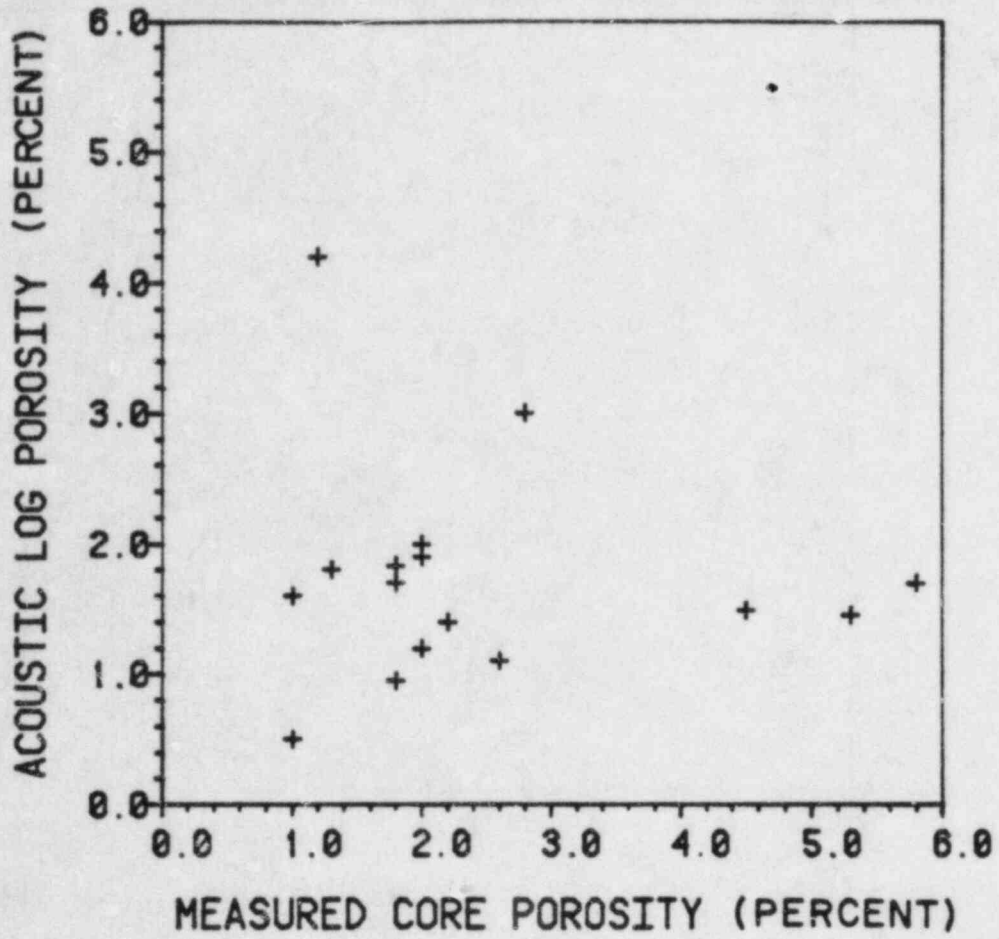

Figure 4.7. Comparison of measured core porosity and value of porosity calculated by the interval acoustic-velocity log, in borehole H4.

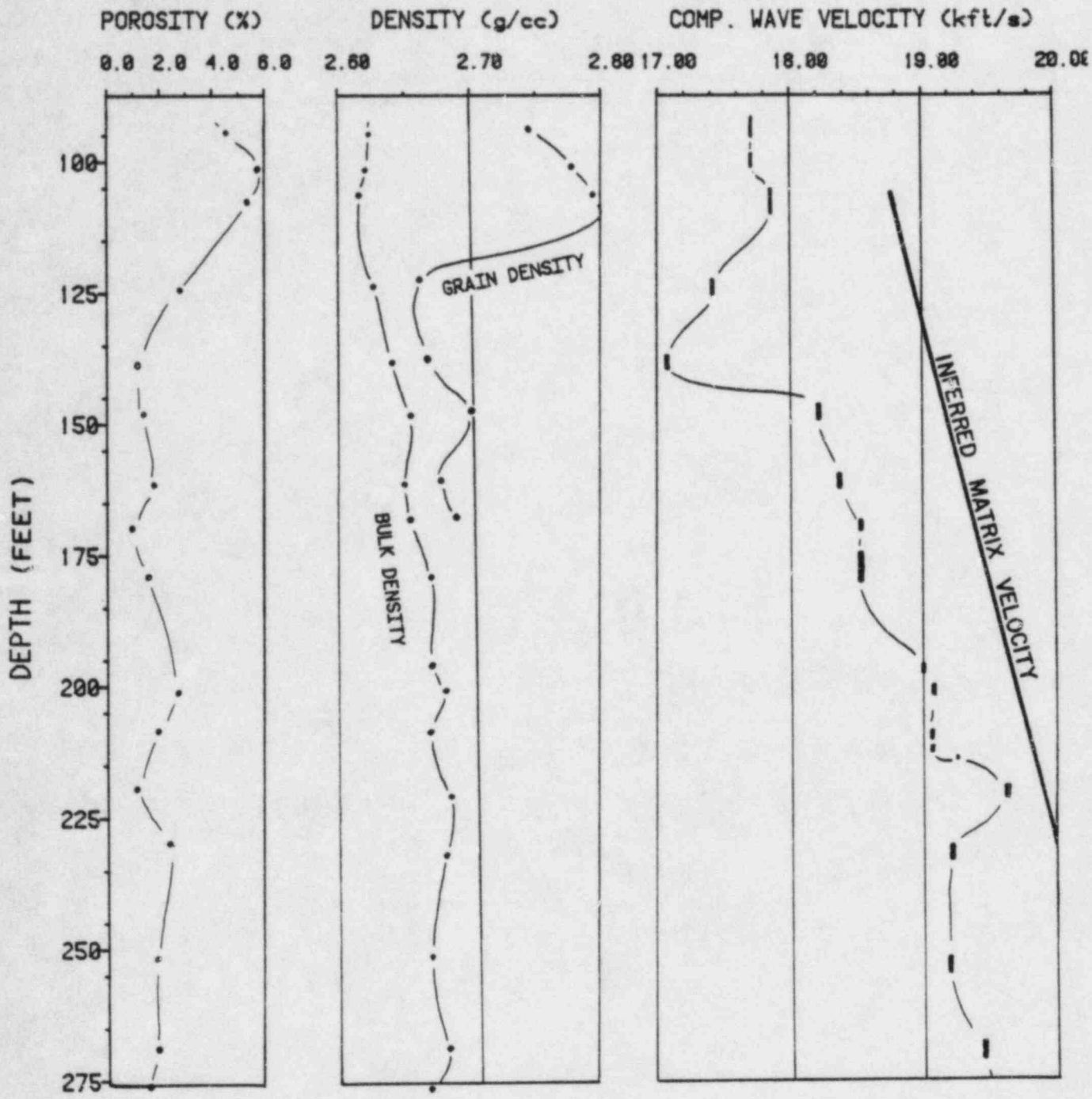

Figure 4.8. Comparison of measured core porosity, rock density, and interval-acoustic velocity for borehole H4.

Equation (4.2) does not provide an accurate expression for porosity at the study site. One possible reason is that rock heterogeneity causes the matrix velocity to vary. Vertical fractures in the vicinity of the borehole also may affect the refraction of the acoustic wave during logging and, hence, alter the apparent velocity. Therefore, the acoustic log is primarily useful for qualitative inferences about the rock mass.

5. GEOSTATISTICAL ANALYSIS OF SINGLE-HOLE, HYDRAULIC-CONDUCTIVITY DATA

Hydraulic conductivity is one of the most important parameters controlling subsurface radionuclide transport, and the rate at which water can flow through the rock. The ratio of hydraulic conductivity to effective porosity is directly proportional to flow velocity, and, thus, the rate of convective-radionuclide transport. The degree to which hydraulic conductivity varies locally within a given rock mass has a direct bearing on overall (effective) hydraulic conductivity of this mass; on directional dependence (anisotropy) of effective hydraulic conductivity; and on hydrodynamic dispersion (the spread of a radionuclide plume during transport). Therefore, it is of utmost importance to characterize the spatial variability of hydraulic conductivity.

The question of spatial variability in fractured rocks has been addressed in two different ways. One way has been to collect statistical information about fracture geometry (orientation, density, length, aperture width and roughness, interconnection, or other characteristics) and then translate this information into hydraulic conductivity by means of a mathematical model (Snow, 1965; Long et al., 1982). Another way is to work with hydraulic conductivity obtained by direct measurement in the field. We prefer the latter approach because: (1) In situ fracture geometry is difficult to ascertain; (2) available mathematical models for the computation of hydraulic conductivity from fracture geometry are of questionable validity (refer to Section 4.1); and (3) direct measurements of hydraulic conductivity can be performed by means of single-hole packer tests. These points are illustrated by the situation at the study site, where 102 single-hole, packer test data are available from seven boreholes. Despite a considerable effort to study fracture geometry at the site, we still know relatively little about the statistical distributions and correlations of such critical fracture characteristics as fracture shape, length, aperture, filling, roughness, and interconnectivity. Even if these characteristics were known, we would still face serious difficulties in translating them into hydraulic-conductivity values in three dimensions, because of both conceptual and computational limitations.

We will, therefore, devote the remainder of this chapter to a description of the spatial variability of single-hole, packer-test results from the study site. The method is applicable to any fractured (or porous) rock; it is not limited to the Oracle granite. The method is based on the premise that log-hydraulic conductivity determined in packer tests, or any other measurable aquifer properties, are random variables generated by a stochastic process in three-dimensional space. The same stochastic process could give rise to an infinite number of different, but equally likely, log-hydraulic conductivity distributions in the rock. This infinite set of equally likely log-hydraulic conductivity distributions is called an ensemble; thus, our measured values are merely one possible realization of this ensemble of possibilities. Another way to appreciate this concept is to view the actual rock mass in the field as one out of an infinity of different but equally likely rock masses, all of which have similar statistical properties.

We work with log-hydraulic conductivity instead of hydraulic conductivity because the former generally is distributed in a manner closer to normal than

the latter (see Appendix D). Hence, log-hydraulic conductivity gives rise to better-defined semivariograms than does hydraulic conductivity.

For simplicity, we assume that the underlying stochastic process is intrinsic. This implies that the ensemble mean does not vary from point to point, and that the spatial relationship among the values of log-hydraulic conductivity can be described by means of a semivariogram function, $\gamma(h)$, defined as

$$\gamma(\underline{h}) = \frac{1}{2} E \{[Y(\underline{x}) - Y(\underline{x} + \underline{h})]^2\}, \qquad (5\text{-}1)$$

where $\underline{x}$ = a position vector (x_1, x_2, x_3);

$Y(\underline{x})$ = log-hydraulic conductivity at point $\underline{x}$;

$\underline{h}$ = an arbitrary displacement vector; and

$E\{\}$ = the expectation symbol.

Just like the mean, the semivariogram is independent of the position vector, $\underline{x}$. In the particular case where $\gamma(\underline{x})$ depends only on the distance, $h = |\underline{h}|$, and not on the direction of the displacement, the semivariogram is said to be isotropic; otherwise, it is anisotropic.

Seven log-hydraulic-conductivity profiles for boreholes M1 and H2 through H7 as determined by constant injection, single-hole packer tests are shown in Figure 5.1. (Again, we mention that some values of hydraulic conductivity are overestimated because of leakage past the packers. See page 42.) Location of these eight boreholes is indicated in Figure 1.2. Distance between the packers in each test was 13 ft. When plotted on log-normal probability paper (Figure 5.2), packer-test results are seen to deviate only slightly from a straight line. This straight line represents a normal distribution of log-hydraulic conductivity (log-normal distribution of hydraulic conductivity), with mean $\mu = 8.04$ and variance $\sigma^2 = 0.83$. More is said about the probability distribution of these data in Appendix D. The degree of spatial correlation between these random variables then is examined by establishing the underlying semivariogram, by discretizing Equation (5.1) in the manner described by Journel and Huijbregts (1978). In the one-dimensional case, where all data plot on a line, the line is subdivided into equal intervals called "distance classes."

All data values plotting within a given distance class are averaged to provide a single representative value for the midpoint of the interval. The distance between two contiguous midpoints is termed lag 1; twice that distance is termed lag 2, etc. The first point of the semivariograms, $\gamma(h)$, corresponding to an h of lag 1, is obtained by averaging the squares of the differences between all pairs of contiguous midpoint values. The second point, corresponding to an h of lag 2, is obtained by averaging the squares of the differences between all pairs of midpoint values separated by two interval lengths.

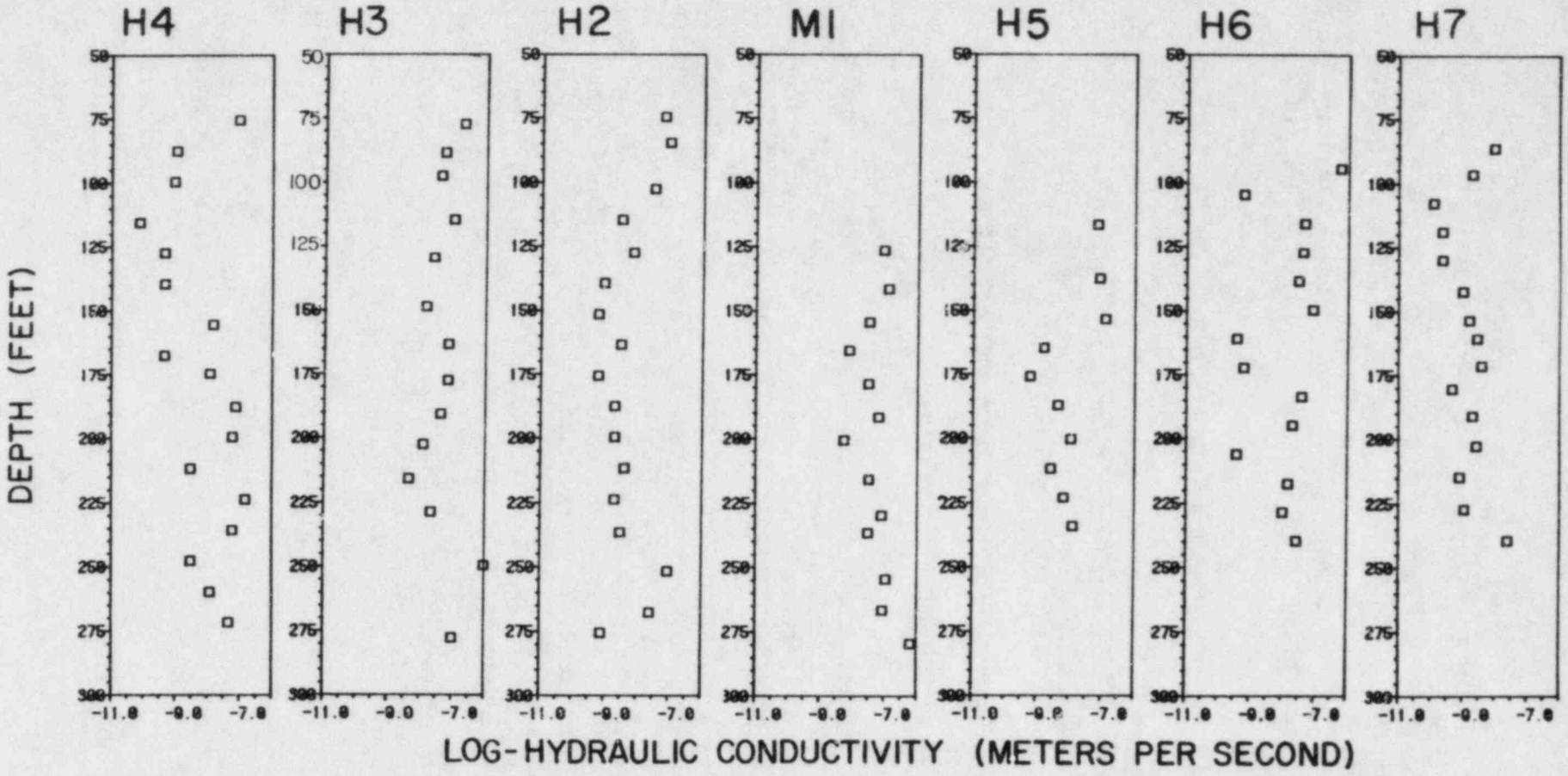

Figure 5.1. Log-hydraulic-conductivity profiles in boreholes M1, H2, H3, H4, H5, H6 and H7. Each point corresponds to the centerpoint of the straddle-packer test interval (13 feet).

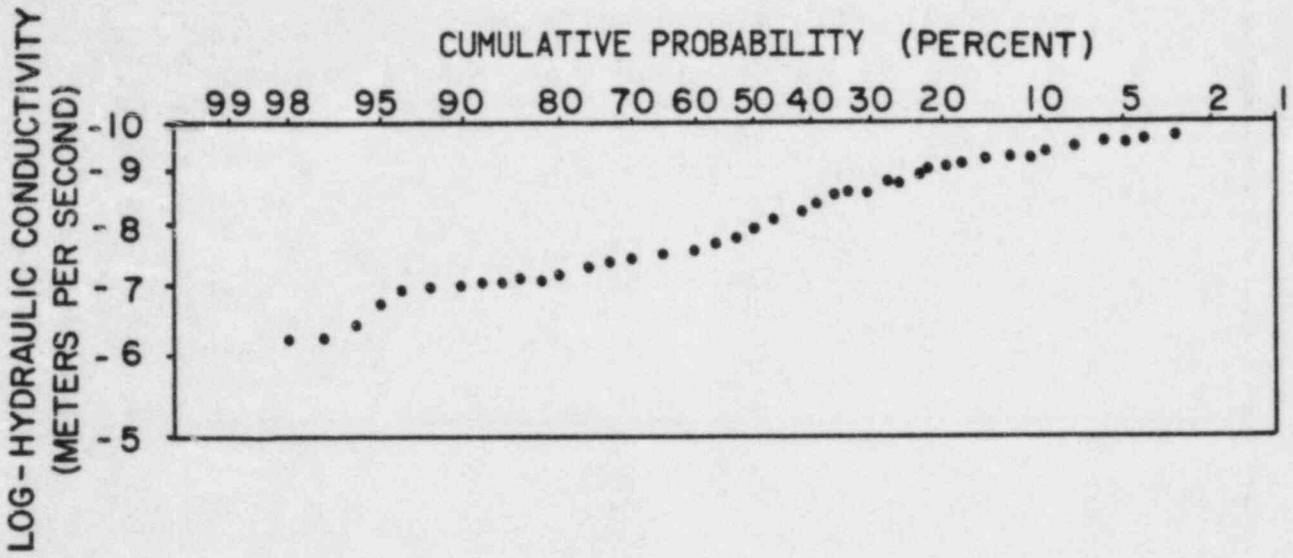

Figure 5.2. Probability plot of the distribution of log-hydraulic conductivity.

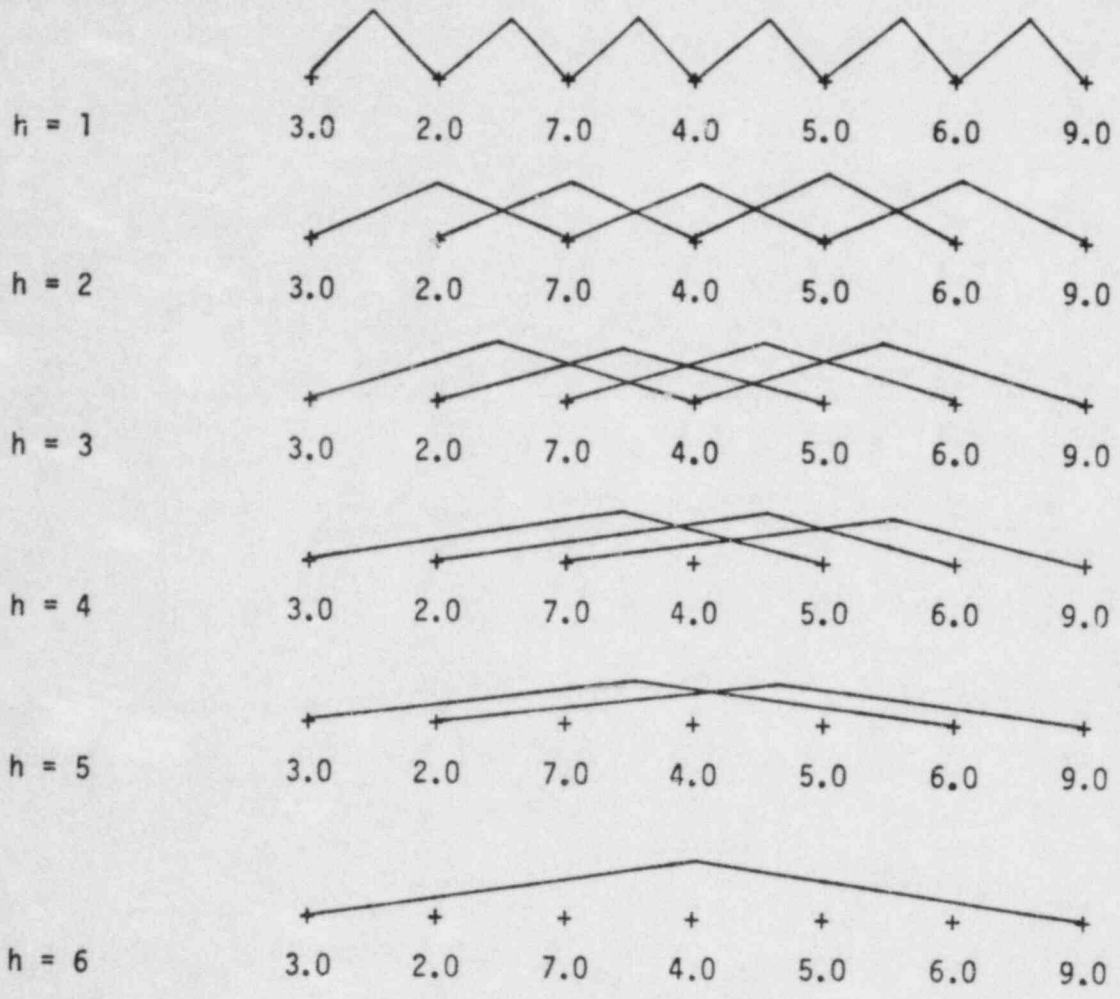

$$\gamma(h) = \left(\frac{1}{2N(h)}\right) \sum_{i=1}^{N(h)} [Z(X_i) - Z(X_i + h)]^2$$

where $Z(X)$ = sample value at point X, and

$N(h)$ = number of sample pairs for a lag h.

Example: For $h = 1$, $\gamma(1) = 3.83$

$$= 1/2(6)[(3-2)^2 + (2-7)^2 + (7-4)^2 + (4-5)^2 + (5-6)^2 + (6-9)^2]$$

Figure 5.3. Example of one-dimensional semivariogram construction (arbitrary units).

This procedure is repeated for increasing lags until the number of available data pairs becomes too small to consider (say, less than 30). This procedure is illustrated in Figure 5.3. The resulting set of points is referred to as "experimental semivariogram" or "sample semivariogram."

When the data are distributed in three-dimensional space, an experimental semivariogram in a given direction can be obtained by defining a solid angle of tolerance, or window, about that direction. All data plotting within the window of a given point are projected on the radius vector emanating from this point in the direction of interest. The radius vector is then discretized in a manner similar to the one-dimensional case, and the process is repeated for each data point. This process for the two-dimensional case is shown in Figure 5.4.

To obtain experimental variograms for the data, we chose a lag of 10 feet. Two experimental semivariograms are shown in Figure 5.5, one obtained in the vertical direction with a solid window of 35° around the vertical, the other averaged over all horizontal directions. The horizontal semivariogram is two-dimensional; it is the average of six semivariograms along different horizontal directions 30° apart, with overlapping windows of 60° each. An experimental semivariogram averaged over all directions is shown in Figure 5.6. Since this semivariogram has no direction, it is sometimes called "isotropic."

A semivariogram must satisfy certain theoretical requirements, such as being conditionally positive definite. One particular form satisfying these requirements, which appears to fit the data in Figures 5.5 and 5.6, is the so-called "spherical model" represented in a given direction by

$$\gamma(h) = \sigma^2 \left[1.5 \frac{h}{a} - .5 \left(\frac{h}{a}\right)^3 \right] \qquad h < a, \text{ and} \qquad (5\text{-}2)$$

$$\gamma(h) = \sigma^2 \qquad h \geq a. \qquad (5\text{-}3)$$

The maximum value of $\gamma(h)$, σ^2, is called the "sill"; it is equal to the variance of the data (in this case, $\sigma^2 = 0.83$). Over distances at which $\gamma(h) < \sigma^2$, the data are mutually correlated. The maximum correlation distance, a, is called the "range."

The range of the semivariogram is found by fitting Equation (5.2) to the data. Since the data are scattered, various fits are possible, and the choice between them is made on the basis of a validation procedure described later in this chapter. This procedure led us to the spherical models shown by the solid curves in Figures 5.5 and 5.6. The range of the vertical semivariogram is 60 feet; the range of the horizontal semivariogram is 30 feet; and the range of the isotropic semivariogram is 30 feet. Since a difference occurs between maximum correlation lengths in vertical and horizontal directions, the log-hydraulic-conductivity field is "statistically anisotropic." This statistical anisotropy should not be confused with hydraulic anisotropy (i.e., directional dependencey of the hydraulic conductivity) which is not considered in this analysis.

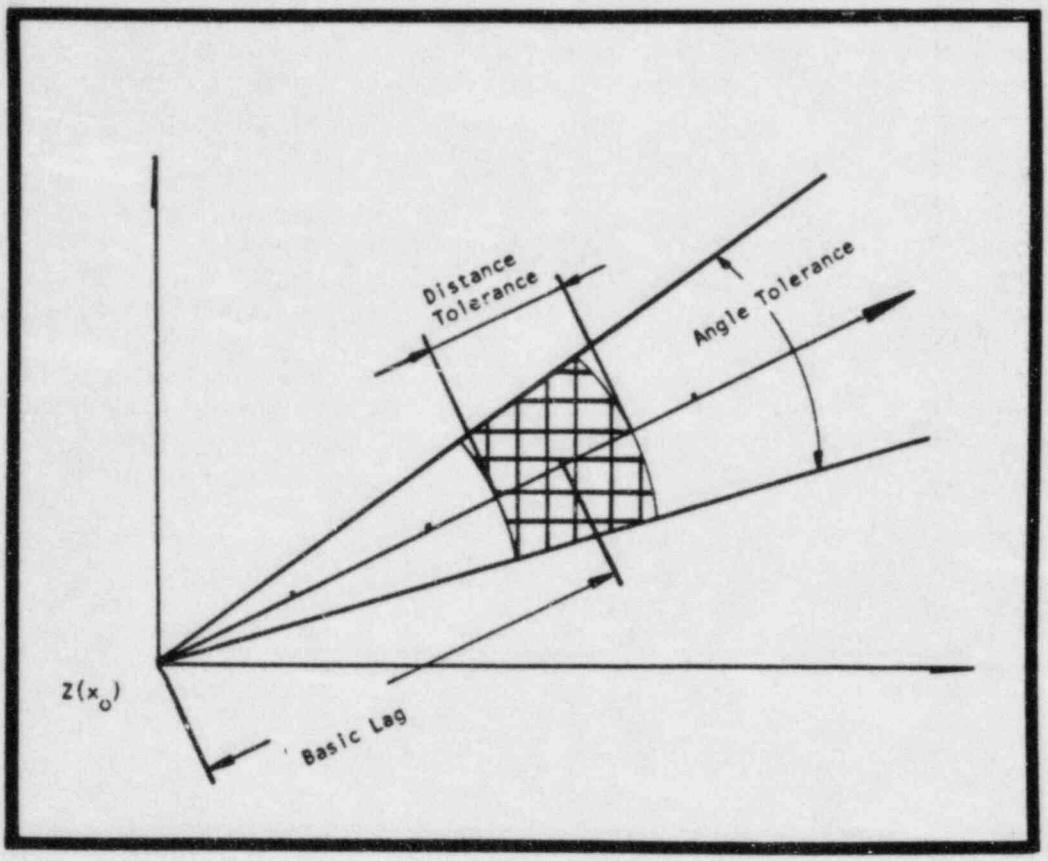

Figure 5.4. Distance class construction for a two-dimensional semivariogram (after Journel and Huijbregts, 1978).

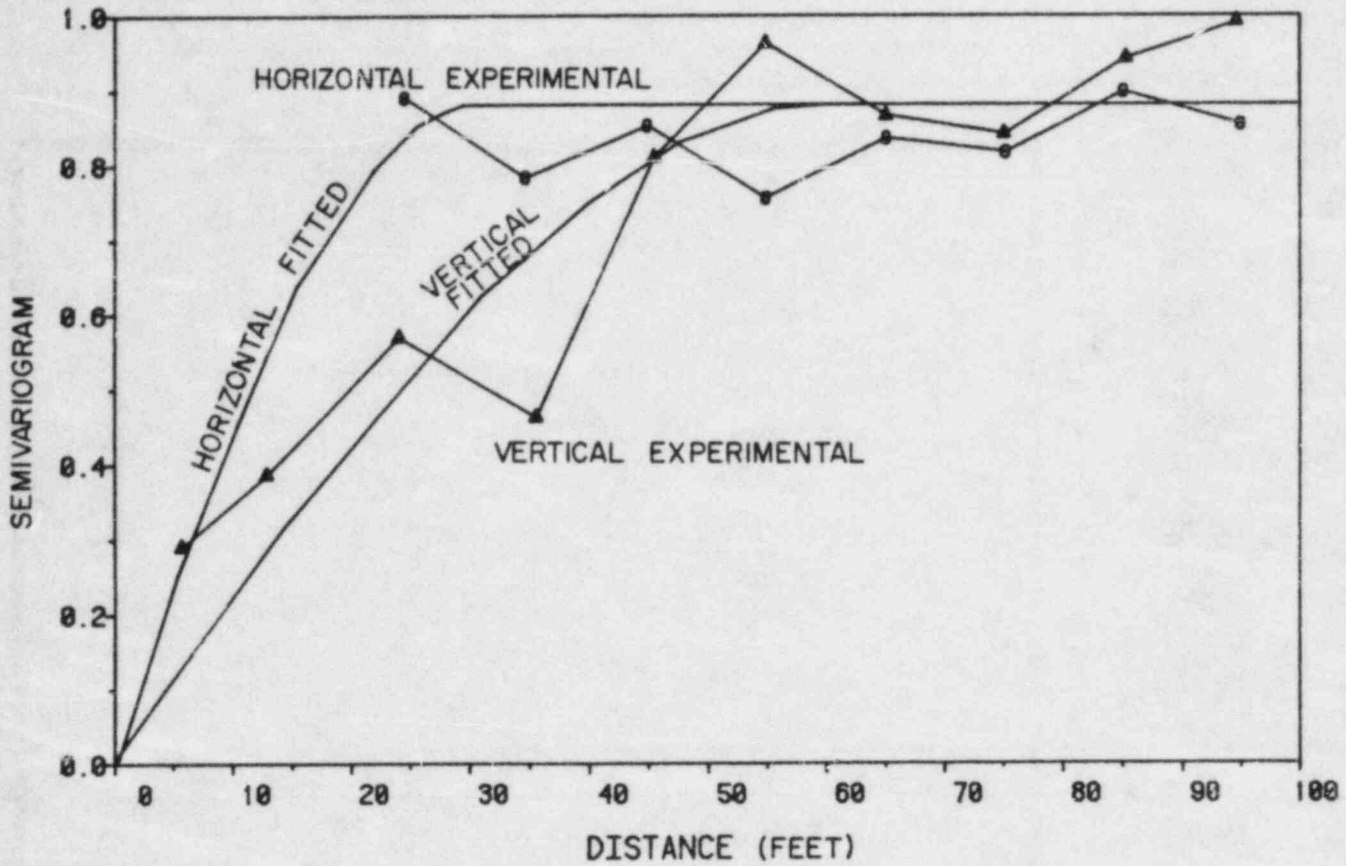

Figure 5.5. Anisotropic semivariogram of log-hydraulic conductivity.

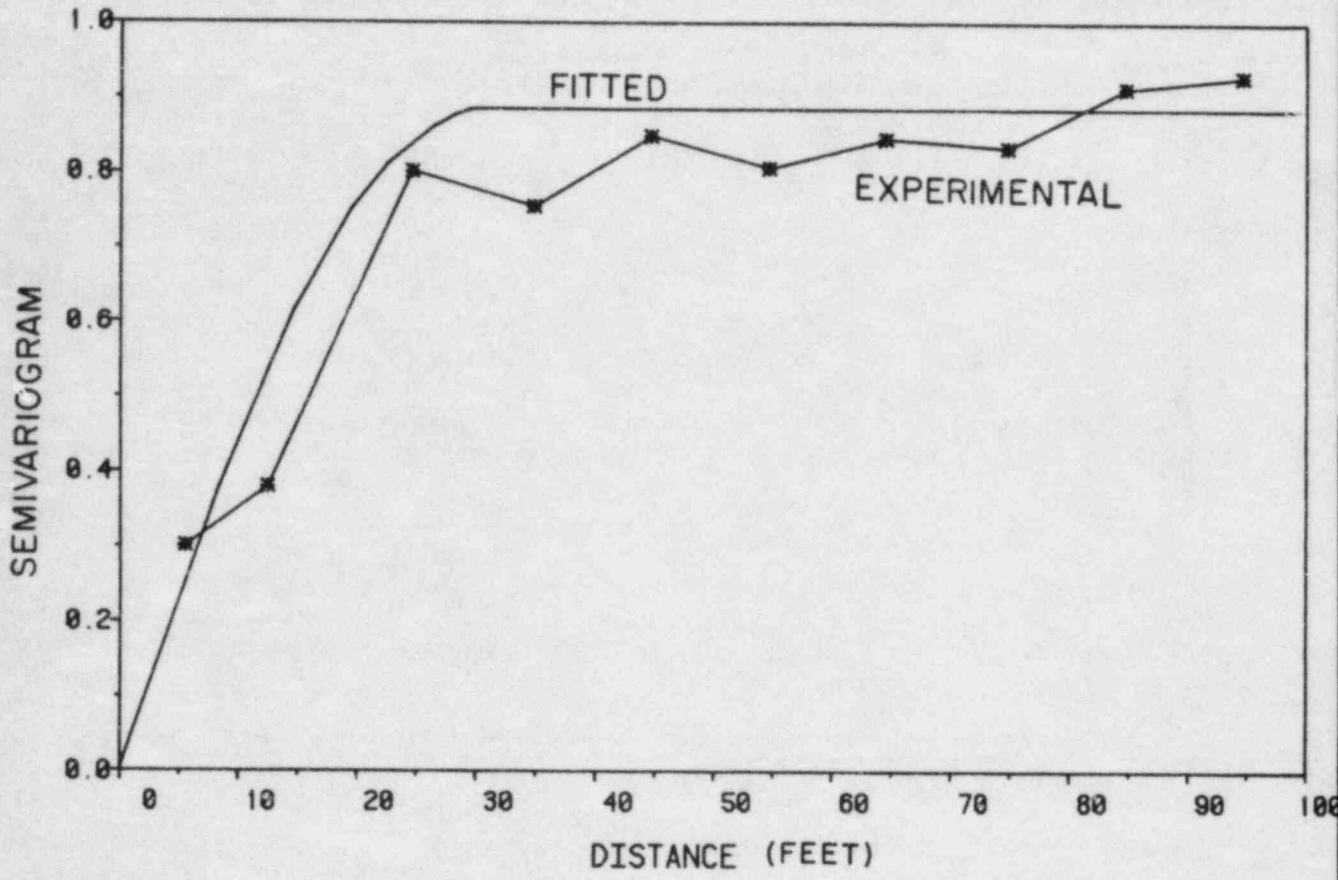

Figure 5.6. Isotropic semivariogram of log-hydraulic conductivity.

The fact that the log-hydraulic-conductivity semivariograms possess distinct sills suggests the lack of a noticeable trend, or "drift," in these values, within the rock volume tested. Such a drift might become noticeable on a larger scale; a systematic decrease in the hydraulic conductivity of fractured granites with depth was observed by Gale et al. (1982) near Stripa, Sweden, as well as by Davison et al. (1982).

Vertical semivariograms also have been obtained for: (1) Neutron-log data, averaged over each packed-off interval, in boreholes M-1 and H-3 (Figure 5.7); and (2) the fracture density in each such interval in holes M1, H2, H3, and H4 (Figure 5.8). Neutron-log data were fitted to a spherical model with a range similar to that of the log-hydraulic-conductivity semivariogram in the vertical direction. Fracture density data in Figure 5.8 can be fitted, among others, to a periodic semivariogram model with a wavelength of 34 feet and an amplitude that diminishes with the lag (this is also known as the "hole effect model"). A similar variogram periodicity was observed in granites by Miller (1979). The fact that the fracture-density and log-hydraulic-conductivity semivariograms differ from each other supports our earlier finding that these two sets of data are not closely interrelated. Only a weak correlation between such data from granites near Stripa, Sweden, was noted by Gale et al. (1982).

In a separate topical report (Winter et al., 1984a), our log-hydraulic conductivity semivariograms are used to calculate dispersivity of the Oracle granite, a parameter that is crucial for the prediction of radionuclide transport. This method is not specific to granites; it can be applied to other fractured rocks, such as basalts and tuffs.

5.1 Three-Dimensional Kriging of Log-Hydraulic Conductivity

In the remainder of this chapter, we use our semivariograms for a different purpose, namely, to estimate three-dimensional distribution of log-hydraulic conductivity between the boreholes at the study site. The method we adopt for this purpose is a geostatistical interpolation procedure called "kriging." This method has several important advantages over other, more conventional interpolation techniques. By considering the statistical-correlation structure of the log-hydraulic-conductivity field as embodied in the semivariograms, kriging provides an unbiased estimate of log-hydraulic conductivity at any point between the boreholes, provided the measurements are considered unbiased. This estimate, obtained as a weighted average of observed values, is better than that provided by any other arithmetic averaging procedure because the estimation error has minimum variance. Kriging also provides information about the magnitude and structure of the estimation error. The log-hydraulic conductivity estimates and the covariance matrix describing the structure of the errors may, in turn, be used to generate random homologs of the actual log-hydraulic-conductivity field; i.e., distributions that are statistically indistinguishable from each other. With these homologs stochastic modeling of fluid flow and contaminant transport in a given fractured rock mass can proceed.

Development of kriging is attributed to Matheron (1971). A recent discussion of applications to hydrogeology was published by Neuman (1982). To estimate the log-hydraulic conductivity, $Y(\underline{x})$, at a point $\underline{x}$, one takes the weighted average

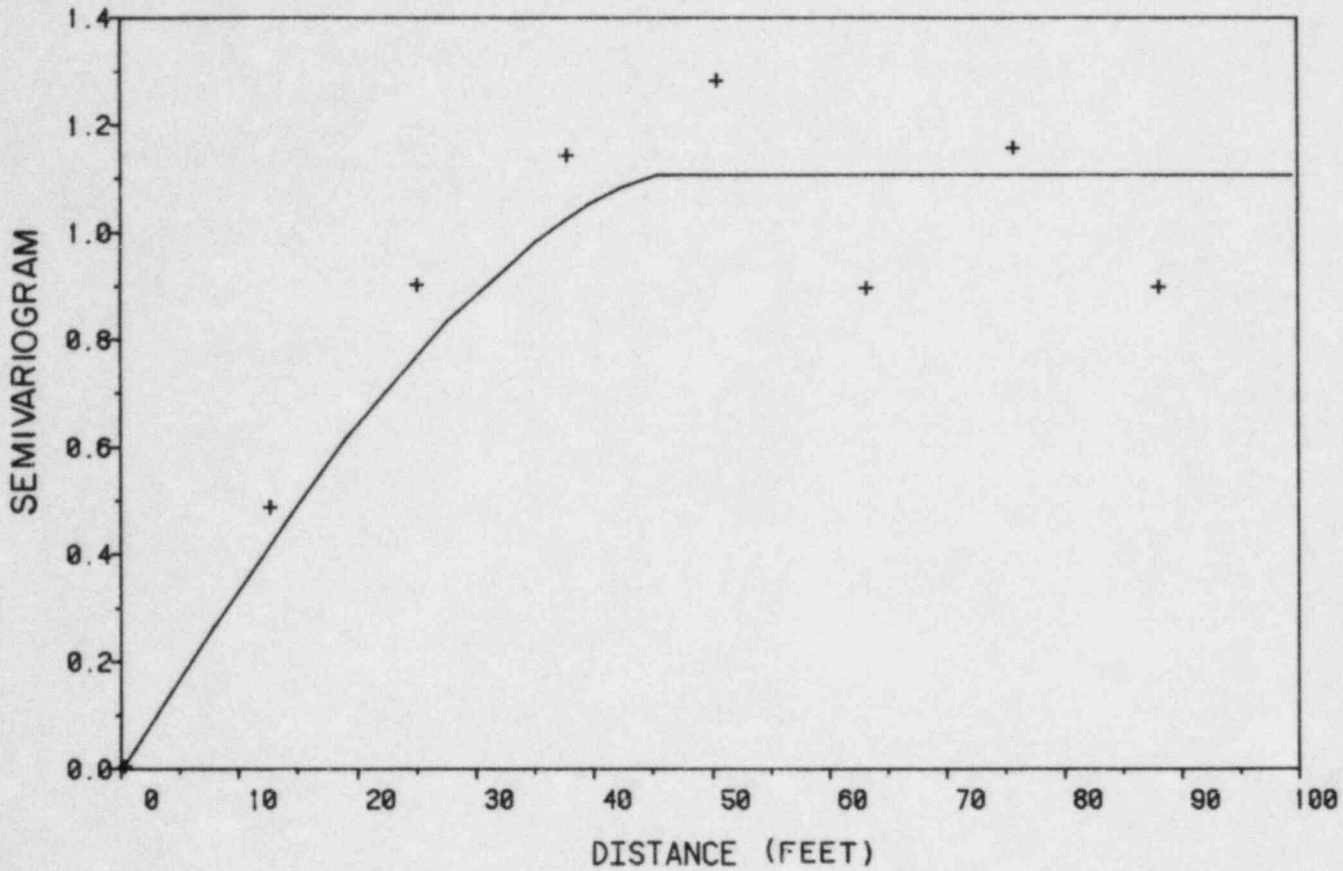

Figure 5.7 Semivariogram of integrated neutron-log response in boreholes M1 and H3.

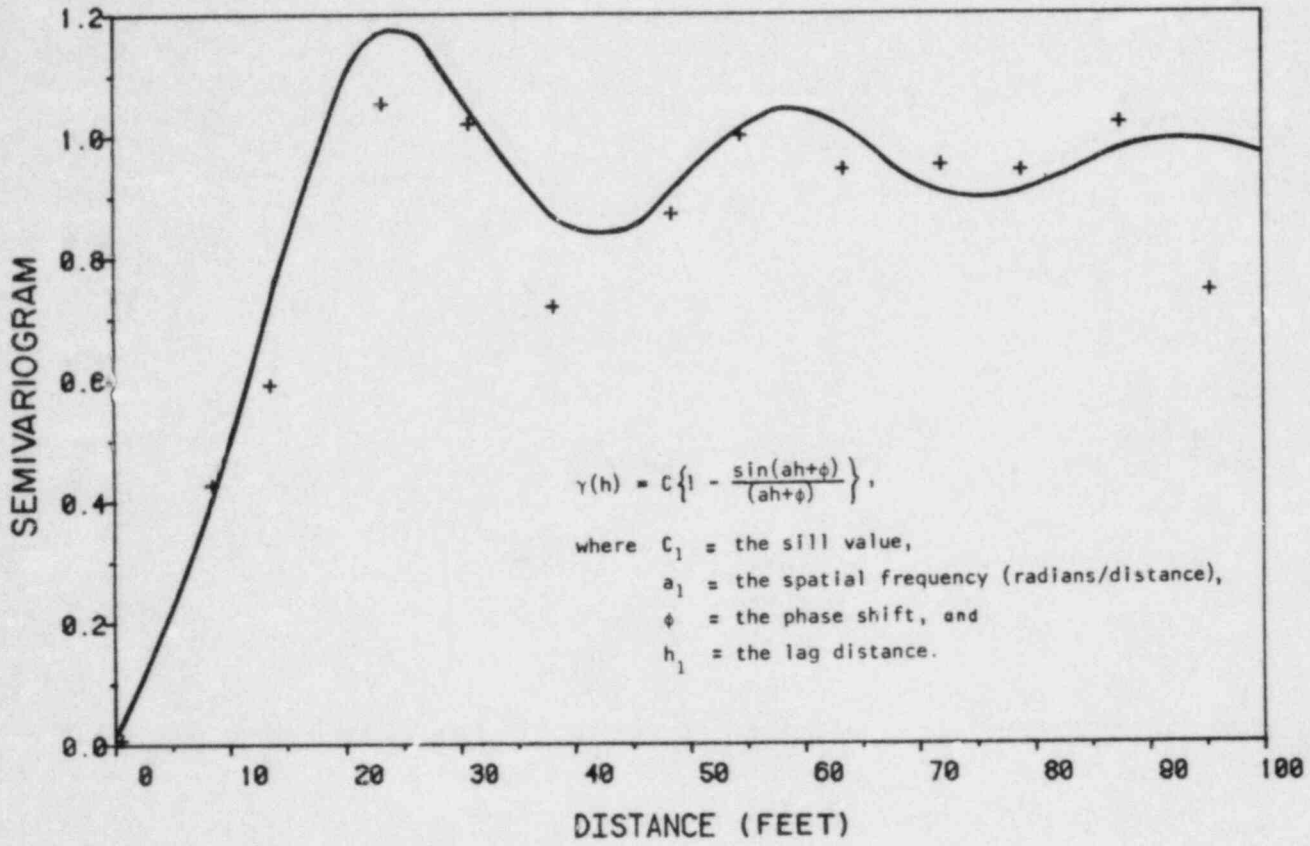

Figure 5.8. Semivariogram of fracture densities in boreholes M1, H2, H3, and H4 (hole-effect model).

$$\hat{Y}(\underline{x}) = \sum_{i=1}^{I} \lambda_i \, Y(\underline{x}_i) \qquad (5\text{-}4)$$

where $\underline{x}_i$ are I measurement points in the neighborhood of $\underline{x}$; $\hat{Y}$ is the "kriging estimate" of Y; and λ_i are "kriging coefficients." The latter are determined to ensure that the estimation error be unbiased:

$$E[\hat{Y}(\underline{x}) - Y(\underline{x})] = 0 \qquad (5\text{-}5)$$

and that its variance,

$$V = E\{[\hat{Y}(\underline{x}) - Y(\underline{x})]^2\} \qquad (5\text{-}6)$$

be minimum. Both criteria are satisfied when λ_j are taken to be the solution of the following (I+1) "kriging equations,"

$$\sum_{j=1}^{I} \lambda_j \gamma(\underline{x}_i, \underline{x}_j) - \lambda_i \sigma_i^2 + \beta = \gamma(\underline{x}_i, \underline{x}_0) \qquad i = 1,2,\ldots,I \text{ , and} \qquad (5\text{-}6a)$$

$$\sum_{j=1}^{I} \lambda_j = 1 \qquad (5\text{-}6b)$$

Here $\gamma(\underline{x}_i, \underline{x}_j)$ is the variogram for $\underline{s} = \underline{x}_i - \underline{x}_j$; σ_i^2 is the variance of the measurement error at $\underline{x}_i$ (assumed to have zero mean and to be uncorrelated to measurement error at $\underline{x}_j$, $j \neq i$); and β is a Lagrange multiplier for the estimation of a value located at $\underline{x}_0$.

After solving Equations (5-6) for all the λ's, the latter are substituted into Equation (5-3) to compute $Y(\underline{x})$. The associated estimation error variance is calculated from

$$V = -\gamma(o) + \sum_{i=1}^{I} \lambda_i \, \gamma(\underline{x}_i, \underline{x}) + \beta \qquad (5\text{-}7)$$

Covariances between estimation errors at different points also can be evaluated (Clifton and Neuman, 1982; Neuman, 1982). The results can be translated into hydraulic-conductivity estimates, K, and the associated error variance, V_K, through (Hines and Montgomery, 1980)

$$R = \exp (2.303 \, Y + 2.303^2 \, V/2) \qquad (5\text{-}8)$$

$$V_K = R^2 \, [\exp (2.303^2 V) - 1] \qquad (5\text{-}9)$$

The values of log-hydraulic conductivity were kriged over a regular three-dimensional grid of points spanning the boreholes. The grid spacing in the vertical direction was 13 feet to coincide with the length of the packer-test intervals. As a result of this vertical spacing, each point in the grid may be viewed to represent a cylinder of rock equal in volume to that of the rock mass affected by a packer test. This volume is called the "data support" of the grid. Horizontal separation between the grid points varied from 20 to 120 feet.

The first step in the analysis is validating the semivariogram through a process called "jack-knifing." This is done by eliminating one datum point at a time, and trying to reproduce the measured log-hydraulic conductivity at this point by kriging only with data surrounding the point. Different semivariograms can be compared among themselves, based on the degree to which they help reproduce known values of log-hydraulic conductivity at all measurement points. Application of this method to the study site data led to the anisotropic spherical semivariograms in Figure 5.5.

A total of 102 data values were available for kriging at the study site, with values ranging from 5.0×10^{-11} to 6.3×10^{-7} m/s. Kriging was done with the anisotropic spherical semivariograms in Figure 5.5. Measurement errors were disregarded. An illustration of the three-dimensional distribution of kriged values of log-hydraulic conductivity is shown in Figure 5.9. The upper weathered zone (see discussion of geophysical logs in Chapter 4) shows a high hydraulic conductivity everywhere except near the diabase dike intercepting borehole H4 between the depths of 60 and 90 feet. The zone below the diabase has relatively low values of hydraulic conductivity (between $10^{-8.5}$ and $10^{-9.5}$ m/s), resulting from calcite from the overlying dike filling the fractures. A zone of relatively high values of hydraulic conductivity, due to the presence of a flat-lying fault, is evident in the lower part of the cross section.

A map of the standard errors of estimation (V from Equation (5-6)) associated with Figure 5.9 is shown in Figure 5.10. Since measurement errors are not considered in our analysis, contours in Figure 5.10 depend entirely on location of the data points in relation to location of the remaining grid points. This explains why the smallest standard errors occur along the boreholes, and the largest standard errors occur between the boreholes. Also, the fault zone at depth 260 feet (approximately) was not tested in some of the boreholes because of excessive leakage around the packer assembly; hence, Figure 5.10 indicates a high estimation error at that depth. Relatively large standard errors also occur above and below the tested portion of each borehole. Note that the maximum standard error cannot exceed the square root of the dispersion variance, σ^2 (i.e., the square root of the semivariogram sill).

As mentioned earlier, an unbiased estimate of the conductivity (as opposed to its log) is given by Equation (5-8). The difference between the logarithm of

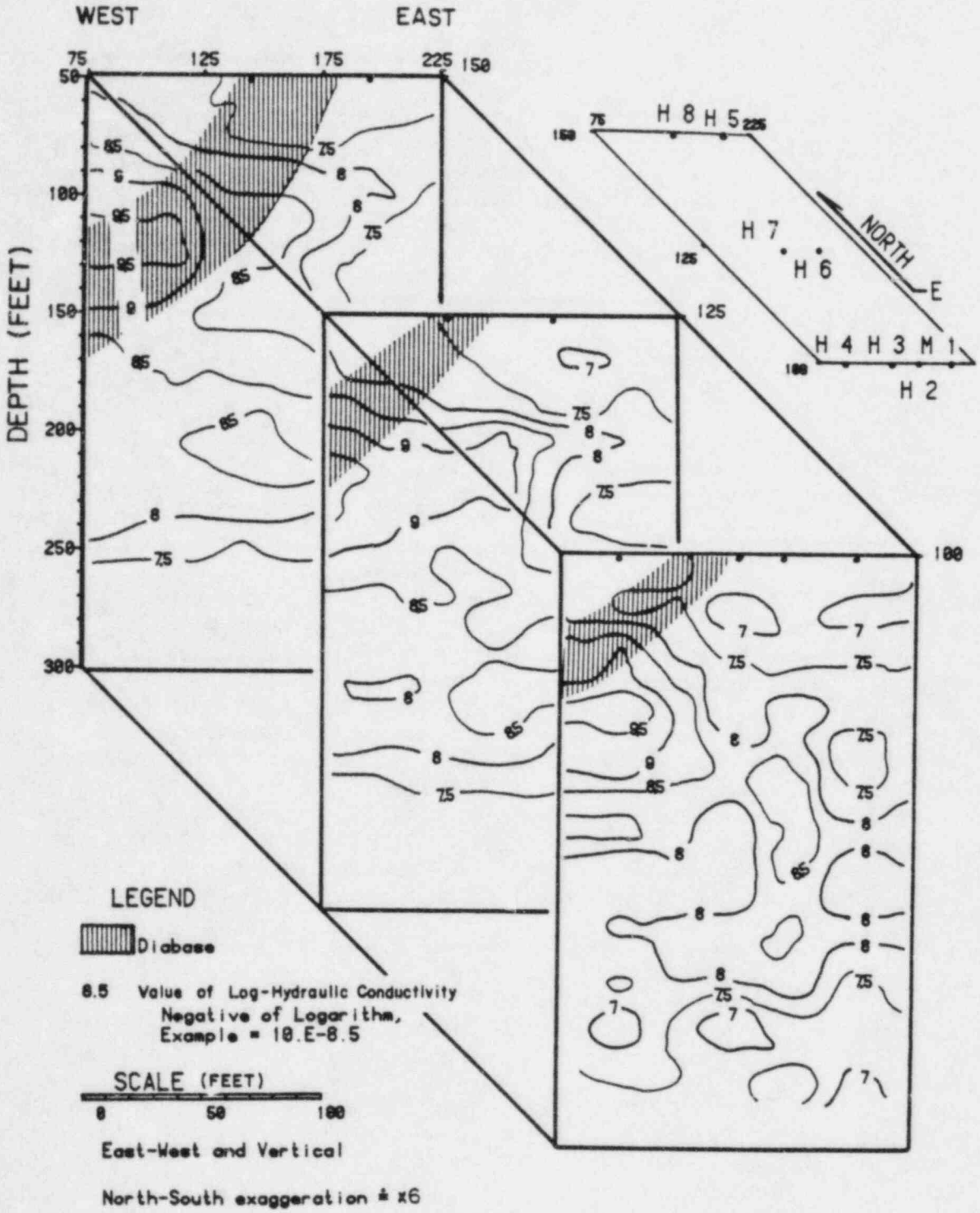

Figure 5.9. Kriged log-hydraulic conductivity in three dimensions.

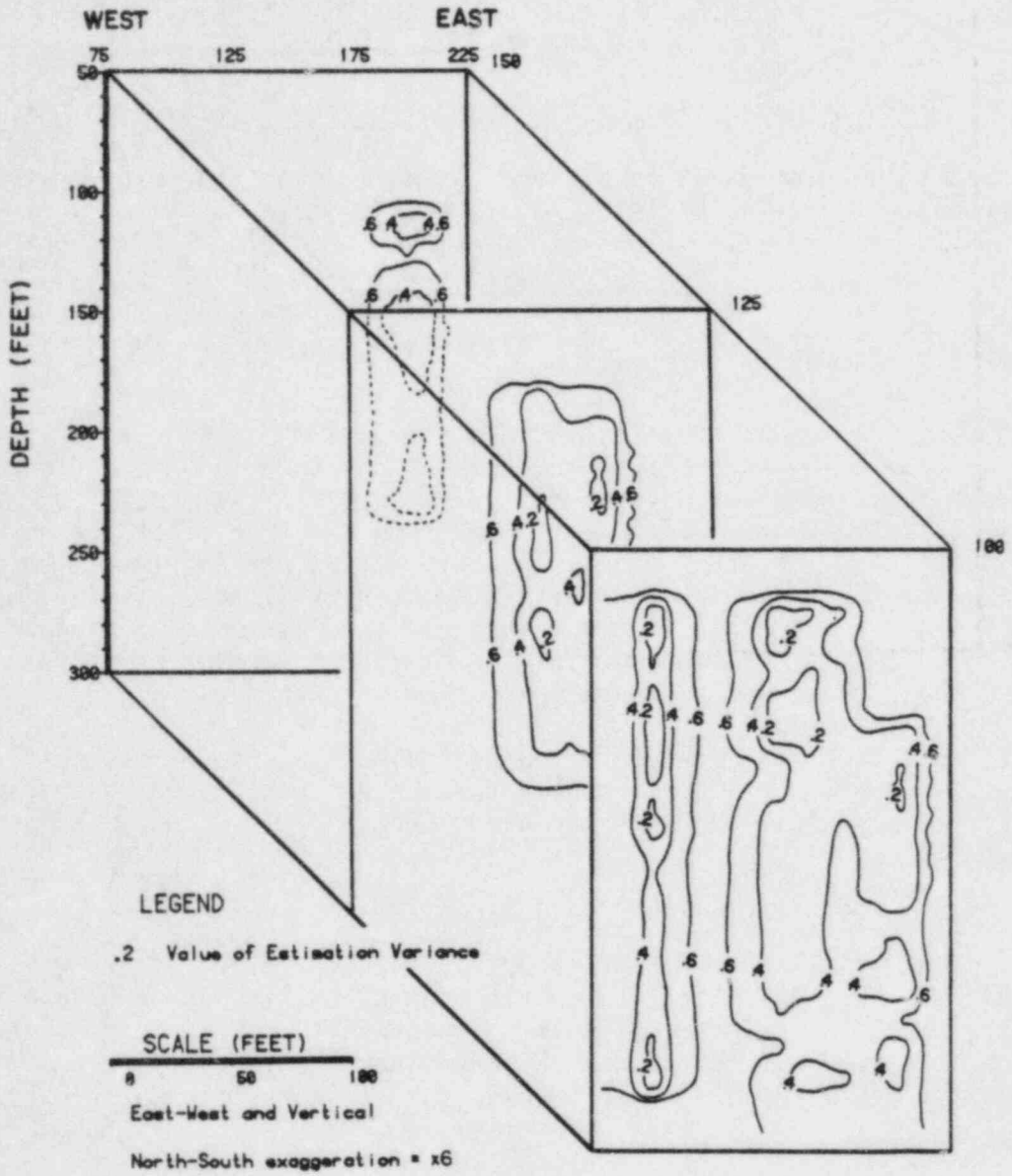

Figure 5.10. Estimation errors associated with Figure 5.9.

this estimate and the kriged estimate of Figure 5.9 is shown in Figure 5.11. Since this difference increases with the estimation variance, V, it is smallest along the wellbores and largest between them. However, for most stochastic modeling applications, only log-hydraulic-conductivity estimates are needed.

5.2 Conditional Simulation of Log-Hydraulic Conductivity

Although kriging provides an optimum estimate of the three-dimensional log-hydraulic-conductivity distribution at a site, this estimate is, nevertheless, associated with an estimation error. Without additional field data, the kriged estimate cannot be improved, and true hydraulic-conductivity distribution at the site remains unknown. True hydraulic-conductivity distribution generally is more variable (i.e., less smooth) than that estimated by kriging (e.g., Figure 5.9).

The purpose of conditional Monte Carlo simulation is to go a step beyond kriging, by generating statistical homologs of the true log-hydraulic-conductivity field at the site; i.e., by generating log-hydraulic-conductivity distributions that, though random and different from the true distribution, have an equal likelihood of occurrence. This simulation process is called conditional because the generated log-hydraulic-conductivity fields preserve measured values along the boreholes; i.e., they are conditioned on available field data. The method should be useful for the investigation of different, but equally likely avenues of contaminant transport at a given site.

Conditional simulation is performed by adding a positive- or negative-random value to the value of log-hydraulic conductivity estimated by kriging at each point. First, one determines the covariance,

$$V_{ij} = E\ \{[\hat{Y}(\underline{x}_i) - Y(\underline{x}_i)]\ [\hat{Y}(\underline{x}_j) - Y(\underline{x}_j)]\} \qquad (5\text{-}10)$$

between the kriging estimation errors at any two points of the grid, by following a procedure outlined in the papers of Clifton and Neuman (1982) and Neuman (1982). Possible errors in the measured data also can be included (if desired) in the conditional simulations. Next, the covariance matrix $\underline{\underline{V}}$ (which includes all V_{ij} values) is decomposed into a lower triangular matrix, $\underline{\underline{M}}$, and its transpose, $\underline{\underline{M}}^T$, as follows:

$$\underline{\underline{V}} = \underline{\underline{M}}\ \underline{\underline{M}}^T. \qquad (5\text{-}11)$$

Since kriging is an unbiased estimator, the mean of the estimation errors is zero. Thus, upon assuming that these errors are normally distributed, we can generate a vector of log-hydraulic conductivity, Y_i^*, at all the grid points, $\underline{x}_i$, simply by writing:

$$\underline{Y}^* = \underline{\hat{Y}} + \underline{\underline{M}}\ \underline{\Psi}. \qquad (5\text{-}12)$$

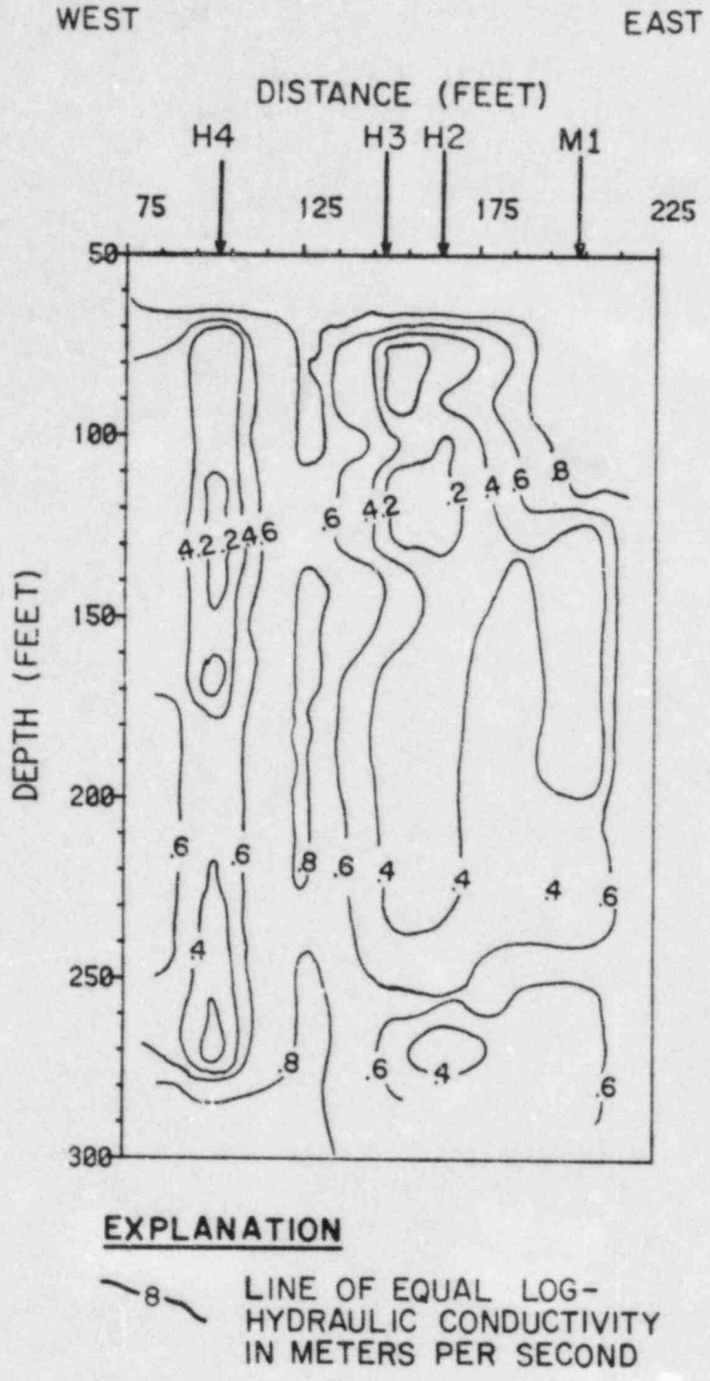

Figure 5.11. Differences between the logarithms of hydraulic conductivity estimated by Equation (5-8), and kriged log-hydraulic conductivity.

Here $\underline{\Psi}$ is a vector of independent random numbers, each of which is drawn from a normal population having zero mean and unit variance. It follows that $\underline{Y^*}$ has a mean equal to $\underline{\hat{Y}}$, and a variance equal to $\underline{V}$. By generating different $\underline{\Psi}$ vectors at random, we can generate different log-hydraulic-conductivity vectors, $\underline{Y^*}$, all of which are normally distributed with the same mean and covariance, and thereby are homologous with each other. Moreover, the Y_i^* values generated in this way at measurement points essentially will be equal to the measured values of log-hydraulic conductivity.

Three log-hydraulic-conductivity cross sections (Figures 5.12a,b,c) were generated by the above method for the vertical plane, connecting boreholes M1, H2, H3 and H4 to illustrate this method. The scale across the top of Figures 5.12a,b,c matches the x-y coordinate system shown in the upper right corner of Figure 5.10. Although these simulated cross sections retain the major features of the kriged cross sections in Figure 5.9, they are much less smooth, showing a greater degree of spatial variability. Since each of these cross sections is equally likely, we cannot tell which is closest to the truth. Therefore, in studying the potential risk of contaminant transport at a given site, one may consider many possible scenarios by generating them conditionally.

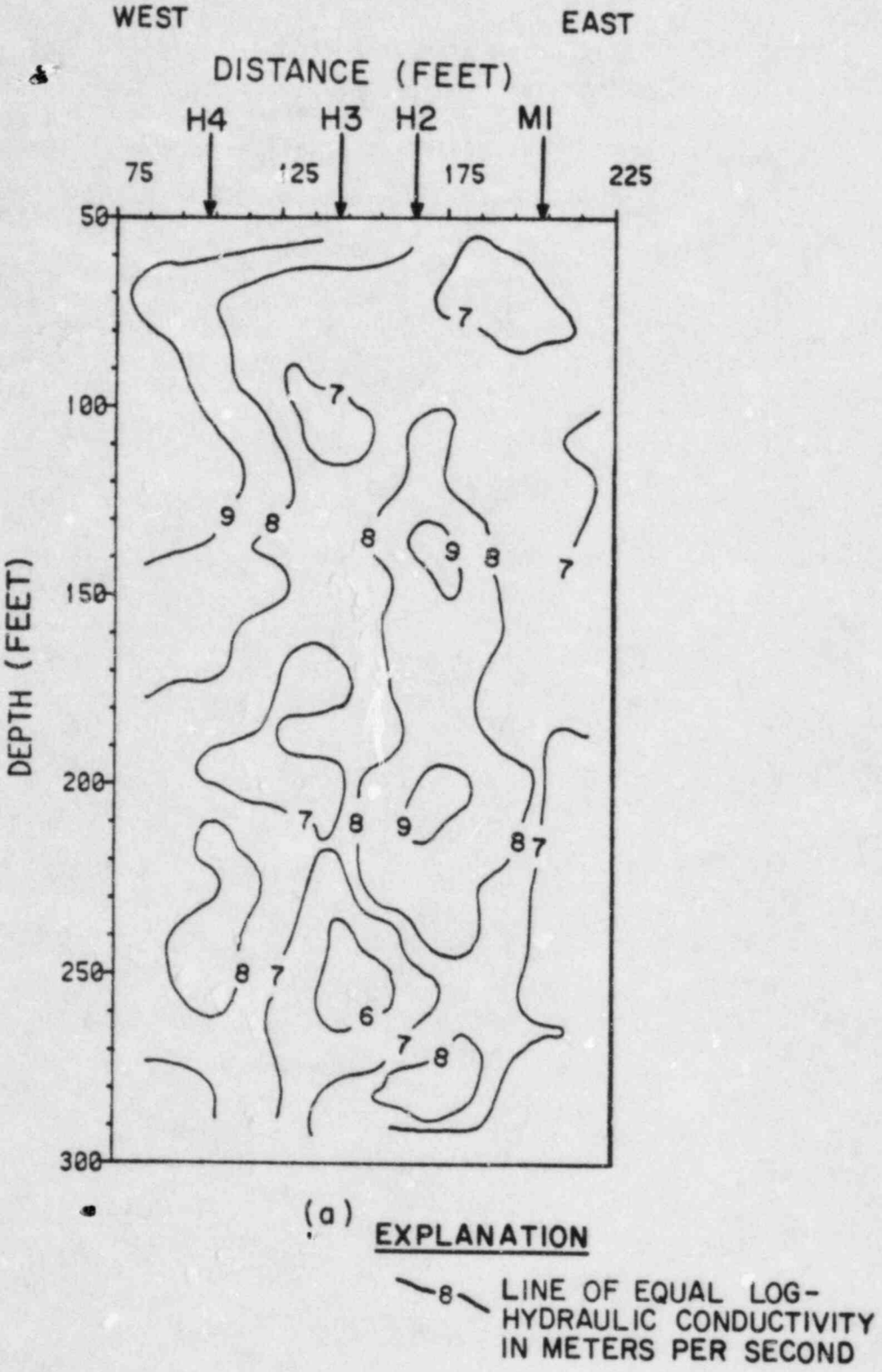

Figure 5.12a. First conditional simulation of log-hydraulic conductivity for a west-east cross section through the Oracle site.

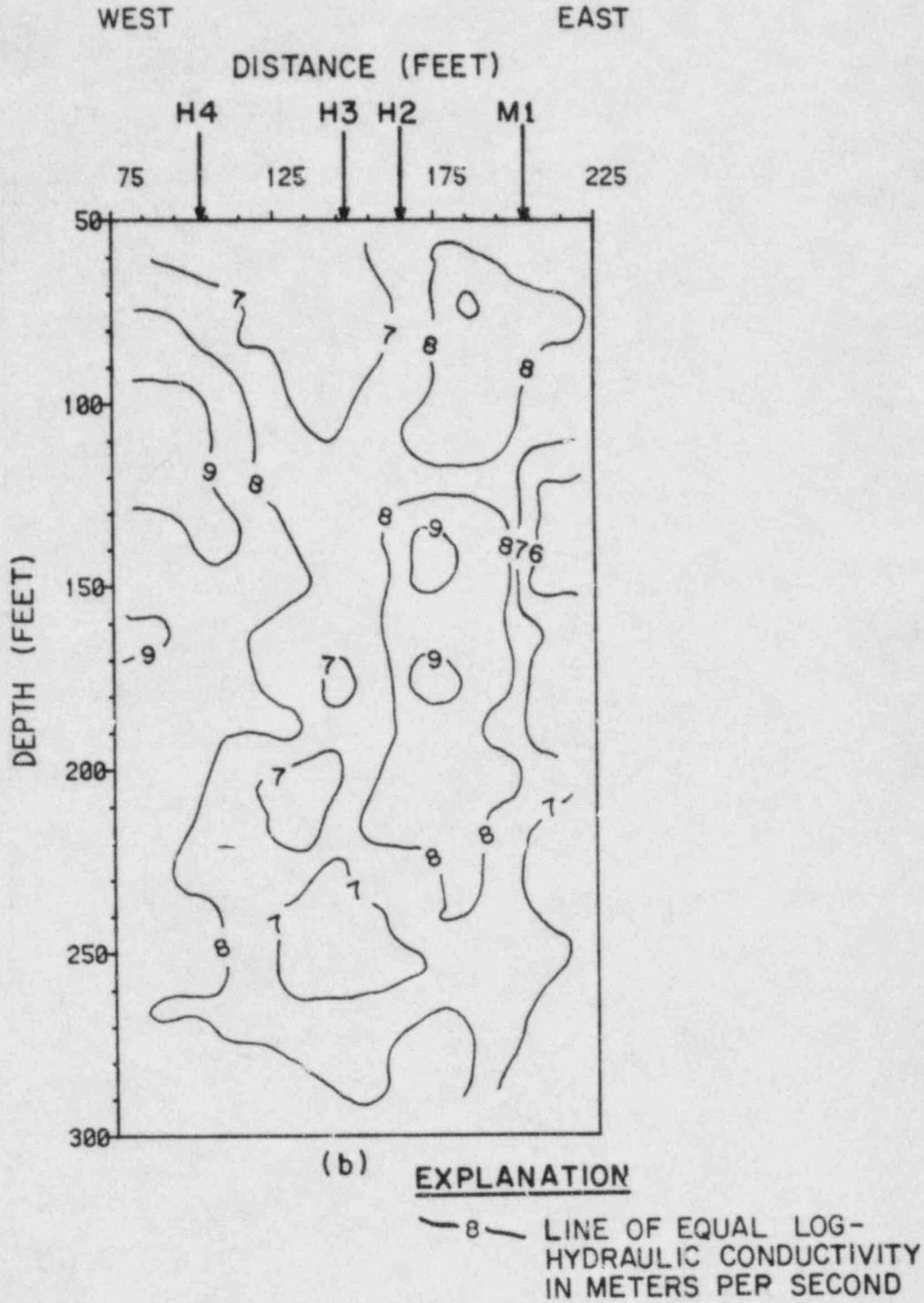

Figure 5.12b. Second conditional simulation of log-hydraulic conductivity for a west-east cross section through the Oracle site.

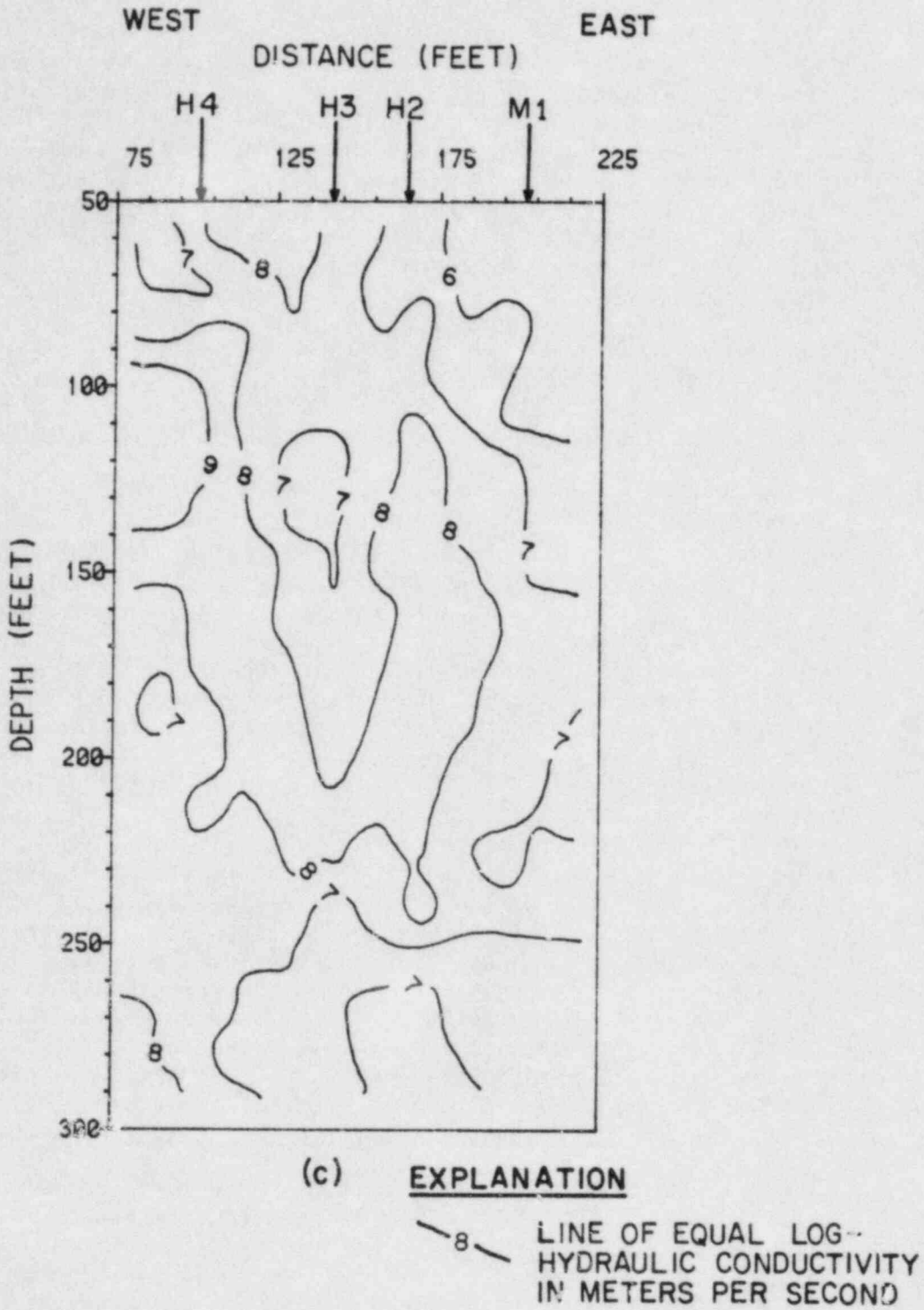

Figure 5.12c. Third conditional simulation of log-hydraulic conductivity for a west-east cross section through the Oracle site.

6. RELEVANCE TO NRC LICENSING OF HIGH-LEVEL RADIOACTIVE WASTE REPOSITORIES

In licensing high-level radioactive-waste (HLW) repositories, the U.S. Nuclear Regulatory Commission (NRC) will be responsible for implementing the U.S. Environmental Protection Agency (EPA) radiological standard for HLW, Part 191 of Title 40 of the Code of Federal Regulations (40 CFR 191). This standard was published as a Notice of Proposed Rulemaking (NPR) on page 58196 of Volume 47 of the Federal Register (47 FR 58196). As the regulatory vehicle for implementing 40 CFR 191, NRC published procedural and technical criteria for its high-level waste rule 10 CFR 60. Procedural criteria were published as a final rule in the Code of Federal Regulations; technical criteria were published as an NPR in 46 FR 35280. A final ruling for 10 CFR 60 was published as 48 FR 28194. NRC is planning to publish regulatory guides to aid in compliance with 10 CFR 60. NRC Regulatory Guide 4.17, on the preparation of site characterization reports, was published. The U.S. Department of Energy (DOE), the sole licensee for HLW disposal, published a Notice of Proposed Rulemaking on guidelines for disposal of HLW, 10 CFR 960 (48 FR 5670).

In paragraph 60.21 of 10 CFR 60, item (6) states that a license application must include "...a description of site characterization work actually conducted by DOE at all sites considered in the application." Item (c) states that a Safety Analysis Report must be submitted including "...a description and analysis of the site at which the proposed geologic repository operations area is to be located...the assessment shall contain an analysis of the geology, geophysics, hydrology,..." and other aspects of the site. NRC Regulatory Guide 4.17 states specifically that hydrological evaluation of a site must include "...information on hydraulic characteristics of the matrix and fluid for each principal hydrogeologic unit..." and the method of determination (paragraph 5.9.2). Among these hydraulic characteristics are "intrinsic permeability," "hydraulic conductivity," "total and effective porosity," and "storage coefficient." Special attention is focused on "the nature of the pore space" and how it controls the intrinsic permeability, the extent to which Darcian flow can be assumed, and the "representative volume" applicable to measureable parameters. Site-characterization studies are to continue through all phases of a repository so that "...a continuing program of surveillance, measurement, testing, and geologic mapping shall be conducted to...accommodate actual field conditions encountered..." (paragraph 60.141). Above all, with regard to the hydrologic characteristics of a site, it will be necessary to "...include data sources and estimated uncertainties..." and to "...discuss any significant consequences of the uncertainties about conclusions drawn from the data..." (NRC Regulatory Guide 4.17-20).

This report is intended as a generic study to illustrate investigation techniques that can be applied to a fractured rock. Site-characterization studies are similar to any subsurface investigation in that a combination of data are necessary to describe a site. First, a general overview of the geology of a site is necessary to conceptually organize the features of a site, such as stratigraphy, fracture patterns, and regional hydrology. During the construction and operation of a repository, additional information also will be obtained. Geological characterization should include field mapping and

description of the lithology, structure, and geologic history of a site. Information obtained can come from aerial photographs and remote-sensing records, analyses of outcrops, core data, geophysical logs, and water samples, as well as nondestructive geophysical techniques, such as gravity, seismic, magnetic, and electrical surveys. During the initial exploration, hydrogeologic units can be defined and plans can be made to perform further tests, based on the scale and heterogeneity of observed features. The first five chapters of this report contain the types of information necessary for the initial planning stages of a hydrogeological investigation.

After the general characteristics of a site have been identified in a geological context, the next step is to quantitatively assess fracture patterns, rock characteristics, and hydraulic characteristics. These characteristics are often interrelated at a large and a small scale; their measurement may depend upon the scale of investigation. For example, Darcian flow may be a reasonable assumption at a regional scale, but may be an invalid working hypothesis for some hydraulic tests. This question was addressed by Hsieh et al. (1983) as part of this project. Results of hydraulic testing are used in this report in conjunction with downhole-geophysical testing, fracture analysis, and geostatistics. A great deal of information can be gained from an integrated analysis of these data. To briefly summarize the applicability of the techniques demonstrated in this report, quantitative investigation can be broken down into three categories: (1) Fracture statistics; (2) geophysical logs; and (3) geostatistical analysis of hydraulic tests, described below.

6.1 Fracture Statistics

Description of the fracture system at a site is necessary to define its structural history, as well as its mechanical and hydraulic properties. A guideline for the description of fractures was published in the International Journal of Rock Mechanics and Mining Science, Vol. 15, 1948. These guidelines set forth standards for proposed techniques in physical description and testing of fractures. Among the fracture characteristics that received the most interest in hydrology are location, aperture, length, orientation, roughness, and continuity or interconnections. Of these, the only reliable values obtained in this study are the location and orientation of fractures from drill cores and acoustic-televiewer logs. Internally, fractures are quite variable and easily disrupted by drilling, so that characteristics such as aperture and roughness are difficult to measure reliably. Analysis of the orientation and spacing of fractures was done primarily through the use of stereonets, spacing-class histograms, and semivariograms. Fractures analyzed as sets can show distinct spatial patterns; techniques that account for their spatial distribution give useful information. Statistical tests also can be performed to examine the periodicity and clustering of fractures into zones. A comparison of fracture statistics can be made based on methods used in this study.

6.2 Geophysical Testing

Downhole- and surface-based geophysical techniques can provide detailed, nondestructive tests of a site. The petroleum industry has been relying on geophysical testing for many years to characterize oil reservoirs; this technology can be applied to repository studies. Applications to crystalline rock

are recent and will improve with experience. Lithologic variations are rapidly assessed by the rock response to nearly all geophysical instruments; core data can be extrapolated laterally and vertically based on geophysical logs. At the study site, the neutron-log response correlated with measured values of hydraulic conductivity. Hence, the neutron log should provide a means for assessing the hydraulic structure of a site. Overall, geophysical tests offer the possibility to rapidly and accurately assess subsurface conditions of a potential repository.

6.3 Analysis of Hydraulic Tests

Accurate appraisal of the spatial distribution of hydraulic conductivity is crucial to the determination of radionuclide transport in the subsurface. Direct measurements by single-hole, straddle-packer injection tests were done at the site, and used in two ways. First, since hydraulic testing is time consuming and difficult to perform, other data were compared with the tests to determine whether a partial replacement could be found for direct tests. Fracture statistics did not prove to offer any correlation to the magnitude of hydraulic conductivity. Neutron-log data, which represent a larger volumetric sample of the rock than direct fracture analyses, did show a correlation over at least two orders of magnitude in measured hydraulic conductivity. Other correlations may be possible; each site should be examined individually. Second, a technique is presented to construct a subsurface cross section of the interpolated distribution of measured hydraulic conductivity. Values obtained in any field study are never precise; they will always contain a degree of uncertainty. This uncertainty, which must be understood in any study or projection of the performance of a potential repository, can be quantitatively assessed, using the geostatistical techniques of kriging and conditional simulation. Chapter 5 explains the approach, which is based on a stochastic description of a geological system, and which allows for statistical variability of measured values. Through the use of conditional simulation, possible variations of spatial distribution of hydraulic conductivity (or any other parameter) readily can be demonstrated.

7. CONCLUSIONS

The following major conclusions can be drawn from this study:

1. An understanding of the manner in which a fractured rock mass has evolved through geologic time is essential for the description of its hydrologic properties. This understanding is particularly important for the classification and organization of fractures into separate sets with distinct geometric and mineralogical properties, as well as for the identification of hydrogeological units.

2. An acoustic televiewer is an invaluable tool for subsurface investigation of fractured crystalline rocks. In addition to providing detailed information about location, orientation, and (to a lesser extent) aperture of individual fractures, televiewer logs also can be used to recover the azimuths of unoriented core samples or to substitute for core, when no core is obtained.

3. Surface and subsurface mapping of fractures in the Oracle granite revealed the presence of six fracture sets. Three of these sets were nearly orthogonal to each other, and their origin was traced to the early stages of magmatic intrusion in the region. The other three sets appeared to be related to later geologic events; thus are they of secondary origin. The same events also caused some movement and hydrothermal activity along directions parallel and subparallel to the three primary sets of suborthogonal fractures.

4. Frequency distribution of fracture spacings at the study site revealed a random component superimposed on systematic tendencies of many fractures to be evenly spaced or to cluster in narrow zones. Where clustering occurred, rock properties often changed sufficiently to appear as anomalies on certain geophysical logs and to produce unusually high values of hydraulic conductivity.

5. Attempts to correlate fractures between boreholes were only marginally successful. This may have been due to possible curvatures of fracture surfaces, spatial variations of apertures within individual fractures, nonuniform mineralogy, lack of fracture continuity between boreholes, and sampling errors. To the extent that correlation was possible, it relied heavily on core and acoustic-televiewer data as well as on various geophysical logs and in situ hydraulic-conductivity measurements.

6. Data from the study site showed an apparent lack of correlation between fracture density and measured hydraulic conductivity. This raises a serious question about the validity of existing conceptual models of fluid flow and contaminant transport through networks of discrete fractures when applied to rocks such as the Oracle granite. An alternative approach suggested in this study is based on a continuum concept coupled with geostatistical analysis of hydrologic-test data.

7. A distinct linear relationship between inverted, integral, neutron-log responses in the Oracle granite and the logarithm of hydraulic conductivity exists over at least two orders of magnitude of hydraulic-conductivity variation. Since this relationship is sensitive to borehole diameter, there is

an important advantage in using one standard nominal borehole diameter in all crystalline-rock investigations, at least until the geophysical tools can be calibrated to igneous and metamorphic rock.

8. Neutron- and acoustic-velocity logs do not correlate well with rock-matrix porosities determined in the laboratory for 18 samples of Oracle granite obtained from retrieved core.

9. Logarithms of scalar-hydraulic-conductivity values obtained from single-hole packer tests at the study site appear to be the realization of a second-order stationary, but anisotropic, stochastic process. The distribution of the values of log-hydraulic conductivity is approximately normal. Their spatial auto-covariance structure can be characterized by an anisotropic spherical semivariogram, with a range (maximum correlation distance) varying from 30 feet in the horizontal direction to 60 feet in the vertical direction.

10. Spatial distribution of scalar-hydraulic-conductivity values from single-hole packer tests at the site can be estimated at any point between the boreholes, by a three-dimensional, stochastic, interpolation technique called kriging. The advantage of this geostatistical approach is that it provides information about the variance and covariance of estimation errors resulting from such interpolation.

11. On the basis of kriging, one can generate an unlimited number of equally likely hydraulic-conductivity distributions in three-dimensional space between the boreholes by conditional Monte Carlo simulation. Thus, one can examine a multitude of different but equally likely paths that a particle of contaminant may take while traveling through the rock mass. We believe that this continuum approach provides a viable alternative to discrete fracture models of fluid flow and contaminant transport through fractured rocks.

8. REFERENCES

Alexander, J., D. H. Hall, and B. C. Storey, 1981, Porosity measurements of crystalline rocks by laboratory and geophysical methods, Institute of Geological Sciences, Report EPNU 81-10, Harwell, England.

Balk, Robert, 1937, Structural behavior of igneous rocks, Geological Society of America, Memoir 5, 177 pp.

Banerjee, A. K., 1957, Geology of the Oracle granite, Ph.D. Dissertation, University of Arizona, Tucson, Arizona.

Clifton, P. M. and S. P. Neuman, 1982, Effects of kriging and inverse modelling on conditional simulation of the Avra Valley aquifer in Southern Arizona, Water Resources Research, Vol. 18, No. 4, pp. 1215-1234

Cloos, Hans, 1922, Strekung and Rutschstreifen in granit zon zobten in Schleisen, Aloh. Preuss. Geol. Landesanst., N.F., 89, 107.

Crittenden, M. D., P. J. Coney, and G. H. Davis, eds, 1980, Cordilleran metamorphic core complexes. Geological Society of America, Memoir 153, 490 pp.

Czubek, J.A., 1979, Modern trends in mining geophysics and nuclear logging methods for mineral exploration, in Geophysics and Geochemistry in the Search for Metallic Ores, P.S. Hood, ed., Geol. Survey of Canada, Economic Geology Rept. No. 31, pp. 231-272.

Davis, G. H., 1981, Regional strain analysis of the superposed deformations in Southeastern Arizona and the Eastern Great Basin, Arizona Geological Society Digest, Vol. XIV, Tucson, Arizona.

Davis, G. H. and J. J. Hardy, 1981, The Eagle Pass detachment, Southeastern Arizona - product of mid-Miocene normal faulting in the Southern Basin and Range, Geological Society of America Bulletin, Vol. 92, Pt. 1, pp 749-762.

Davis, J. C., 1973, Statistics and Data Analysis in Geology, John Wiley & Sons, New York.

Davison, C. C., W. S. Keys and F. L. Paillet, 1982, Use of borehole geophysical logs and hydrologic tests to characterize crystalline rock for nuclear-waste storage, Whiteshall Nuclear Research Establishment, Manitoba, and Chalk River Nuclear Laboratory, Ontario, Canada, U.S. Office of Nuclear Waste Isolation, Technical Report ONWI-418, N.T.I.S., U.S. Dept. of Commerce, Springfield, VA 22161, 103 pp.

Dobrin, M. B., 1976, Introduction to Geophysical Prospecting, McGraw-Hill, New York.

Drewes, H. D., 1981, Tectonics of Southern Arizona, U. S. Geological Survey, Professional Paper 1144.

Dyck, A.V., ed. 1975, Borehole geophysics applied to mineral prospecting: a review, Canadian Geological Survey, Paper 75-31.

Gale, J. E., P. A. Witherspoon, C. R. Wilson and A. Rouleau, 1982, Hydrogeological characterization of the Stripa site, OECD/NEA Stripa Symposium, Stockholm, Sweden, October 25-27, 1982.

Glenn, W. E., and P. H. Nelson, 1979, Borehole logging techniques applied to base metal ore deposits, in Geophysics and Geochemistry in the Search for Metallic Ores, P. J. Hood, ed, Geological Survey of Canada, Economic Geology Report 31, pp. 273-294.

Hines, W. W., and D. C. Montgomery, 1980, Probability and Statistics in Engineering and Management Science, John Wiley, New York.

Hodgson, R. A., 1961, Classification of structures of joint surfaces, Amer. Journal of Science, Vol. 259.

Hsieh, P. A., S. P. Neuman and E. S. Simpson, 1981, Pressure testing of fractured rocks--a methodology employing three-dimensional hole tests, U.S. Nuclear Regulatory Commission, Washington, D.C., NUREG/CR-3213, 176 pp.

Hudson, J. A., and S. D. Priest, 1979, Discontinuites and rock mass geometry, Int. J. Rock Mech. Min. Sci., Vol. 16, pp. 339-362.

Journel, [illegible] and R. Froidevaux, 1982, Anisotropic hole-effect modeling, Mathematical Geology, Vol. 145, No. 3, pp. 217-239.

Journel, A. G., and C. Huijbregts, 1978, Mining Geostatistics, Academic Press, New York, 600 pp.

[illegible] S. B., S. J. Reynolds, P. E. Da[illegible] M. Shafiqullah, D. E. Livingston, and P. D. Pushkar, 1980, Evidence for multiple intrusion and deformation within the Santa [illegible]alina-Rincon-Tortolita crystalline complex, southeastern Arizona, in Crittenden, M. D., P. J. Coney, and G. H. Davis, eds., Cordilleran metamorphic core complexes, Geologic Society of America, Memoir 153, pp. 217-267.

Keys, W. S., 1984, A synthesis of borehole geophysical data at the underground Research Laboratory, Manitoba, Canada, Office of Crystalline Respository Development Technical Report 84I/OCRD 15, 42 pp.

Keys, W. S., 1979, Borehole geophysics in igneous and metamorphic rocks, 20th Ann. Symp., Trans. Society of Professional Well Log Analysts, pp. 001-0026.

Keys, W. S., and L. M. MacCary, 1971, Application of borehole geophysics to water-resources investigations, Chapter E1, in U.S. Geological Survey, Report TWI 2 (Book 2, Collection of Environmental Data), 126 pp.

Keys, W. S., and J. K. Sullivan, 1979, Role of borehole geophysics in defining the physical characteristics of the Raft River geothermal reservoir, Idaho, Geophysics, Vol. 44, No. 6, pp. 1116-1141.

Knapp, R. B., and D. L. Norton, 1981, Preliminary numerical analysis of processes related to magma crystallization and stress evolution in cooling pluton environments, Amer. Journal of Science, Vol. 281, pp. 35-68.

Law, A. M., and W. D. Kelton, 1982, Simulation Modeling and Analysis, McGraw-Hill, New York, 400 pp.

Law, A. M., and S. G. Vincent, 1983, UNIFIT: An interactive computer package for fitting probability distributions to observed data, Tucson, Arizona.

Long, J. C. S., J. S. Remer, C. R. Wilson, and C. A. Witherspoon, 1982, Porous media equivalents for networks of discontinuous fractures, Water Resources Research, Vol. 18, No. 3, pp. 645-658.

Lowell, J. D., 1968, Geology of the Kalamazoo orebody, San Manuel District, Arizona, Economic Geology, Vol. 63, pp. 645-654.

Matheron, G., 1971, The theory of regionalized variables and its application, Les Cahiers du Centre de Morphologie Mathematique de Fountainbleau, France.

McEwen, T. J., 1980, Fracture analysis of crystalline rocks: Field measurements and field geomechanical techniques, Institute of Geological Sciences, Natural Environment Research Council Report No. ENPU 80-11, Harwell, United Kingdom.

Miller, S. M., 1979, Determination of spatial dependence in fracture set characteristics by geostatistical methods, M. S. Thesis, University of Arizona, Tucson, Arizona.

Nelson, P. H., and W. E. Glenn, 1975, Influence of bound water on the neutron log in mineralized igneous rocks, 16 Ann. Symp., Trans. Society of Professional Well Log Analysts, pp. M1-M7.

Nelson, P. H., B. Paulsson, R. Rachiele, and L. Anderson, 1979, Preliminary report on geophysical and mechanical borehole measurements at Stripa (Sweden), Swedish-American Cooperative Program on Radioactive Waste Storage, Report No. 16, LBL-8280 SAC-16 UC-70.

Neuman, S. P., 1982, Statistical characterization of aquifer heterogeneities: An overview, Geological Society of America, Special Paper 189.

Paillet, F., 1980, Acoustic propagation in the vicinity of fractures which intersect a fluid-filled borehole, Trans. Society of Professional Well Log Analysts, 21st Annual Logging Symposium, Lafayette, LA, June 1980, p. DD1-DD33.

Pirson, S. J., 1963, Handbook of Well-Log Analysts, Prentice-Hall, New York.

Priest, S. D., and J. A. Hudson, 1976, Discontinuity spacings in rock, Int. J. Rock Mech. Min. Sci., Vol. 13, pp. 135-148.

Romm, E. W., and B. V. Pozinenko, 1963, Investigation of seepage in fractured rocks (in Russian), Trudy Unigri, No. 214, Leningrad, U.S.S.R.

Schimschal, Ulrich, 1981, The relationship of geophysical measurements to hydraulic conductivity at the Brantley damsite, New Mexico, Geoexploration, No. 19, pp. 115-125.

Schlumberger Ltd., 1978, Schlumberger Log Interpretation Principles, Vol. I, 277 Park Avenue, New York, N.Y.

Schwartz, F. W., L. Smith, and H. S. Crowe, 1983, Stochastic analysis of ground-water flow and contaminant transport in a fractured rock system. Unpublished manuscript presented at the Spring, 1983, Fractured Rock Symposium of the American Geophysical Union, Baltimore, Maryland.

Simmons, G., T. Todd, and W. S. Baldridge, 1975, Toward a quantitative relationship between elastic properties and cracks in low porosity rocks, American Journal of Science, Vol. 275, pp. 318-345.

Snow, D. T., 1965, A parallel-plate model of fractured permeable media, Ph.D. dissertation, the University of California, Berkeley, California.

Snow, D. T., 1970, The frequency and apertures of fractures in rock, Int. J. Rock Mech. Min. Sci., Vol. 7, pp. 23-40.

Wilson, C. R., and P. A. Witherspoon, 1970, An investigation of laminar flow in fractured rocks, Geotechnical Report No. 70-6, University of California, Berkeley, California.

Winter, C. L., S. P. Neuman, and C. M. Newman, 1984a, Prediction of far-field subsurface radionuclide dispersion coefficients from hydraulic conductivity measurements, U. S. Nuclear Regulatory Commission, Washington, D.C., NUREG/CR-3612, 56 pp.

Winter, C. L., C. M. Newman, and S. P. Neuman, 1984b, A perturbation expansion for diffusion in a random velocity field, S.I.A.M. Jour. Appl. Math., Vol. 44, No. 2, pp. 411-424.

Wyllie, M. R. J., and M. B. Spangler, 1952, Application of electrical resistivity measurements to be problem of fluid flow in porous media, Bull. Amer. Assoc, Petroleum Geol., Vol. 36, No. 2, pp. 359-403.

APPENDIX A: SUMMARY OF BOREHOLE DATA

A.1 Core and Fracture Logging. Core was obtained from boreholes H4 and M1 (Figure 1.3 and Table 1.1). A partial core from borehole M1 was obtained to study hydraulic properties on nonfractured rock sections; little attention was paid to recovering fractured intervals. (The core was obtained for Rock Mass Sealing Project, NRC 04-78-271. Borehole M1 eventually will be sealed as part of this project.) The core from borehole H4 was obtained for this project; the core was later oriented using the acoustic-televiewer strip charts; and the composition and aperture size of all the fractures were recorded. (See Figure A.1 for a sample strip chart.) The composition data included the percentage of chlorite, weathered clays (typically kaolinite), red iron oxides, yellow iron oxides, crystalline quartz, and calcite. The strike and dip of every fracture was recorded by orienting the core with the televiewer data. An average of 0.74 fracture per foot was identified. Depths were referenced to televiewer depths (top of casing), and the data were entered (in coded form) in a computer file. Criteria for classifying aperture widths on visual examination of core from borehole H4 are listed in Table A.1.

Fractures in the other boreholes (H2, H3, M1) were classified into fracture types by examination of acoustic-televiewer images of the boreholes. Three classes were identified, X, A and B. Distinct images were designated X-type; intermediate images were designated A-type; and small, indistinct images were designated B-type. This classification is meant to be used only as an approximate correlation tool. Chip samples and drillers logs provided additional lithologic information for boreholes H2, H3, and M1.

A.2 Borehole Geophysics. A significant proportion of the data used in studying the fracture system was provided by borehole-geophysical data. These data were obtained by members of the U.S. Geological Survey. W. Scott Keys, U.S. Geological Survey, Denver, Colorado, was at the site in March, 1981 and recorded logs in boreholes M1, H2, H3, and H4 (as indicated in Table A.2). Ken Hollett, U.S. Geological Survey, Tucson, Arizona, was at the site in January 1981, December 1982, and April 1983; he ran logs of boreholes H5, H6, and H7, as well as secured additional data in the first four boreholes. This report would not be possible without their efforts.

Data obtained from each logging tool were used to evaluate physical, mechanical, and chemical properties of the granite. Fracture orientations were obtained with the acoustic televiewer. Fracture locations were detected with varying sensitivity by all the logs. Lithologic variations were found by acoustic-velocity, gamma, electrical, gamma-gamma, and neutron logs; use of these logs is documented in Chapters 4 and 5.

A full description of the practical use of these logs is available in manuals published by service companies, such as Schlumberger and Dresser-Atlas; they are usually available at no cost. References to logging crystalline rock include: Keys and McCary (1971); Dyck (1975); Czubek (1979); Keys (1979); and Nelson and Glenn (1975).

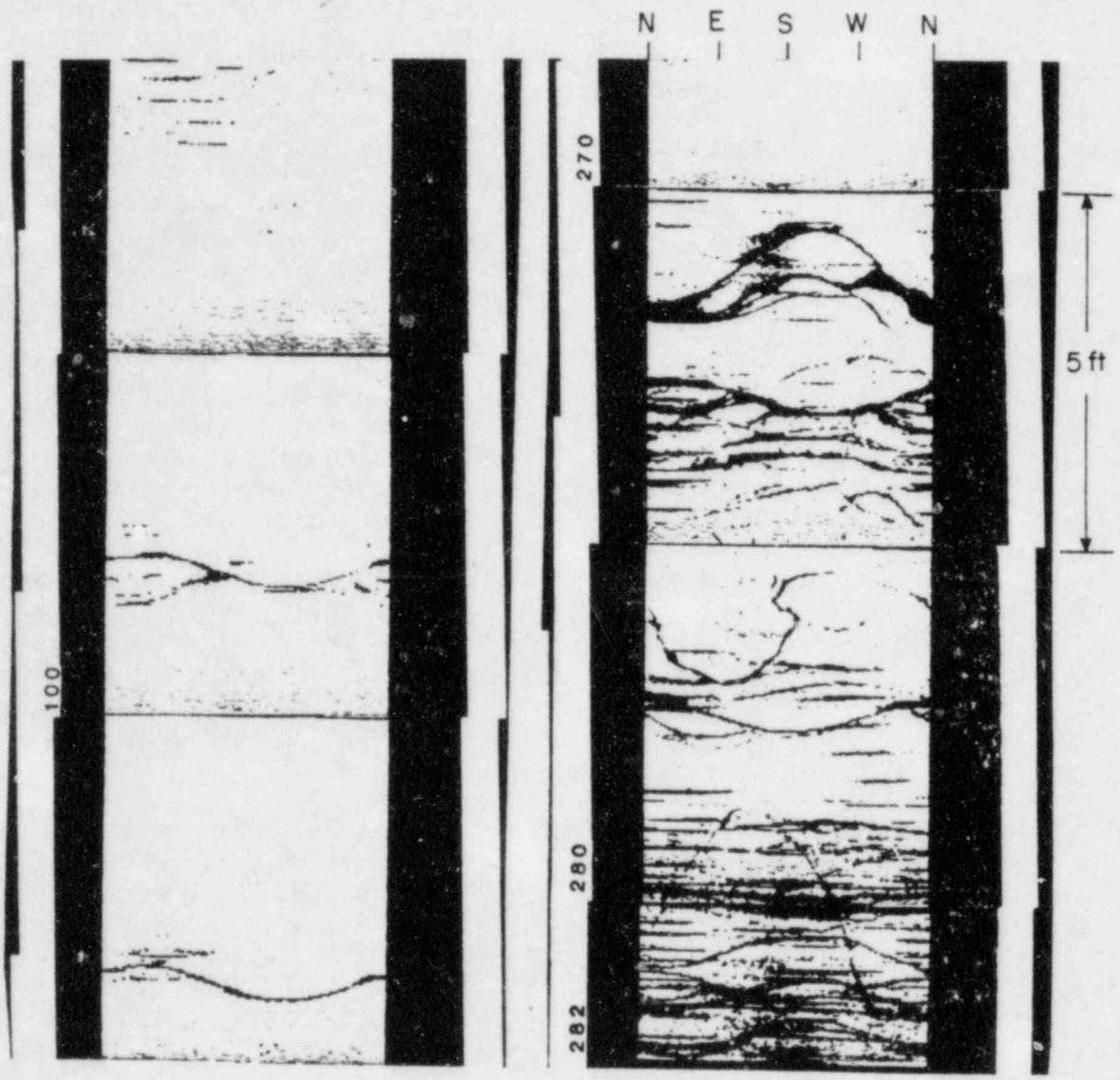

Figure A.1. Examples of acoustic-televiewer logs.

Table A.1 Criteria for classifying aperture widths based on visual examination of core from borehole H4.

X - (Major flow channels): Fracture broke apart on removal from core barrel; obviously was open when in situ. Fracture surface deeply weathered and friable.

A - (Partly open): Same as X except that exposed fracture surface showed portions with little or no weathering.

B - (Possibly open/essentially closed): Fracture aperture filled or nearly filled with calcite, permitting little present-time flow but indicating past flow. Fracture may or may not break apart on removal from core barrel.

C - (Closed): Fracture remained unbroken when core was removed from core barrel; if broken, surfaces meshed tightly together. If exposed, fracture surface showed no visual sign of weathering, but may contain minerals such as chlorite.

Table A.2 Summary of geophysical logging performed by the U.S. Geological Survey. (All logs were run from the bottom of the casing to the total depth whenever possible. D designates logging performed by W. Scott Keys, Denver, Colorado office. T designates logging performed by Ken Hollett, Tucson, Arizona office.)

LOG	BOREHOLES							
	M1	H2	H3	H4	H5	H6	H7	H8
Caliper	D	D	D	D	T	T	T	T
Temperature	T	T	T					
Neutron	D	D	D	D	T	T	T	T
Gamma-gamma					T	T	T	
Gamma	D	D	D	D			T	T
Acoustic televiewer	D	D	D	D				
Acoustic velocity	D	D	D	D				
Single-point resistance		T		D			T	
16-inch normal					T	T		
64-inch normal					T	T	T	

A brief description of the logging tools used at the site follows:

A.2.1 Caliper Log: The borehole diameter was measured by a three-arm mechanical probe. The arms were opened at the bottom of the hole by a motor. As the tool was brought up the borehole, the spring-loaded arms followed the shape of the hole. Resolution of the borehole diameters was approximately 0.05 inches. Single fractures that intercepted the borehole at angles greater than 20° from the horizontal were detected by the arms at different depths.

A.2.2 Gamma-Gamma: Gamma rays from a source in the downhole probe were scattered into the rock formation around the hole; some were scattered back to a downhole detector. Scattering was related to the electron density of the rock and was proportional to bulk density for most rocks. Measurements were sensitive to hole diameter. No results were reported for this tool in this study, but it appeared capable of detecting subtle lithologic variations.

A.2.3 Gamma: This probe measured gamma radiation emitted by (naturally occuring) radioactive isotopes. Most of the radiation was from potassium-40 and isotopes of the uranium and thorium series. The response was approximately proportional to the weight concentration of radioactive material.

A.2.4 Acoustic Televiewer: A reflected acoustic image of the inside of a borehole was obtained from this tool; its use is noted in the first part of this Appendix. The borehole televiewer is manufactured by Simplec Manufacturing Company of Dallas, Texas, under license by Mobil Oil Corporation. In operation, a rotating transducer scans the borehole wall with a 1.3-mHz acoustic signal. The signal is pulsed at 1300 to 1500 cycles per second, and the transducer serves as both a transmitter and receiver. Orientation of the tool is recorded by a flux-gate magnetometer. The log (Figure A.1) is a record of reflected acoustic amplitude. Borehole-wall irregularities, such as fractures, attenuate the signal; they are recorded as dark zones on Polaroid-film images of the oriented-scan traces. Near-horizontal sinusoidals of several fractures are shown in Figure A.1.

The aperture or width of fractures obtained by visual inspection of the core retrieved from borehole H4 was compared to the televiewer response. A relative scale can be assigned to the apertures. Fracture apertures in the core as small as 0.1 mm have been detected by the televiewer, but the tool does not discriminate between filled and open fractures, and it is affected by small-scale irregularities in the borehole wall. It is very useful for orienting core and for determining fracture orientation, and it will provide data in major fracture zones where core is lost.

A.2.5 Acoustic Velocity: Velocity of a compressional acoustic wave is measured by this tool. A pulsed source emits 20 to 35-kHz acoustic energy into the formation. Two receivers on the tool detect the wave as it passes through the formation, and the interval-transit time is recorded. In densely fractured zones or in irregularly shaped boreholes the first arrival can be missed; detection of the next pulse, or cycle, results in recording an

abnormal velocity. This misreading by the tool is known as cycle skipping; it often leads to an uninterpretable log, except that most fracture zones were detected by cycle skipping. Velocities measured in the granite were between 16,000 and 22,000 feet per second.

APPENDIX B: GLOSSARY

The following definitions are modified from the Glossary of Geology, American Geological Institute, 2nd ed., 1980.

Anastamose: A descriptive term referring to a feature characterized by an interlaced or braided pattern of channels. The veins of a leaf or the channels of a braided stream are described as having an anastamose pattern.

Andesite: A dark-colored, fine-grained extrusive rock that, when porphyritic, contains phenocrysts, composed primarily of zoned acid-plagioclase and one or more of the mafic minerals (e.g., biotite).

Antithetic: A descriptive term pertaining to minor normal faults that are of opposite orientation to the major fault with which they are associated.

Aphanitic: A descriptive term referring to the texture of an igneous rock in which crystalline components are not distinguishable by the unaided eye.

Aplite: A light-colored hypabyssal igneous rock characterized by fine-grained xenomorphic-granular texture. Said of an igneous rock having the characteristics and/or texture of aplite, such as a comparatively fine- and even-grained rock free of dark minerals.

Augen: In foliate metamorphic rocks such as schists and gneisses, large, lenticular mineral grains or mineral aggregates having the shape of an eye in cross section, in contrast to the shapes of other minerals in the rock.

Augen gneiss: A general term for a gneissic rock containing lenticular mineral grains or aggregates representing either deformed original phenocrysts or porphyroblasts of metamorphic origin.

Basalt: Dark- to medium-dark-colored, commonly extrusive (locally intrusive, as dikes), mafic igneous rock, composed chiefly of calcic plagioclase (usually labradorite) and clinopyroxene in a glassy or fine-grained groundmass; the extrusive equivalent of gabbro. Apatite and magnetite are common accessories.

Batholith: A large, generally discordant, plutonic mass that has more than 40 square miles (100 km^2) in surface exposure, and is composed predominantly of medium- to coarse-grained rocks of granodiorite and quartz monzonite composition.

Breccia: A coarse-grained clastic rock composed of large (greater than 2 mm diameter), angular, and broken rock fragments that are cemented together in a fine-grained matrix.

Brecciation: Formation of a breccia, as by crushing a rock into angular fragments.

Chlorite: A group of platy, monoclinic, usually greenish minerals of general formula: $(Mg, Fe^{+2}, Fe^{+3})_6AlSi_3O_{10}(OH)_8$.

Conchoidal: A descriptive term for a type of mineral or rock fracture that gives a smoothly curved surface. It is a characteristic habit of quartz and of obsidian.

Diabase: An intrusive rock whose main components are labradorite and pyroxene that is characterized by ophitic texture.

Exfoliation: The process by which thin (from less than a centimeter to several meters) concentric shells, slabs, sheets, scales, flakes, or plates of rock are successively broken, loosed, spalled, peeled, or stripped from the bare outer surface of a larger rock mass. Exfoliation is caused by the action of physical, thermal, or chemical forces producing differential stresses within an expanding rock, such as by rapid temperature changes in a desert region, or by the release of confining pressure of a once deeply buried rock as it is brought nearer to the surface by erosion.

Fault breccia: A tectonic breccia composed of angular fragments resulting from the crushing, shattering, or shearing of rocks during movement on a fault, from friction between the walls of the fault, or from distributive ruptures associated with a major fault.

Fault gouge: Soft, uncemented, pulverized, clayey or clay-like material, commonly a mixture of minerals in finely divided form, found along some faults or between the walls of a fault and filling, or partly filling a fault zone.

Foliation: A general term for a planar arrangement of textural or structural features in any type of rock.

Gneiss: A foliated rock formed by regional metamorphism in which bands or lenticles of granular minerals alternate with bands and lenticles in which minerals with flaky or elongate prismatic habits predominate.

Latite: A porphyritic extrusive rock having plagioclase and potassium feldspar (probably mostly sanidine) present in nearly equal amounts as phenocrysts, little or no quartz, and a finely crystalline to glassy groundmass.

Lineation: A general, nongeneric term for any linear structure in a rock of whatever scale.

Lystric Fault: A fault that is identifiable on a large scale by an undulating fault plane. Lystric refers to the smooth, spoon-shaped nature of the large wavelength undulating surface.

Massif: A massive topographic and structural feature in an orogenic belt, commonly formed of rocks more rigid than those of its surroundings.

Mylonite: A compact, chertlike rock without cleavage, but with a streaky or banded structure, produced by the extreme granulation and shearing of rocks that were pulverized and rolled during over-thrusting or by action of intense dynamic metamorphism in general.

Mylonite Gneiss: A metamorphic rock that is intermediate in character between mylonite and schist.

Mylonitization: Deformation of a rock by extreme microbrecciation, due to mechanical forces applied in a definitive direction, without noteworthy chemical reconstitution of granulated minerals.

Myrmekite: A wart-like intergrowth of plagioclase feldspar (generally oligoclase) and vermicular quartz, generally replacing potassium feldspar, formed during the later stages of consolidation in an igneous rock or during a subsequent period of plutonic activity. The quartz occurs as blobs, drops, or vermicular shapes within the feldspar.

Ophitic: A descriptive term for the holocrystalline, hypidiomorphic-granular texture of an igneous rock (especially diabase) in which lath-shaped plagioclase crystals are partially or completely included in pyroxene crystals.

Outcrop: That part of a geologic formation or structure that appears at the surface of the Earth.

Pegmatite: An exceptionally coarse-grained (most grains one cm or more in diameter) igneous rock, with interlocking crystals, usually found as irregular dikes, lenses, or veins, especially at the margins of batholiths.

Pegmatitic: A descriptive term for the texture of an exceptionally coarsely crystalline igneous rock.

Perthite: A variety of alkali feldspar consisting of parallel or subparallel intergrowths in which the potassium-rich phase (usually microcline) appears to be the host from which the sodium-rich phase (usually albite inclusions) exsolved.

Phaneritic: A descriptive term for the texture of an igneous rock in which the individual components are distinguishable megascopically.

Phenocryst: A relatively large, conspicuous crystal in a porphyritic rock.

Porphyritic : A descriptive term for the texture of an igneous rock in which larger crystals (phenocrysts) are set in a finer groundmass that may be crystalline, or glassy, or both.

Quartz Monzonite: In U.S. usage, granitic rock in which quartz comprises 10% to 50% of the felsic constituents, and in which the alkali feldspar/total feldspar ratio is between 35% and 65%, the approximate intrusive equivalent of rhyodacite. With an increase in plagioclase and felsic minerals, it grades into granodiorite; with more alkali feldspar, it grades into a granite.

Rhyolite: A group of extrusive igneous rocks, generally porphyritic and exhibiting flow texture, with phenocrysts of quartz and alkali feldspar (especially orthoclase) in a glassy to cryptocrystalline groundmass.

Schlieren: In some igneous rocks, irregular streaks or masses that contrast with the rock mass but have shaded borders. They may represent segregations of dark or light minerals, or altered inclusions elongated by flow.

Trachyandesite: An extrusive rock intermediate in composition between trachyte and andesite.

Trachybasalt: An extrusive rock intermediate in composition between a trachyte and a basalt.

Trachyte: A group of fine-grained, generally porphyritic, extrusive rocks having alkali feldspar, minor mafic minerals (biotite, hornblende, or pyroxene) as the main components, and possibly a small amount of acid plagioclase.

Vermicular Quartz: Quartz occurring in worm-like forms intergrown with or penetrating feldspar, as in myrmekite.

Xenomorphic: A descriptive term for the texture or fabric of an igneous rock having or characterized by crystals not bounded by their own crystal faces and having their form impressed upon them by preexisting adjacent mineral crystals.

APPENDIX C

Summary of Hydraulic Conductivity Values Measured from Single-Hole, Pressure Injection Tests

The values of hydraulic conductivity used in this report were calculated from single-hole, pressure injection tests conducted between 1982 and 1983 by Paul Hsieh, Gary Stiles, and Jim Posedly of the University of Arizona. The results for boreholes H5, H6, and H7 are reported here for the first time. Hydraulic conductivity was calculated under the assumption of prolate ellipsoidal flow under steady-state conditions and follow the technique of Hsieh et al. (1983).

We used these values of hydraulic conductivity to illustrate the use of geostatistics in the assessment of the properties of a variable rock mass. In some cases, especially in boreholes M1 and H3, the packer tests were subject to leakage above and below the packed-off intervals. However, at low injection pressures steady-state conditions commonly were reached with moderate leakage (less than 10% of the total flow). Values calculated for leaky tests are noted in Table C.1. Although these values probably are higher than true values, we use them to demonstrate our technique as described in Chapter 5.

The zone around the fault zone could not be properly tested because of excessive leakage. This introduces some bias toward smaller values of hydraulic conductivity. If this zone were to be properly tested, it would require a longer packer assembly in order to span the intensely fractured zone. The values of hydraulic conductivity calculated for the study site are listed in Table C.1.

Table C.1

Measured Values of Hydraulic Conductivity

BOREHOLE	DEPTH (FT)	HYD. COND. (M/S)	LOG HYD. COND. (M/S)
H4	-76.0	6.03E-08	-7.220
4	-88.0	7.08E-10	-9.150
4	-100.0	6.03E-10	-9.220
4	-116.0	5.01E-11	-10.300
4	-128.0	3.02E-10	-9.520
4	-140.0	3.02E-10	-9.520
4	-156.0	1.00E-08	-8.000
4	-168.0	3.02E-10	-9.520
4	-175.0*	7.94E-09	-8.100
4	-188.0*	5.01E-08	-7.300
4	-200.0*	3.98E-08	-7.400
4	-212.0	2.00E-09	-8.700
4	-224.0	1.00E-07	-7.000
4	-236.0	3.98E-08	-7.400
4	-248.0	2.00E-09	-8.700
4	-260.0*	7.94E-09	-8.100
4	-272.0*	3.02E-08	-7.520
H3	-63.5*	3.55E-07	-6.450
3	-77.5	2.00E-07	-6.700
3	-88.5	5.25E-08	-7.290
3	-89.5	6.03E-08	-7.220
3	-97.5*	3.98E-08	-7.400
3	-114.5	1.00E-07	-7.000
3	-129.5*	2.40E-08	-7.620
3	-148.5	1.41E-08	-7.850
3	-163.5	7.24E-08	-7.140
3	-164.5	5.01E-08	-7.300
3	-177.5	6.76E-08	-7.170
3	-190.5	4.17E-08	-7.380
3	-202.5	1.20E-08	-7.920
3	-215.5	4.47E-09	-8.350
3	-228.5	2.19E-08	-7.660
3	-249.5*	2.51E-06	-5.600
3	-277.5*	1.00E-07	-7.000

Table C.1

Measured Values of Hydraulic Conductivity--Continued

BOREHOLE	DEPTH (FT)	HYD. COND. (M/S)	LOG HYD. COND. (M/S)
H2	-74.5*	6.03E-08	-7.220
2	-84.5*	8.91E-08	-7.050
2	-102.5	3.02E-08	-7.520
2	-114.5	3.02E-09	-8.520
2	-127.5	7.08E-09	-8.150
2	-139.5*	8.91E-10	-9.050
2	-151.5	6.03E-10	-9.220
2	-163.5	3.02E-09	-8.520
2	-175.0	6.03E-10	-9.220
2	-187.5	2.00E-09	-8.700
2	-199.5	2.00E-09	-8.700
2	-211.5	3.98E-09	-8.400
2	-223.5*	2.00E-09	-8.700
2	-236.5	3.02E-09	-8.520
2	-251.5*	8.91E-08	-7.050
2	-267.5	2.51E-08	-7.600
2	-275.5	7.94E-10	-9.100
M1	-126.5	8.51E-08	-7.070
1	-141.5	1.20E-07	-6.920
1	-154.5*	3.16E-08	-7.500
1	-165.5*	7.59E-09	-8.120
1	-178.5	3.09E-08	-7.510
1	-191.5*	6.31E-08	-7.200
1	-200.5*	5.37E-09	-8.270
1	-215.5	3.24E-08	-7.490
1	-229.5	7.94E-08	-7.100
1	-236.5*	3.02E-08	-7.520
1	-254.5	1.07E-07	-6.970
1	-266.5*	8.71E-08	-7.070
1	-279.5*	6.31E-07	-6.200
H5	-116.7	6.76E-08	-7.170
5	-137.1*	8.13E-08	-7.090
5	-153.3*	1.23E-07	-6.910
5	-164.6	1.55E-09	-8.810
5	-175.8	5.89E-10	-9.230
5	-187.1	4.37E-09	-8.360
5	-200.3	1.07E-08	-7.970
5	-211.6	2.57E-07	-8.590
5	-222.8	6.46E-09	-8.190
5	-234.0	1.26E-08	-7.900

Table C.1

Measured Values of Hydraulic Conductivity--Continued

BOREHOLE	DEPTH (FT)	HYD. COND. (M/S)	LOG HYD. COND. (M/S)
H6	-94.4	5.75E-07	-6.240
6	-104.7	5.75E-10	-9.240
6	-115.9*	4.17E-08	-7.380
6	-127.2*	3.98E-08	-7.400
6	-138.4*	2.95E-08	-7.530
6	-149.7*	8.32E-08	-7.080
6	-160.9	3.72E-10	-9.430
6	-172.2	6.03E-10	-9.220
6	-183.4*	3.89E-08	-7.410
6	-194.7*	2.00E-08	-7.700
6	-205.9	3.63E-10	-9.440
6	-217.2	1.45E-08	-7.840
6	-228.4	1.00E-08	-8.000
6	-239.7	2.69E-08	-7.570
H7	-86.1	9.55E-09	-8.020
7	-96.4	1.91E-09	-8.720
7	-107.6	1.20E-10	-9.920
7	-118.9	2.29E-10	-9.640
7	-130.1	2.34E-10	-9.630
7	-142.4	1.00E-09	-9.000
7	-153.6	1.58E-09	-8.800
7	-160.8	2.82E-09	-8.550
7	-171.4	3.80E-09	-8.420
7	-180.4	4.57E-10	-9.340
7	-191.0	1.95E-09	-8.710
7	-202.7	2.57E-09	-8.590
7	-214.8	7.94E-10	-9.100
7	-227.1	1.10E-09	-8.960
7	-239.4	2.40E-08	-7.620

* Denotes test with significant leakage around packers.

Appendix D

Fitted Probability Functions for Log-Hydraulic Conductivity

The statistical description of the frequency distribution of hydraulic conductivity measured in oil fields and aquifers is generally regarded to fit a lognormal distribution (Neuman, 1982). A histogram of the logarithm of values that can be described as lognormal will have a "bell-shaped" or normal distribution about the mean. The log of measured hydraulic-conductivity values obtained from the Oracle granite (Appendix C) does not appear to have a histogram with the symmetry of a normal distribution. Two histograms are shown in Figure D.1 which were generated using groupings of 0.5 and 1.0 log unit for the data shown in Appendix C. Both have a skewed or asymmetric appearance. Since the probability distribution function (PDF) that describes the Oracle data may not be the lognormal PDF, a comparison of three possible distributions are tested to see how well they fit the data. The normal distribution (for the log of the values) was compared to two skewed distributions, the Weibull and gamma, to see which model best fits the data. Three PDF's and the functions that determine the curves are shown in Figure D.2. The normal is determined by two parameters: The mean which establishes the origin of Figure D.2 (part c), and the variance which sets the scale. The Weibull (Figure D.2, part a) and the gamma (Figure D.2, part b) require three parameters: (1) A location parameter sets the origin and is equal to the lower limit of the data; (2) a scaling parameter, β, sets the magnitude of the curve, and (3) a shape parameter, α, alters the basic shape of the distribution and is the most critical parameter. All three cases illustrated are for the case where $\beta = 1$.

A fit to the data can be analyzed according to many statistical tests. In this case, three tests are applied. First, the curve parameters are fit to the data for all three models. A comparison can then be made of the theoretical and measured values of the mean, variance, and coefficients of skewness and kurtosis. Then the "goodness" of the fit is quantitatively tested by the chi-square and Kolmogorov-Smirnov tests which show the discrepancy between the theoretical and measured distributions. A third qualitative test of the models is done by the standard technique of plotting the data on probability paper and examining the fits qualitatively. Probability paper linearizes the theoretical cumulative distribution for each model so a plot of the field data on the paper will result in a straight line if the data can be described by the particular probability model.

The first test was done by estimating the probability-function parameters (scale, shape, and location) through the use of a maximum-likelihood estimation. This test, and the others, was done with a commercially available PDF fitting program, UNIFIT, written by A. M. Law and S. Vincent (1983). The theory of the computational procedure largely follows Law and Kelton (1982). Results of the fit and a comparison of the field data and theoretical point statistics are shown in Table D-1. The shape of the fitted Weibull and gamma distributions are determined by α, the shape parameter (Figure D.2). The

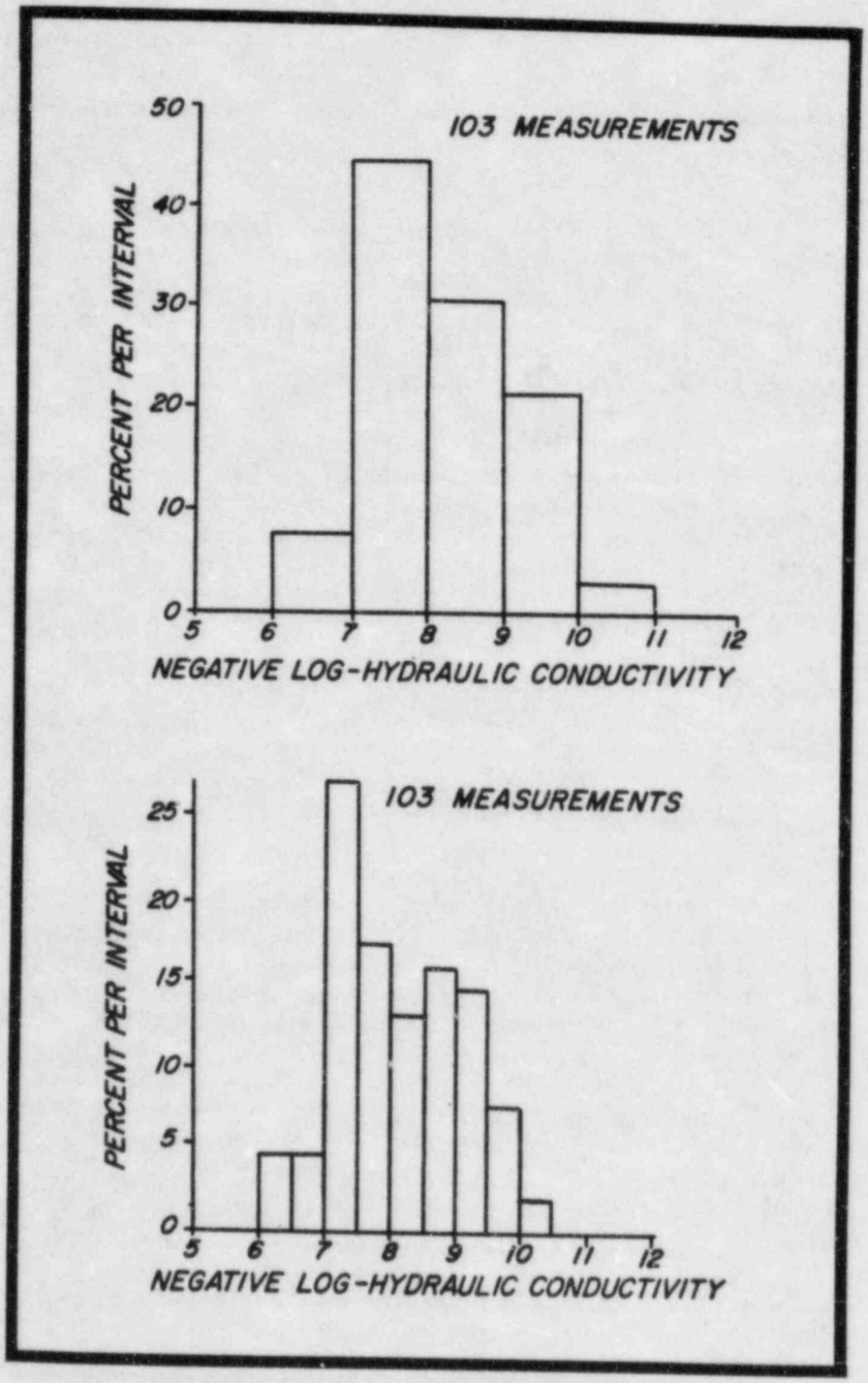

Figure D.1. Histograms of Log-Hydraulic Conductivity.

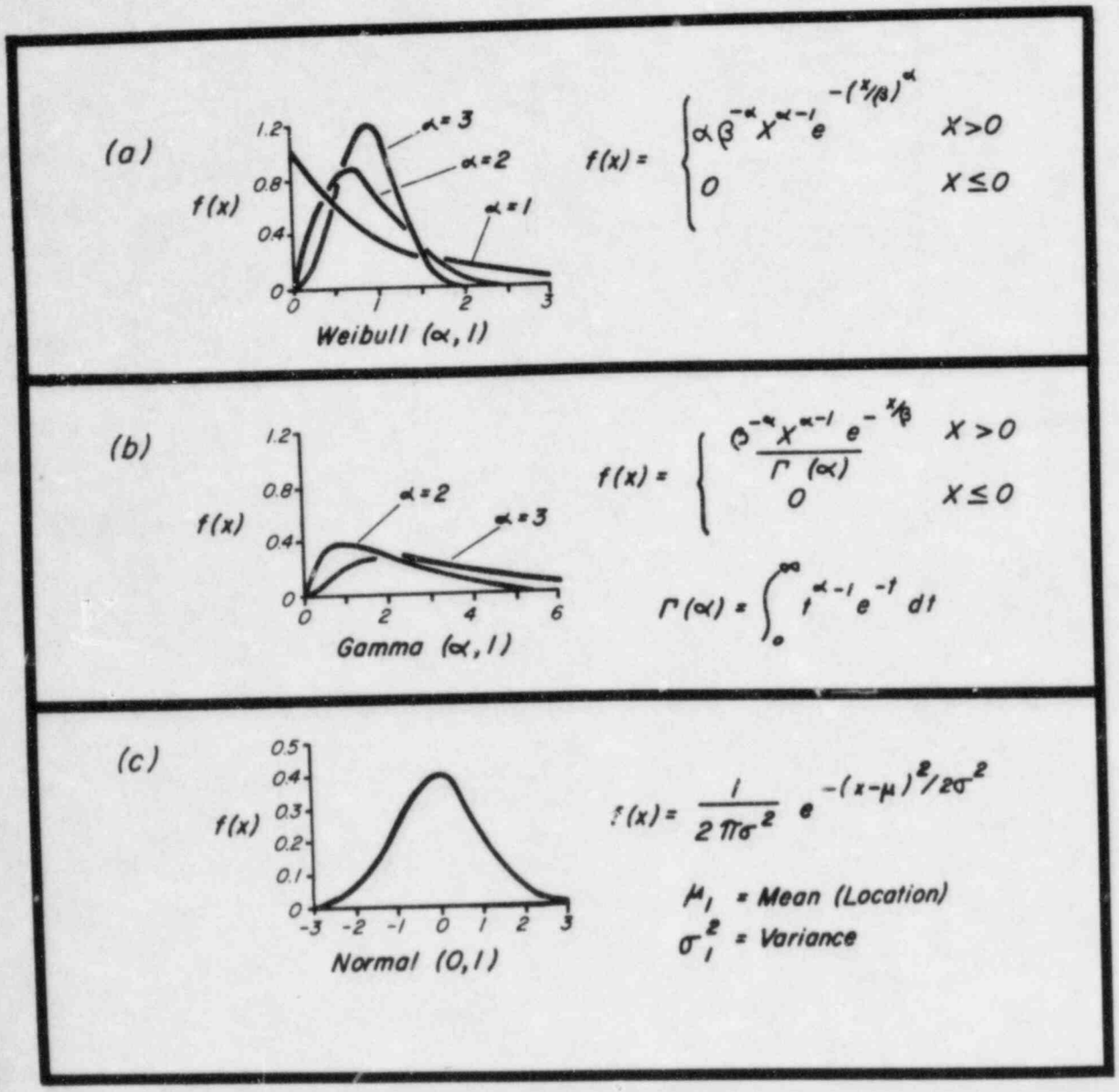

Figure D.2. Probability-distribution functions.

Table D.1 Probability-Distribution Fitting Statistics

FITTED PARAMETERS* (maximum-likelihood estimates)

	Location	α_1 Shape	β Scale
Weibull	6.20	1.96	2.05
Gamma	6.20	2.40	0.77
Normal	8.05	-	0.91

DISTRIBUTION CHARACTERISTICS

	Mean	Variance	Coefficient of Skewness	Coefficient of Kurtosis
Data	8.05	0.83	0.26	2.10
Weibull	8.02	0.93	0.64	3.28
Gamma	8.05	1.42	1.29	5.49
Normal	8.05	0.83	0.00	3.00

TEST STATISTICS

	$\chi^2(10)$	$\chi^2(18)$	K-S	K-S, Alpha Level
Weibull	15.6	11.9	0.082	.20
Gamma	31.5	14.9	0.112	.10
Normal	30.9	27.6	0.122	.10

* Refer to Figure D.1 for a description of the parameters.

Weibull has a sharper peak than the gamma and approximates the data histogram better than the gamma. Quantitative comparison is done using the chi-square (χ^2) and Kolmogorov-Smirnov (K-S) tests. The χ^2 test is dependent upon the frequency class width or data groupings chosen to generate a histogram since it is essentially the sum of the difference between a theoretical histogram and the histogram of the measured data. To minimize the possible bias introduced by selecting improper groupings, the data are grouped into intervals of equal probability that result in histogram classes of similar width. Oracle data were grouped into 8 intervals which represent 12.5% of the data per interval, and 10 intervals that represent 10.0% of the data per interval. The larger the value of the χ^2 statistic, the greater the discrepancy is between the theoretical and observed histograms. Statistics are shown in Table D.1; they indicate the Weibull provides the best fit, although the gamma and normal distributions are not unreasonable. The K-S test also can be applied to the models. This test compared the cumulative probability distribution and is not dependent upon a subjective grouping of the data. It does require that a complete range of data exist in order to represent a continuous function with the discrete data points. At the study site, the data occur regularly between the values of -10.3 and -6.2 so this condition is met. Like the χ^2 test, a large value of the K-S test indicates a greater discrepancy between a fitted model and the measured data. The results of the K-S test agrees with the χ^2 test and show that the skewed Weibull distribution provides the best match to the log-hydraulic conductivity. It also is possible to determine the degree of confidence one has using the K-S test, through the use of a value known as the alpha level. An alpha level is a measure of how well the data mean will be reproduced by the model distribution (the hypothesis test for the mean). The larger the value, the better the distribution model will represent the data. The alpha level is used to construct the confidence intervals of a distribution commonly seen, for example, in linear regressions as 90 or 95% confidence intervals about the regression line through a set of points. As the alpha level increases, the better the fit of the line will be to the data, or in this case, to the model distribution. This statistic agrees with the findings of the χ^2 test and allows for a quantitative interpretation of the K-S test.

The third test applied to the data is a comparison of the cumulative probability functions associated with each model. A qualitative comparison can be made of the three models shown in Figure D-3. The K-S statistic tested the fit as well, but is influenced by a few major differences between the data and the theoretical distribution. All three tests compare favorably when presented in this manner.

The observed skew or asymmetry of the observed distribution of log hydraulic conductivities is best modeled by a Weibull distribution. The lognormal distribution (a normal distribution of log values) does not appear to be as adequate in the statistical description of the frequency distribution of the 102 measured values of hydraulic conductivity. Other studies of the hydraulic conductivity of granite rock (Gale et al., 1982; Snow, 1965) showed that the observed distribution was lognormal.

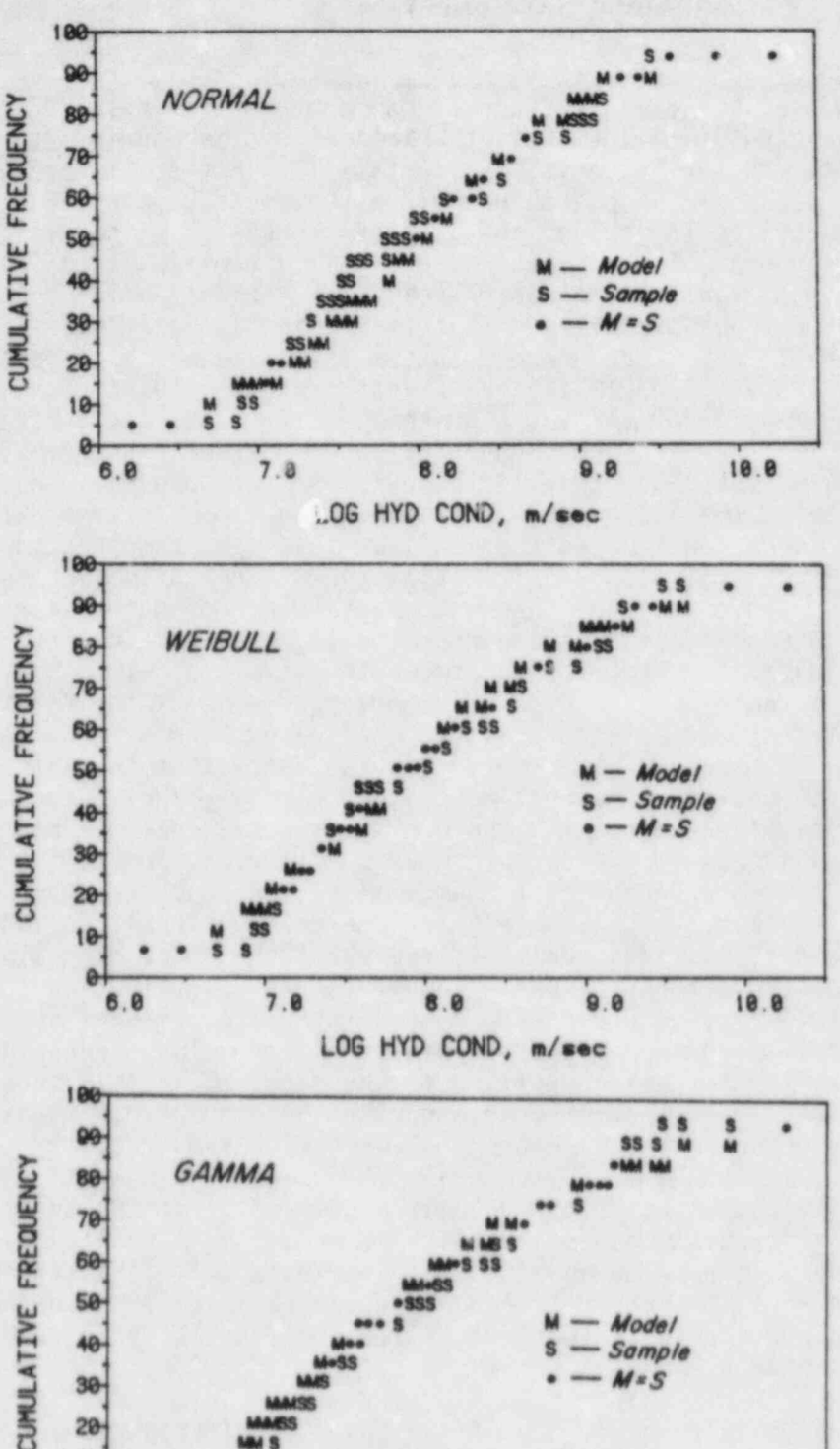

Figure D.3. Comparison of three cumulative-probability plots filled to log-hydraulic conductivity.

*U.S. GOVERNMENT PRINTING OFFICE: 1985-461-721:20266

NRC FORM 335 (11) U.S. NUCLEAR REGULATORY COMMISSION

BIBLIOGRAPHIC DATA SHEET

1 REPORT NUMBER (Assigned by TIDC, add Vol. No., if any)
NUREG/CR-3736

2 Leave blank

3 TITLE AND SUBTITLE
Field and Theoretical Investigations of Fractured Crystalline Rock near Oracle, Arizona

4 RECIPIENT'S ACCESSION NUMBER

5 DATE REPORT COMPLETED
MONTH: May YEAR: 1985

6 AUTHOR(S)
J. W. Jones, E. S. Simpson, S. P. Neuman, W. S. Keys

7 DATE REPORT ISSUED
MONTH: August YEAR: 1985

8 PERFORMING ORGANIZATION NAME AND MAILING ADDRESS (Include Zip Code)
Department of Hydrology and Water Resources
University of Arizona
Tucson, AZ 85721

9 PROJECT/TASK/WORK UNIT NUMBER
Task 1

10 FIN NUMBER
FIN B5753

11 SPONSORING ORGANIZATION NAME AND MAILING ADDRESS (Include Zip Code)
Division of Radiation Programs and Earth Sciences
Office of Nuclear Regulatory Research
U.S. Nuclear Regulatory Commission
Washington, DC 20555

12a TYPE OF REPORT
Topical technical report

12b PERIOD COVERED (Inclusive dates)
1982-1984

13 SUPPLEMENTARY NOTES

14 ABSTRACT (200 words or less)

A combination of geophysical and hydraulic testing has been conducted in granite near Oracle, Arizona. The purpose of the work is to determine relationships, if any, among (1) fracture distribution, (2) geophysical properties, and (3) hydraulic properties of fractured rock of low hydraulic conductivity. To date, eight vertical borings spaced 20 to 50 feet apart, ranging from 250 to 300 feet in depth, have been drilled. The data obtained from neutron, gamma, acoustic-velocity, electrical-resistivity, and acoustic-televiewer logs, with the results of over 100 single-hole, straddle-packer injection tests make possible a detailed description of the fracture system. Geophysical logs readily detect fractures and are sensitive to subtle lithologic variations of the granite. Orientation and distribution of individual fractures were determined from the interpretation of the acoustic-televiewer data, and from the analysis of core obtained from one borehole. Fracture densities over the 13-foot long straddle-packer test intervals did not correlate with measured hydraulic conductivity measurements. A strong correlation between the neutron-log response and measured hydraulic conductivity does exist; it was used to supplant conductivity measurements. The geostatistical technique of kriging provided a three-dimensional map of hydraulic conductivity that can be compared with subsurface interpretations of the geophysical logs.

15a KEY WORDS AND DOCUMENT ANALYSIS

15b DESCRIPTORS

Hydrology, saturated fractured rocks, geophysical interpretations, statistical analysis

16 AVAILABILITY STATEMENT
Unlimited

17 SECURITY CLASSIFICATION (This report)
Unclassified

18 NUMBER OF PAGES

19 SECURITY CLASSIFICATION (This page)
Unclassified

20 PRICE
$

UNITED STATES
NUCLEAP REGULATORY COMMISSION
WASHINGTON, D.C. 20555